Novel Control Approaches for the Next Generation Computer Numerical Control (CNC) System for Hybrid Micro-machines

Wenbin Zhong

A thesis submitted for the degree of Doctor of Philosophy

Centre for Precision Manufacturing

Department of Design, Manufacture and Engineering Management

University of Strathclyde

July 2018

This thesis is the result of the author's original research. It has been composed by the author and has not been previously submitted for examination which has led to the award of a degree.

The copyright of this thesis belongs to the author under the terms of the United Kingdom Copyright Acts as qualified by University of Strathclyde Regulation 3.50. Due acknowledgement must always be made of the use of any material contained in, or derived from, this thesis.

Signed: Wenbin Zhong

Date: 04/07/2018

Abstract

It is well-recognised that micro-machining is a key enabling technology for manufacturing high value-added 3D micro-products, such as optics, moulds/dies and biomedical implants etc. These products are usually made of a wide range of engineering materials and possess complex freeform surfaces with tight tolerance on form accuracy and surface finish.

In recent years, hybrid micro-machining technology has been developed to integrate several machining processes on one platform to tackle the manufacturing challenges for the aforementioned micro-products. However, the complexity of system integration and ever increasing demand for further enhanced productivity impose great challenges on current CNC systems. This thesis develops, implements and evaluates three novel control approaches to overcome the identified three major challenges, i.e. system integration, parametric interpolation and toolpath smoothing. These new control approaches provide solid foundation for the development of next generation CNC system for hybrid micro-machines.

There is a growing trend for hybrid micro-machines to integrate more functional modules. Machine developers tend to choose modules from different vendors to satisfy the performance and cost requirements. However, those modules often possess proprietary hardware and software interfaces and the lack of plug-and-play solutions lead to tremendous difficulty in system integration. This thesis proposes a novel three-layer control architecture with component-based approach for system integration. The interaction of hardware is encapsulated into software components, while the data flow among different components is standardised. This approach therefore can significantly enhance the system flexibility. It has been successfully verified through the integration of a six-axis hybrid micro-machine.

Parametric curves have been proven to be the optimal toolpath representation method for machining 3D micro-products with freeform surfaces, as they can eliminate the high-frequency fluctuation of feedrate and acceleration caused by the discontinuity in

the first derivatives along linear or circular segmented toolpath. The interpolation for parametric curves is essentially an optimization problem, which is extremely difficult to get the time-optimal solution. This thesis develops a novel real-time interpolator for parametric curves (RTIPC), which provides a near time-optimal solution. It limits the machine dynamics (axial velocities, axial accelerations and jerk) and contour error through feedrate lookahead and acceleration lookahead operations. Experiments show that the RTIPC can simplify the coding significantly, and achieve up to ten times productivity than the industry standard linear interpolator. Furthermore, it is as efficient as the state-of-the-art Position-Velocity-Time (PVT) interpolator, while achieving much smoother motion profiles.

Despite the fact that parametric curves have huge advantage in toolpath continuity, linear segmented toolpath is still dominantly used on the factory floor due to its straightforward coding and excellent compatibility with various CNC systems. This thesis presents a new real-time global toolpath smoothing algorithm, which bridges the gap in toolpath representation for CNC systems. This approach uses a cubic B-spline to approximate a sequence of linear segments. The approximation deviation is controlled by inserting and moving new control points on the control polygon. Experiments show that the proposed approach can increase the productivity by more than three times than the standard toolpath traversing algorithm, and 40% than the state-of-the-art corner blending algorithm, while achieving excellent surface finish.

Finally, some further improvements for CNC systems, such as adaptive cutting force control and on-line machining parameters adjustment with metrology, are discussed in the future work section.

Acknowledgements

It is difficult to wonder what the PhD life means to a person until I started to reflect the last four years of my PhD during the writing-up. I believe that it has been the most rewarding time of my life so far. I have met people who inspired me in my career choice and attitude to life. I have encountered things that challenged my understanding and broadened my horizon. I have received encouragement and trust at the difficult times. All those experiences will continue shaping who I am in the future.

Table of Contents

List of Tables

List of Figures

XIII

Nomenclature

t	Time
ρ	Radius of curvature
λ	Safety factor
ε	Contour error
F	Feedrate
J	Maximum jerk
S	Arc length
T	Interpolation period
a_t	Tangent acceleration
a_n	Centripetal acceleration
A_i	The maximum acceleration of axis i
A_t^{max}	Maximum tangent acceleration
A_t^{min}	Minimum tangent acceleration
$\boldsymbol{C}(u)$	Represents a parametric curve with parameter u
F_{cmd}	The command feedrate
F_{lmt}	The feedrate limitation
$N_{i,p}$	B-spline basis function
P_i	The B-spline control points
Q_i	The given toolpath points
t_{look}	The lookahead length
V_i	The maximum velocity of axis i

Abbreviations

3D	3 Dimensional
ADC	Analog-to-digital Converter
AM	Additive Manufacturing
API	Application Programming Interface
ASIC	Application Specific Integrated Circuit
AUTOSAR	AUTomotive Open System ARchitecture
CAD	Computer-aided Design
CAGD	Computer-aided Geometric Design
CAM	Computer-aided Manufacturing
CAN	Controller Area Network
CAPP	Computer-aided Process Planning
CCD	Charge-coupled Device
CCM	CORBA Component Model
CDC	Communications Devices Class
CNC	Computer Numerical Control
COM	Component Object Model
CORBA	Common Object Request Broker Architecture
CPS	Cyber-physical System
DAC	Digital-to-analog Converter
DFU	Device Firmware Upgrade
DLL	Dynamic Link Library
DRI	Dispersed Reference Interferometry
DSP	Digital Signal Processing
EDA	Electronic Design Automation
EDM	Electrical Discharge Machining
EJB	Enterprise JavaBeans
EtherCAT	Ethernet for Control Automation Technology
FEA	Finite Element Analysis
FIFO	First-In-First-Out
FPGA	Field Programmable Gate Array
HDL	Hardware Description Language
HMI	Human-machine Interface

ICT	Information and Communication Technology
IDL	Interface Definition Language
IGES	Initial Graphics Exchange Specification
JTAG	Joint Test Action Group
LIGA	Lithographie Galvanoformung Abformung (German acronym)
MAC	Media Access Controller
MEMS	Micro-Electric-Mechanical Systems
MPU	Memory Protection Unit
NURBS	Non-Uniform Rational B-Splines
OAC	Open Architecture Control
OMAC	Open Modular Architecture Controllers
OMG	Object Management Group
OSACA	Open System Architecture for Controls within Automation Systems
OSE	Open System Environment for Manufacturing
PCB	Printed Circuit Board
PHY	Physical Layer
PVT	Position-Velocity-Time
RMII	Reduced Media-Independent Interface
RMS	Reconfigurable Manufacturing System
RTIPC	The Real-time Interpolator for Parametric Curves
RTOS	Real-time Operating System
SCARA	Selective Compliance Assembly Robot Arm
SDRAM	Synchronous Dynamic Random Access Memory
SFPU	Single Floating Point Unit
STEP	Standard for the Exchange of Product Model Data
VMD	Virtual Module Driver

List of Publications

Journal papers:

1. W. Zhong, X. Luo, W. Chang, F. Ding, and Y. Cai, "A real-time interpolator for parametric curves", Internation Journal of Machine Tools and Manufacture, vol. 125, pp. 133–145, 2018.
2. W. Zhong, and X. Luo, "A new real-time global toolpath smoothing algorithm for freeform surface machining", CIRP Journal of Manufacturing Science and Technology, under review.
3. X. Luo, W. Zhong, and W. Chang, "A generic control architecture for hybrid micro-machines", Micromachines, vol. 9, pp. 305-316, 2018.

Conference papers:

1. R. Walker, W. Zhong, X. Kong, and X. Luo, "Design and integration of a high-precision material handling system with a six-axis hybrid micro-machine", in 6th International Conference on Nanomanufacturing, London, UK, 2018, accepted.
2. W. Chang, W. Zhong, F. Ding, F. Wardle, and X. Luo, "Development of a compact ultra-precision six-axis hybrid micro-machine", in 2017 World Congress on Micro and Nano Manufacturing, Kaohsiung, Taiwan, 2017.
3. W. Zhong, W. Chang, L. Rubio, and X. Luo, "A local tool path smoothening scheme for micromachining", in 16th International Conference of the European Society for Precision Engineering and Nanotechnology, Nottingham, UK, 2016, pp. 317-318.
4. W. Zhong, W. Chang, L. Rubio, and X. Luo, "Reconfigurable software architecture for a hybrid micro machine tool", in 21st International Conference on Automation and Computing, Glasgow, UK, 2015, pp. 389-392.

Book chapter:

X. Luo, W. Chang, W. Zhong, F. Wardle, "Chapter 8 Hybrid Machine Tool Design", in X. Luo, Y. Qin, "Hybrid Machining: Theory, Methods, and Case Studies", Elsevier, in press.

Chapter 1   Introduction

1.1   Background

Micro-manufacturing, in the broad term, refers to techniques to manufacture a variety of miniaturized/micro products/systems, such as micro-electric-mechanical systems (MEMS), micro-mechanical devices, and micro-medical components, etc. It can be classified into MEMS-based (or lithography-based) micro-manufacturing and non-MEMS-based (or non-lithography-based) micro-manufacturing [1]. MEMS-based micro-manufacturing involves techniques such as photolithography, chemical etching, LIGA, laser ablation, etc. While common non-MEMS-based micro-manufacturing techniques include micro-mechanical cutting, micro-forming, laser machining, electrical discharge machining (EDM), etc. MEMS-based micro-manufacturing has become mature in the industry for many years, it mainly focuses on creating planer or 2.5D structures on silicon, while non-MEMS-based micro-manufacturing is still in the developing stage, its ability to create complex 3D structures on a wide range of materials has attracted a lot of attention from both academia and industry. Therefore, micro-manufacturing refers to non-MEMS-based approaches in the rest of the thesis.

Back to 2005, a panel of scientists from the U.S. conducted an international investigation on the research and development of micro-manufacturing techniques for the U.S. government. In the published investigation report [2], they defined micro-manufacturing as the creation of high-precision 3D products using a variety of materials and possessing features with sizes ranging from tens of micrometres to a few millimetres. They emphasized that the importance of micro-manufacturing, as a new technology, is that it is an enabling technology to bridge the gap between the nano- and micro-worlds, as shown in Figure 1-1. They therefore recommended the U.S. government to invest in it as a strategic technology to enhance the competitive advantage of the U.S. While in the UK, the Technology Strategy Board carried out a study on high value manufacturing in 2012, the micro- and nano-manufacturing

processes were identified as one of the most significant process technologies that have the potential to bring sustainable growth and major economic benefits to the UK [3].
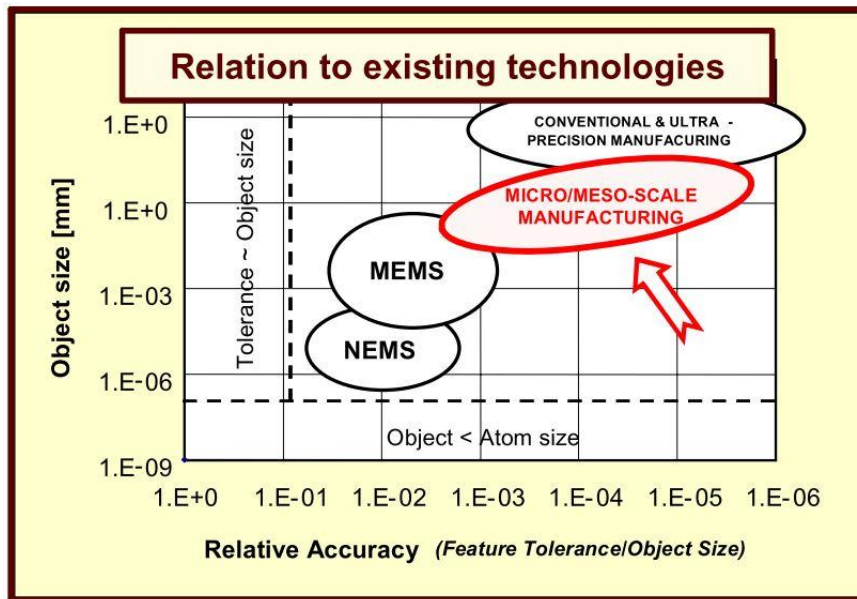
Figure 1-1 Micro-manufacturing size/precision domain [2]
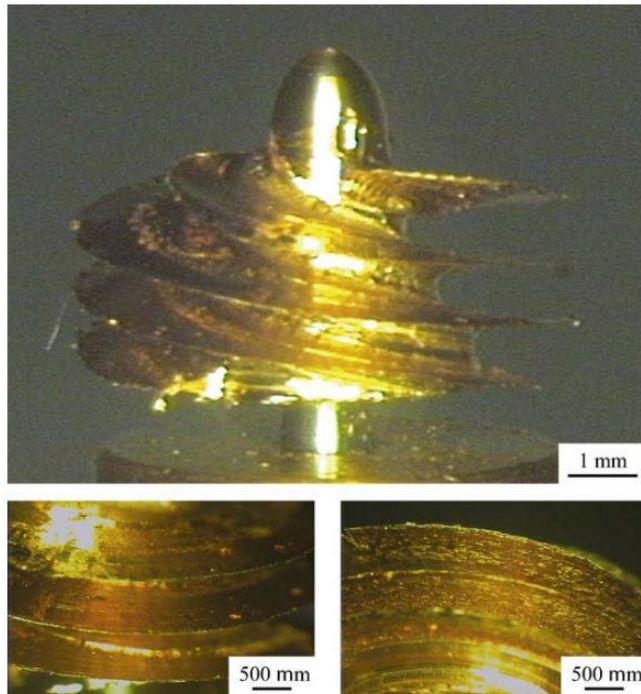
Figure 1-2 Machined result of a micro-inducer [4]

Figure 1-2 shows a machined micro-inducer used in the blood pump system [4]. The micro-inducer possesses complex freeform surfaces and requires good surface finish. It was machined by conventional micro-machining method, and took 42 hours, which definitely can be improved. In this regard, it is of great importance to carry out research to improve micro-manufacturing processes for higher productivity and accuracy. It is worth noting that micro-milling is the most flexible and versatile process among current micro-manufacturing processes when manufacturing very complex 3D micro-products [5], while achieving superior surface finish. In recent years, hybrid micro-machining technology has been developed to integrate several micro-manufacturing processes on one platform to utilize the so-called "1+1=3" effect, which means that the advantages of the hybrid process is more than double of the advantages of the single processes [6]. The benefits of the hybrid machining process include [7]: (1) It can improve the machinability of the difficult-to-machine materials, such as ceramics, hardened steel, and super alloys, etc.; (2) It eliminates the re-alignment errors and the set-up time if the workpiece should go through sequential processes on different machines. Therefore, it provides new possibilities for high-efficiency and high-accuracy machining of the aforementioned difficult-to-machine materials. Chavoshi and Luo [8] have provided a good review of current hybrid micro-processes, and classified those processes into assisted and combined hybrid micro-machining processes, as show in Figure 1-3.
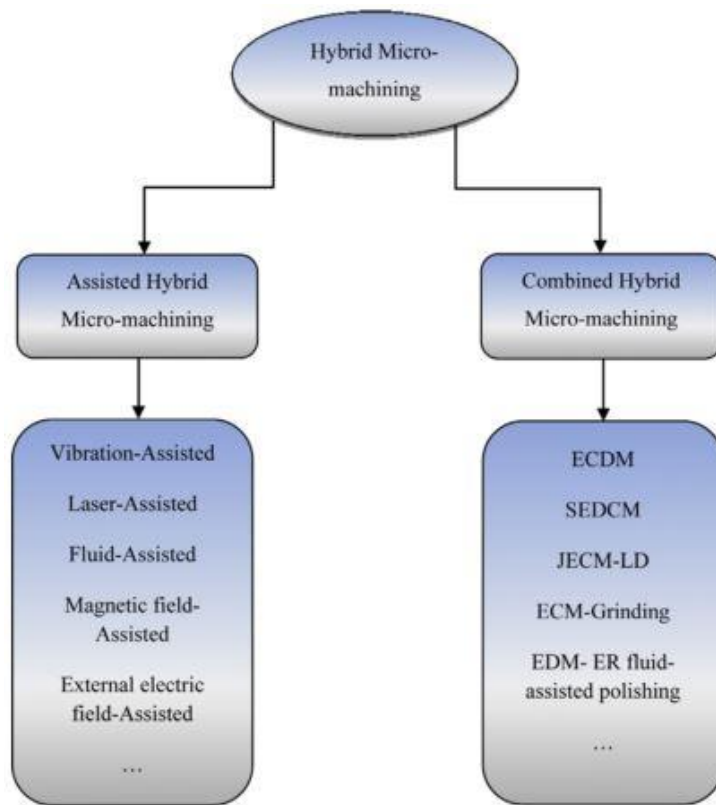
Figure 1-3 Classification of hybrid micro-machining processes [8]

Hybrid micro-machining raises a number of issues when scaling down those processes from macro level to micro level, such as process dynamics, tooling, material handling, assembly, metrology and control etc. Some effects considered to have little or no influence at macro level will become dominant factors that influence the resulting machining accuracy and surface quality in micro level [9], [10]. This thesis will only focus on some issues within the control system for hybrid micro-machining.

There is a growing trend for the hybrid micro-machines to integrate more functional modules, in addition to the modules for the add-on processes, for even higher efficiency and accuracy, such as in-line metrology system for in-process surface measurement, material handling system for automatic workpiece loading and unloading. Machine developers tend to choose those modules from different vendors to satisfy the performance and cost requirements. For example, vendor A provides the most cost-effective laser solutions, while vendor B supplies motion control

module with satisfied specifications. However, those modules often possess proprietary hardware and software interfaces and the lack of plug-and-play solutions lead to tremendous difficulty in system integration, which will result in complex and inflexible CNC system, as well as high developing cost and long lead time. For example, the laser module uses RS232 communication bus, while the motion control module adopts the FireWire communication bus. Both of them have different data protocols. A lot of programming work will be required to coordinate the two functional modules.

Moreover, the conventional approach of machining 3D micro-products with freeform surfaces is to generate the toolpath using the computer-aided manufacturing (CAM) software. The toolpath is generally composed of a large number of short linear segments. This approach results in the following undesirable problems:

(1) To achieve higher contour accuracy, more segments are needed to approximate the original surface, which pose huge burden for data transfer and memory of the CNC system;

(2) The discontinuity in the first derivatives along the toolpath leads to high frequency fluctuation of feedrate and acceleration, which will decrease machining efficiency and surface finish.

Therefore, the next generation CNC system for hybrid micro-machines will need to address the aforementioned challenges to realise lower development cost, higher productivity and machining quality.

1.2 Aim and objectives

As discussed in section 1.1, this thesis aims to provide novel control approaches to overcome the major challenges within the CNC system for hybrid micro-machines. These new control approaches will provide solid foundation for the development of

next generation CNC system for hybrid micro-machines. In order to achieve this aim, the following objectives are set:

- To review current state-of-the-art commercial hybrid machines and their CNC systems as well as relevant literature to identify the challenges of current control approaches.
- To propose a novel control architecture for CNC system of hybrid micro-machines to address the system integration challenge, and demonstrate its effectiveness through the integration of a complex hybrid micro-machine.
- To develop a real-time interpolator for parametric curves to tackle the interpolation challenge, and perform machining trails to validate the approach.
- To develop a real-time global toolpath smoothing algorithm to bridge the gap in toolpath representation, and validate it through machining trials.

1.3   Research methodology

The aim and objectives of this thesis have been clearly defined in the previous section. This section will describe how the research will be carried out to achieve these objectives.

First of all, extensive review will be conducted in both industry and academia to identify the challenges for the novel control approaches. Then a novel control architecture will be developed to address these challenges. The proposed parametric interpolation algorithm and toolpath smoothing algorithm will be also incorporated in the control architecture, which makes it a ready solution for hybrid micro-machine developers. The effectiveness of the control architecture will be demonstrated through the integration of a six-axis hybrid micro-machine.

The parametric interpolation algorithm and the toolpath smoothing algorithm should be executed in the real-time kernel of the control architecture. However, the selected real-time motion control module is not open enough for user specific algorithms. As a result, an experimental test-bed should be developed for the implementation and

verification of these algorithms. The verification of these algorithms is performed by numerical experiments and freeform machining experiments. The industry standard and state-of-the-art algorithms will be used as benchmarks in the machining experiments. The overview of this research is shown in Figure 1-4.
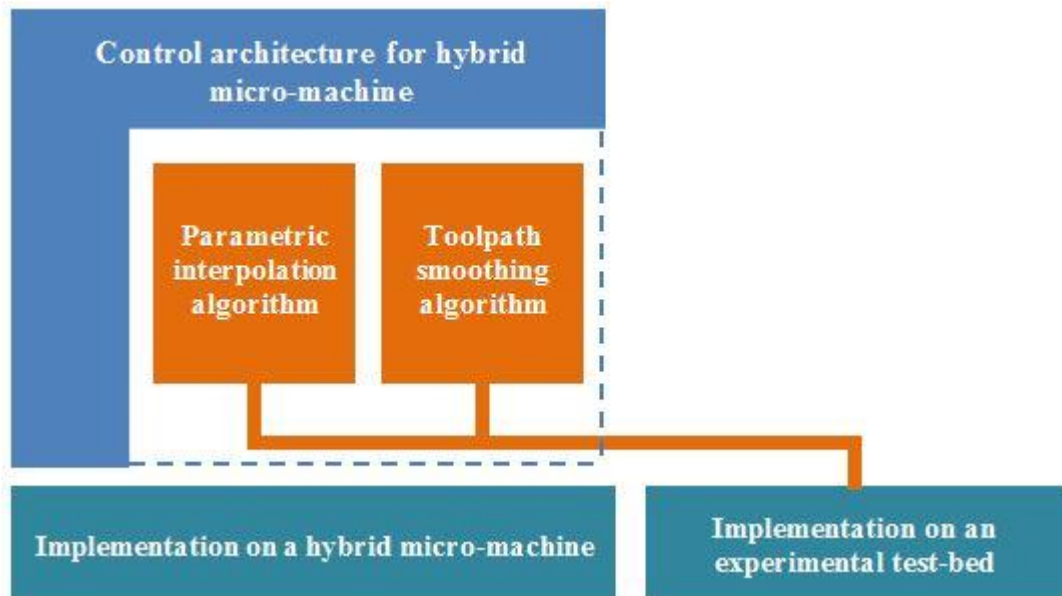
Figure 1-4 The overview of the research

1.4 Structure of the thesis

This thesis consists of 7 chapters. The main contents of each chapter are listed below.

Chapter 1 introduces the background and significance of hybrid micro-machining, and defines the scope and objectives of the research work.

Chapter 2 reviews the current state-of-the-art commercial hybrid machines and their CNC systems as well as the relevant literature. The system integration, the parametric interpolator and the toolpath smoothing are identified as the three major challenges.

Chapter 3 proposes a novel CNC system control architecture taking into consideration of the identified challenges. The effectiveness of the control

architecture is demonstrated through the integration of a six-axis hybrid micro-machine.

Chapter 4 develops a test-bed for the implementation and verification of the proposed parametric interpolator and the toolpath smoothing algorithm.

Chapter 5 develops the proposed real-time interpolator for parametric curves (RTIPC). The validation of the RTIPC is carried out with benchmarks of the industry standard linear interpolator and the state-of-the-art PVT interpolator.

Chapter 6 develops the proposed global toolpath smoothing algorithm. The superiority of this approach is demonstrated by freeform surface machining experiments in comparison with the standard toolpath traversing algorithm and the state-of-the-art corner blending algorithm.

Chapter 7 summarises the major contributions and conclusions of this thesis. In addition, further improvements of the CNC system are discussed.

Chapter 2　　Literature review

2.1　Introduction

High value-added 3D micro-products, such as optics, moulds/dies and biomedical implants etc. are increasingly in demand. These products are usually made of a wide range of engineering materials and possess complex freeform surfaces with tight tolerance on form accuracy and surface finish. The tolerance is usually in sub-micron level. Hybrid micro-machining, such as micro-milling with laser deburring, micro-grinding with laser pre-heating, has emerged as a solution to tackle the manufacturing challenges in machinability and productivity for these products, especially when they are made of hard-to-machine materials, such as ceramics, harden steel, super alloys, etc. Hybrid micro-machines are the platforms to realize the advantage of hybrid process, i.e. the so-called "1+1=3" effect, as discussed in section 1.1. This chapter firstly reviews the state-of-the-art hybrid micro-machines, and then identifies the CNC system requirements for hybrid micro-machines considering the characteristics of the machine and the 3D micro-product. The current commercial CNC systems are surveyed to highlight the gaps to the identified requirements, and existing efforts on new control approaches in the literature are also reviewed.

2.2　State-of-the-art commercial hybrid micro-machines

Hybrid micro-machines are distinct from conventional machines, as they accommodate more than one process on the machine, and the combination of processes varies significantly with the requirement of the application, such as ultrasonic assisted diamond turning process was developed to reduce the severe tool wear when machining steel parts [11], laser-assisted micro-milling was developed to produce freeform surfaces on hard-brittle materials [12], etc. This section surveys the state-of-the-art commercial sequential and assisted hybrid machines in order to highlight the characteristics of these machines and their CNC systems.

2.2.1 Sequential hybrid machines

Sequential hybrid machines perform the machining processes sequentially to make use of the advantages of each process for the best machining results. For example, micro-milling process can be used to remove bulk materials rapidly, and then micro-EDM is used for finishing operation. Another popular configuration is to conduct the additive manufacturing (AM) and conventional subtractive manufacturing sequentially. AM has the unique advantage in building complex inner structures, while milling process can be performed afterward to obtain high dimensional accuracy and good surface finish. Currently, most of the commercial hybrid machines belong to this category.

2.2.1.1 Hybrid machine for EDM + mechanical machining

The DT-110 Hybrid μEDM machine [13], developed by Mikrotools in Singapore, is a three-axis hybrid machining centre, which combines micro-milling, micro-turning and EDM processes on the single machine bed. The strokes of the X, Y and Z axes are 200 mm, 100 mm and 100 mm, respectively. The motion resolution and repeatability are 0.1 μm and 1 μm respectively for each axis. The machine adopts an air bearing milling spindle with a maximum rotational speed of 200,000 rpm. A charge-coupled device (CCD) is also integrated into this machine for on-machine inspection. The hybrid machine can adopt turning operation to fabricate a shaft and then machine it to a micro pin using wire EDM. These micro pins can be used as electrodes to machine micro holes on any conductive materials in the following EDM process. Figure 2-1 shows the images of the machine and its demonstation part.

This machine adopts a PC-based CNC system using Delta Tau's Power PMAC card, which features 800 MHz or 1.0 GHz CPU, and 1 GB or 2 GB memory. Because the EDM process is required to take place in a tank with non-conductive liquid inside, the machined parts have to be uploaded from the outside into the tank. Therefore, the machine still requires another set-up for the second process, which decreses the efficiency.

(a) The DT-110 Hybrid µEDM machine   (b) 70 µm thick micro fins

Figure 2-1 The DT-110 Hybrid µEDM machine and its demonstration part [13]

2.2.1.2 Hybrid machine for additive manufacturing + milling

The LUMEX Avance-25 machine [14], developed by Matsuura Machinery Corporation, combines laser sintering additive manufacturing with high-speed milling, as shown in Figure 2-2. The hybrid AM process includes three steps:

- Powder distribution: The metal powder is distributed spread out on the base plate. The powder thickness is 0.05 mm for the 500 W laser.

- Laser processing: The metal powders are melted and sintered by the laser. When the processing is finished, the next layer of powder will be distributed.

- Milling: The outer surface of the part is precisely milled with a ball end mill. The milling process takes place after each pre-set number of layers.

The hybrid AM process enables manufacturing of parts with complicated internal structures. The travel ranges for the X/Y/Z axes are 260/260/100 mm, the maximum feedrate for the three axes are 60/60/30 m/min. The machine can accommodate a workpiece as large as W256 x D256 x H185 mm. The supported materials include

maraging steel, Ti-6Al-4V titanium alloy, stainless steel 630/316L, cobalt chrome super alloy, nickel alloy 718, and AlSi10Mg.

This hybrid machine is equipped with Matsuura's I-Tech Avance control system, which is specially designed for the hybrid process. However, for most hybrid machine vendors, designing a CNC system for a new machine from scratch will be a huge challenge and not economical.

(a) The LUMEX Avance-25 machine   (b) Artificial tooth made of cobalt chrome

Figure 2-2 The LUMEX Avance-25 machine and its demonstration part [14]

Similarly, the DMG MORI Ltd developed the LASERTEC 65 3D hybrid machine [15] by adding the AM process onto a 5-axis milling machine bed, as shown in Figure 2-3. The travelling distances of the X, Y and Z axes on the gantry are 735 mm, 650 mm and 560 mm, respectively. The rotating angles of the B and C axes (on the base) are 120° and 360°, respectively. Fibre coupled diode laser of 2000W is equipped on the machine and its wavelength is 1030 nm. The laser spot size can be set as 3 mm or 1.6 mm. The metal deposition is carried out through a powder nozzle which is up to 10 times faster than using powder bed. The maximum standard spindle speed is 10,000 rpm.

This machine chooses SIEMENS SINUMERIK 840D sl as its CNC system, which offers the maximum performance thanks to its drive-based numerical control unit with multicore processor. The controller can be perfectly embedded in the Siemens ecosystem using PROFINET. However, the integration of the broad range of third-party functional modules is not convenient. For example, if the laser module uses RS232 interface instead of PROFINET, a lot of work will be involved to adapt the hardware and software interfaces of the laser module for the control system.

(a) The LASERTEC 65 3D hybrid machine   (b) Cooled injection mould

Figure 2-3 The LASERTEC 65 3D hybrid machine and its domonstation part [15]

2.2.1.3 Hybrid machine for laser machining + milling

The Posalux COMBI hybrid machine [16] integrates a FEMTO-laser on milling machine, as shown in Figure 2-4. The ultrashort laser pulse, which is down to 200 fs, can avoid material deposition and recast. It also enables to machine a wide range of materials, such as steel, brass, ruby, and ceramic, etc. The laser heat affected zone is avoided due to cold ablation. The milling process is carried out to make large structures on the workpiece, while the laser is then used for high-precision micro-hole drilling on the workpiece. The hole diameter can be down to 30 μm, while the hole depth diameter ratio can reach up to 10. The machine also integrates a camera for positioning, a focal length measurement device, and the dust extraction function.

The machine is also equipped with a SIEMENS SINUMERIK 840D sl CNC system. The milling process and laser drilling process are carried out independently, which should be coordinated simultaneously for higher productivity.

(a) The Posalux COMBI hybrid machine   (b) Watch plate

Figure 2-4 The Posalux COMBI hybrid machine and its demonstration part [16]

2.2.2 Assisted hybrid machines

Unlike sequential hybrid machines, assisted hybrid machines only contain one main process for machining, and the second process is used to improve the machining conditions of the main process. For example, the laser assisted micro-grinding is superior to conventional micro-grinding when grinding hard-brittle materials, which is because the laser can pre-heat the workpiece and soften the material.

2.2.2.1 Hybrid machine for ultrasonic + mechanical machining

Ultrasonic hybrid machining process is one of the most popular and successfully commercialised assisted hybrid processes. It allows economical machining of 3D micro-products with complex geometries, and hard-to-machine materials, such as ceramics, glass, corundum, tungsten carbide and even composites. A reduction of the process force by up to 40% can be achieved by the ultrasonic hybrid process compared with conventional machining process. Therefore, it allows higher feedrate, longer tool life, and significantly better surface finish of up to Ra < 0.1 µm. The

number and depth of micro cracks in hard-brittle materials is reduced to a minimum [17].

A 5-axis ultrasonic hybrid machine, ULTRASONIC 20 linear [17], has been developed by DMG MORI Ltd, as shown in Figure 2-5. It is capable of ultrasonic-assisted milling, grinding and drilling. It is equipped with a high speed spindle with a maximum rotational speed of 60,000 rpm. The piezoelectric effect ultrasonic actuator is integrated with the tool holder. It will result in the axial oscillation of the tool with a frequency range of 15-55 kHz and a maximum amplitude of 10 µm. The maximum travel distances for X/Y/Z axes are 200/220/280 mm.

The machine is also equipped with the SIEMENS SINUMERIK 840D sl CNC system. The integration of the ultrasonic actuator on the machine is relatively easy, as it is not tightly coupled with the mechanical machining process. As a result, this machine adopts the control approaches that are the same as conventional machines, which is not optimised for 3D micro-products. For example, the surfaces of 3D micro-products are approximated by a large amount of small segments.

(a) The ULTRASONIC 20 linear machine   (b) Structure part mould

Figure 2-5 The ULTRASONIC 20 linear machine and its demonstration part [17]

2.2.3 Summary of the review of hybrid machines

The above review shows that various hybrid processes have been established to solve the manufacturing challenges for specific 3D micro-products. The combination of micro-manufacturing technologies is largely determined by the characteristics of the application, such as material and geometry requirements. More hybrid processes will be developed to achieve high-efficiency high-accuracy machining of future 3D micro-products. To achieve the desired hybrid process, a wide range of functional modules should be integrated, such as EDM, laser, and ultrasonic actuator etc. However, the CNC systems used on the current hybrid machines are still designed for conventional machines. They are not flexible enough for the "real" hybrid machining, i.e. all the functional modules collaborate seamlessly rather than working independently. Moreover, the control approaches are not optimised for 3D micro-products in toolpath representation and interpolation, as these novel control approaches is still excluded from the outdated standard.

2.3 Requirements of CNC system for hybrid micro-machines

2.3.1 Flexibility of system integration

In addition to the add-on process modules, there is a growing trend to integrate more functional modules on the hybrid micro-machine, such as in-line metrology system to measure and evaluate the freeform surfaces, material handling system to efficiently handle the miniature 3D micro-products, etc. Machine developers tend to choose those modules from different vendors to satisfy the performance and cost requirements. Therefore, those selected modules often possess proprietary hardware and software interfaces and the lack of plug-and-play solutions lead to tremendous difficulty in system integration, which will result in complex and inflexible CNC system, as well as high developing cost and long lead time.

Successful development of a hybrid micro-machine requires a systematic design approach. From the control aspect, the flexibility of CNC system that allows easy integration of multiple modules is a critical requirement. The integration includes not only the hardware connection but also the intelligent coordination of different modules. The Open Architecture Control (OAC) concept was created as a potential solution to the demand of control flexibility back to 1990s, and has been promoted by many global consortiums, such as the OSE (Open System Environment for Manufacturing) in Japan [18], the OMAC (Open Modular Architecture Controllers) in the U.S. [19], the OSACA (Open System Architecture for Controls within Automation Systems) in Europe [20]. Pritschow et al. [21] summarised the criteria to assess the openness of a CNC system:

- Portability: Modules can be integrated to a new platform without any changes, while maintaining their capabilities.
- Extendibility: New modules can be added without any conflicts.
- Interoperability: Modules can exchange data between each other in a defined way.
- Scalability: The functionality and performance can adapt to the requirements of user.

However, the openness of CNC has not been standardised, and the intellectual property problem has hindered the development of open CNC. As an alternative solution, the PC-based solutions with a homogenous and standardized environment were favoured, as shown in Figure 2-6. Despite the significant amount of research had been conducted, the OAC remained in the laboratory level, and had little impact in industry, the interest in further development of the OAC had declined. However, the concept of OAC can help sharpen the development of the proposed control approaches, and also provides criteria to assess current CNC systems for hybrid micro-machines.
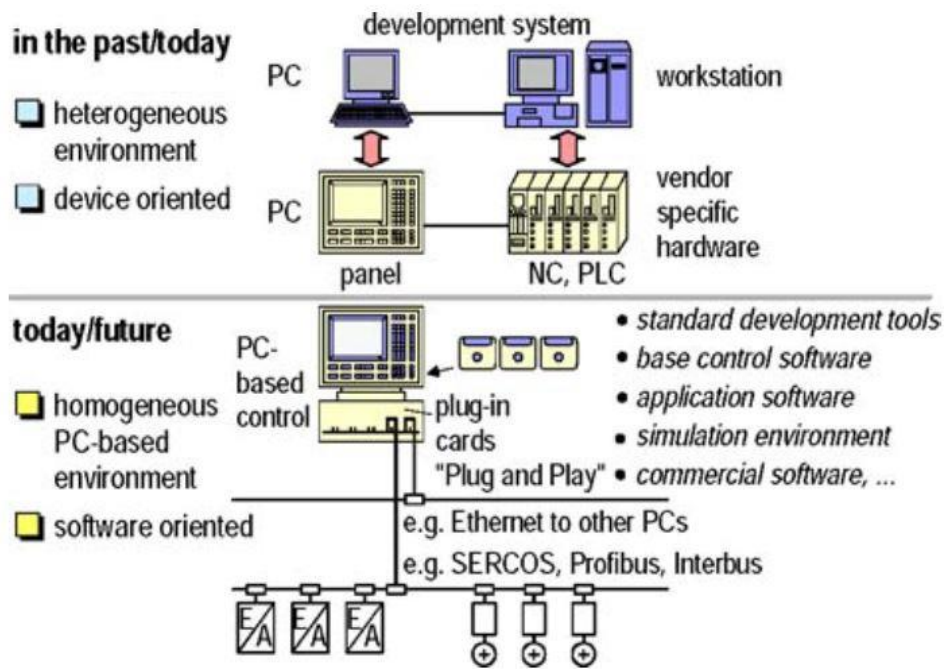
Figure 2-6 PC-based software-oriented control systems [21]

2.3.2 Parametric toolpath interpolation

Figure 2-7 shows how the geometric data of 3D micro-products is converted to manufacturing code in current practice. Firstly, the freeform surfaces are designed in computer-aided design (CAD) software. Some engineering analyses will be carried out at this stage as well, such as finite element analysis (FEA) to predict the behaviour of the product in real-world. When the geometric modelling is finished, computer-aided process planning (CAPP) is carried out to decide the processes and processes' parameters to manufacture the specific product. However, the CAPP is immature [22], process planning generally depends on the experience of the process planner. CAM is then executed to generate the toolpath for the CNC system with the given process parameters. At this stage, the geometric data of the product is represented by a large number of short linear or circular segments. This is due to that the linear interpolator (G01) and the circular interpolator (G02, G03) are the only interpolators defined in the RS274 standard [23].
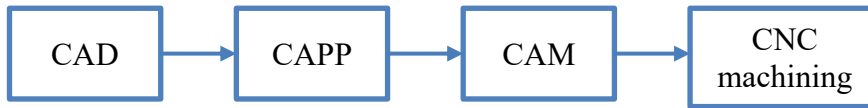
Figure 2-7 3D micro-product data: from design to manufacturing

However, this approach results in the following undesirable problems when machining the 3D micro-products:

(1) Micro-products possess smaller features with higher curvatures compared with macro-products. They require shorter segments to approximate the original surface, which decreases the toolpath continuity further.

(2) The geometric data loss is inevitable, which is due to the approximation of original freeform surfaces with discontinuous segments. To achieve higher approximation accuracy, more segments are needed, which poses a huge burden for the data transfer and memory of CNC systems.

(3) The segments are not continuous in the first derivatives at the join points. The abrupt change in velocity direction will result in infinite acceleration which will saturate the drives. The current interpolators solve the problem by decelerating the velocity to zero at the end of each segment and then start accelerating again at the beginning of the next segment. The high frequency fluctuation of feedrate and acceleration will reduce the average feedrate and causes vibration. As a result, it will lead to a low productivity and poor machined surface finish.

Actually, parametric curves are the *de facto* standard in representing the freeform surfaces of 3D micro-products in CAD. The ISO 10303 standard [24], which is informally known as STEP (Standard for the Exchange of Product Model Data), chose the NURBS (Non-Uniform Rational B-Splines) for the geometric data exchange. Similarly, the IGES (Initial Graphics Exchange Specification) [25] developed by the American National Standard supports various entities represented by parametric curves. In mathematics, parametric curves are represented in parametric form, each coordinate of the curve is given by an explicit function of an

19

independent parameter, in a form of $\boldsymbol{C}(u) = \big(x(u), y(u)\big)\ u \in [a, b]$, where $\boldsymbol{C}(u)$ represents a curve defined in the XY plane with the independent parameter u at the interval $[a, b]$. Parametric representation has a number of advantages, as summarized by Piegl and Tiller [26], most importantly including easy to extend to higher dimensions, intuitive for geometric design, etc.

Parametric curves have been proven as the optimal toolpath representation method for CNC systems when machining those 3D micro-products [27], [28]. They can preserve the features of the freeform surfaces without the enormous amount of segments. More importantly, they have huge advantage in continuity over the linear or circular toolpath. There are two kinds of continuity associated with curves, i.e. geometric continuity and parametric continuity [29]. If the nth derivatives of both curves at the join point have the same direction, then G^n geometric continuity is achieved at the join point. If the derivatives have the same magnitude as well, then C^n parametric continuity is achieved. For hybrid micro-machining applications, at least C^2 continuity is required to guarantee continuous velocity and acceleration along the toolpath. It is easy for parametric curves to achieve the C^2 continuity, while the linear or circular segmented toolpath can only achieve G^0 or C^0 continuity.

As a result, the capability of parametric toolpath interpolation is of great importance for CNC systems of hybrid micro-machines.

2.3.3 Toolpath smoothing

Despite the huge advantages of the parametric toolpath mentioned in the previous section, it is still excluded from the RS274 standard. Most of the CAM software does not export parametric toolpath [30]. The linear segmented toolpath is still dominantly used on the factory floor due to its straightforward coding and excellent compatibility with various CNC systems. To bridge the gap in toolpath representation as well as to fulfil the potential of the parametric interpolator, CNC systems for hybrid micro-machines should have built-in toolpath smoothing approaches.

2.3.4 Summary of requirements of CNC system for hybrid micro-machines

The flexibility of CNC system that allows easy integration of multiple modules is a critical requirement. PC-based CNC systems are preferable to hybrid micro-machines, as PC has unprecedented I/O capabilities to accommodate various hardware and software interfaces used by different vendors. A parametric interpolator is of great importance for high-speed high-accuracy machining of 3D micro-products with complex freeform surfaces. A built-in toolpath smoothing approach is essential to bridge the gap in the toolpath representation and fulfil the potential of the parametric interpolator. C^2 continuity is required for the toolpath in order to achieve the smooth feedrate and acceleration profiles.

2.4   Commercial CNC systems

This section surveys the state-of-the-art commercial CNC systems against the challenges identified in section 2.3. Table 2-1 summarises the features of five CNC systems, which have been applied in hybrid machines or ultra-precision machines.

PC-based CNC systems tend to have a higher degree of openness, but the openness is restricted to the non-kernel part of the CNC system. The flexibility is limited to human-machine interface (HMI) customisation with the given CNC application programming interfaces (APIs). PC-based solutions will be the future of CNC systems for hybrid micro-machines, as PC has unprecedented I/O capabilities to exchange data with various communication interfaces used by different module vendors, such as RS232, Ethernet, FireWire, etc. This allows easy incorporation of new hardware, as well as adaption of software for different data protocols. However, due to the countless possibilities of configurations for hybrid micro-machines, a one-size-fits-all solution for the coordination of those modules to achieve the desired hybrid process is impossible. High standard expertise and large amount of time are necessary for the seamless integration. Therefore, a generic control architecture for hybrid micro-machines is invaluable to accelerate to the integration.

All the listed CNC systems support one or more advanced interpolation methods for specific parametric curves, in addition to the standard linear and circular interpolator. However, those methods are patented and use different kind of syntaxes. It requires good expertise to use them for various freeform surfaces of the 3D micro-products. A general parametric interpolator that can unify the machining of freeform surfaces is highly desirable. Particularly, the PVT interpolator has been promoted by Delta Tau and Aerotech, the advantages of disadvantages about this interpolator will be reviewed in the next section.

The toolpath smoothing approaches used in the five CNC systems can be categorised into the following types:

- Corner rounding: a small curve is inserted to connect two linear segments at the corner, which is a local smoothing approach.
- NURBS smoothing: a NURBS curve is used to approximate a sequence of linear segments, which is a global smoothing approach.
- Corner blending: the velocities of involved axes are scheduled directly at the corner to create a smooth transition, no curve planning is needed. It is a local smoothing approach.

The advantages and disadvantages of those approaches compared with existing literature will be reviewed in section 2.6.

Table 2-1 Features of commerical CNC systems

Features	Heidenhain iTNC 530 [31]	FANUC Series 30i [32]	SIEMENS SINUMERIK 840D [33]	Delta Tau Power PMAC [34]	Aerotech A3200 [35]
PC-based	No	No	Depends on configuration	Yes	Yes
Open architecture	No	No	Partially open	Partially open	Partially open
Interpolation	Line, circle, helical, spline	Line, circle, exponential, helix, involute, cylindrical, NURBS	Line, circle, helix, spline, polynomial, involute	Line, circle, PVT, spline	Line, circle, PVT, Bézier
Toolpath smoothing	Corner rounding	NURBS smoothing	Corner rounding NURBS smoothing	Corner blending	Corner rounding
Application machine tools	KERN Pyramid Nano [36]	FANUC ROBONANO [37]	DMG MORI LASERTEC 65 3D hybrid [15]	Mikrotools Hybrid μEDM [13]	Strathclyde Micro-3D Hybrid Micro-machine [38]

In summary, the current CNC systems are not open enough for the integration of a broad range of functional modules, and there is a lack of generic control architecture for hybrid micro-machines. Moreover, there is no parametric interpolation approach for general parametric curves, and the toolpath smoothing methods vary significantly.

2.5　Review of parametric interpolation

2.5.1　Mathematical challenges

The problem of parametric interpolation can be described as:

Given the curve $C(u)$, find the reference position, which is corresponding to parameter u_k, that the tool should travel to at the kth interpolation period.

Generally, the re-parametrization of u with time t is required to determine each reference position at each interpolation period, i.e. solve the function $u = u(t)$. However, the re-parametrization should be subject to the machine dynamics constraints and contour error tolerance:

(1) Axial velocities and accelerations should be constrained to avoid saturating axes. They are the first and second derivatives of the corresponding parametric function over time, respectively. As shown in Eq. 2-1 and 2-2, respectively.

$$\begin{cases} \|\dot{x}(t)\| = \left\|\dfrac{dx}{du}\dfrac{du}{dt}\right\| \le V_x \\ \|\dot{y}(t)\| = \left\|\dfrac{dy}{du}\dfrac{du}{dt}\right\| \le V_y \end{cases} \tag{2-1}$$

where V_i denotes the maximum velocity of axis i.

$$\begin{cases} \|\ddot{x}(t)\| = \left\|\dfrac{d^2x}{du^2}\left(\dfrac{du}{dt}\right)^2 + \dfrac{dx}{du}\dfrac{d^2u}{dt^2}\right\| \le A_x \\ \|\ddot{y}(t)\| = \left\|\dfrac{d^2y}{du^2}\left(\dfrac{du}{dt}\right)^2 + \dfrac{dy}{du}\dfrac{d^2u}{dt^2}\right\| \le A_y \end{cases} \tag{2-2}$$

where A_i denotes the maximum acceleration of axis i.

 (2) Feedrate is the resultant value of axial velocities, as expressed in Eq. 2-3. The jerk, which is the second derivative of the feedrate over time, should be confined to guarantee smooth motion profiles, as shown in Eq. 2-4

$$F(t) = \sqrt{\dot{x}(t)^2 + \dot{y}(t)^2} \qquad\qquad 2\text{-}3$$

$$\left\| \ddot{F}(t) \right\| \leq J \qquad\qquad 2\text{-}4$$

where $F(t)$ denotes the actual feedrate as a function of time. J denotes the maximum jerk, which controls the characteristics of the "S-curve" profile of the feedrate.

(3) The contour error ε increases with increasing feedrate, as shown in Figure 2-8, the feedrate should be limited to achieve high contour accuracy.
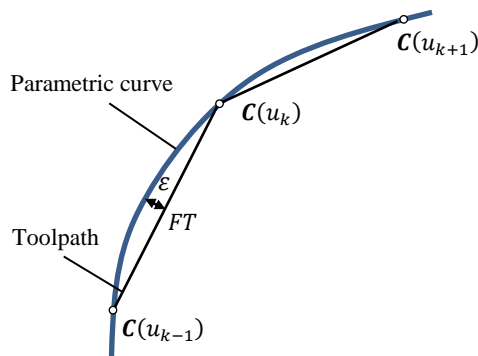
Figure 2-8 Contour error estimation

Therefore, the interpolation of parametric curves becomes an optimization problem, the time-optimal solution is highly desirable, in which case the tool traverses the curve in minimum time while satisfying above constraints. Timar and Farouki [39] worked out the time-optimal solution for polynomial curves subject to only axial acceleration bound. It is generally impractical to find the time-optimal solutions subject to all the prescribed bounds for general parametric curves, because it involves solving many non-linear differential equations. Currently, two technical routes have been developed for the interpolation of parametric curves, i.e. arc length parametrization and recursive Taylor's expansion.

2.5.2 Arc-length parametrization

The feedrate is the differential of arc length S over time, which makes the interpolation straightforward, i.e. discrete point for each interpolation period can be

calculated by incrementing the arc length. However, the arc length parametrization is extremely difficult, as it requires solving the inverse function of the non-linear integral function for arc length evaluation, as shown in Eq. 2-5. In general, this problem has no analytic solution, some numerical techniques may help achieve the approximated arc length parametrization [40].

$$S(u) = \int_{u_1}^{u_2} \left\| \frac{d\mathbf{C}(u)}{du} \right\| du \qquad \qquad 2\text{-}5$$

where

$$\frac{d\mathbf{C}(u)}{du} = \left(\frac{dx(u)}{du} \quad \frac{dy(u)}{du} \right) \qquad \qquad 2\text{-}6$$

and

$$\left\| \frac{d\mathbf{C}(u)}{du} \right\| = \sqrt{\left(\frac{dx(u)}{du} \right)^2 + \left(\frac{dy(u)}{du} \right)^2} \qquad \qquad 2\text{-}7$$

Erkorkmaz et al. [41]–[44] proposed an interpolator for NURBS, it used a 7th order polynomial to approximate the arc length parametrization. Similarly, Liu et al. [45] adopted a cubic polynomial to generate piecewise approximation of arc length parametrization for NURBS. Although near arc length parametrization is possible with some numerical methods, the approximation error will accumulate along the curve, especially for the curve with large curvature variation or uneven parametrization [46]. Furthermore, the numerical method is not applicable for general parametric curves, and the process is computationally intensive.

2.5.3 Recursive Taylor's expansion

Alternatively, Shpitalni, Koren and Lo [47] developed the recursive Taylor's expansion method. Given the feedrate F and current interpolation point u_k, the next interpolation point can be calculated by

$$u_{k+1} = u_k + \frac{FT}{\left\|\dfrac{d\boldsymbol{C}(u)}{du}\right\|} \qquad\qquad 2\text{-}8$$

where T is the interpolation period. Fanuc has applied this work to its NURBS interpolator [48]. Eq. 2-8 was deduced with the first-order approximation of the Taylor's expansion, Cheng, Tsai and Kuo [49] worked out the second-order approximation. Zhao, Zhu and Ding [50] made a step further by proposing a compensation scheme to reduce the truncation error. However, because the Taylor's expansion is performed recursively, the error will not accumulate. If T is very small and the curve does not have extremely large curvature, the second-order approximation is adequate. As a result, this thesis will use the second-order approximation of the recursive Taylor's expansion to develop the general parametric interpolator for its efficiency and high accuracy. The problem now is how to schedule the feedrate within the Taylor's expansion while satisfying the constraints.

Yeh and Hsu [51] provided the idea on how to confine the contour error based on the curvature. Yong and Narayanaswami [52] improved the idea by detecting feedrate sensitive corners offline. Nam and Yang [53] proposed a recursive trajectory generation method to limit the jerk, while Liu et al. [54] developed the time interval modulation method to achieve the same goal. However, none of them have dealt with all the important constraints. To meet as many constraints as possible, many researchers have developed various complicated algorithms. Sencer et al. [55] aimed to obtain the analytic solution to the feedrate which was expressed in cubic B-Spline form, but the process was computationally inefficient, the algorithm was run on the Matlab with long processing time. Sun et al. [56] proposed the curve evolution based feedrate scheduling method, it was an off-line process as well. Xavier et al. [57] developed the velocity profile optimization (VPOp) method, which is an iterative algorithm that computes the intersection of the given constraints. However, the contour accuracy was not considered and the efficiency of this method was not reported.

The lookahead technique is commonly used to alleviate the computation load while satisfying the constraints. Lin et al. [58] proposed a real-time lookahead technique

for their NURBS interpolator, the curve was split into sub-curves according to the curvature. Annoni et al. [59] used similar lookahead technique to acquire segmented small curves and then chose different feedrate for each sub-curve. However, the curvature is usually changing continuously along the curve, the changing rate within each sub-curve is not uniform. So the above methods did not make the most of the continuity of the curve. Jin et al. [60] realized their lookahead method by calculating the length of deceleration repeatedly at each interpolation period. This kind of lookahead technique can determine deceleration position rapidly and tend to achieve near time-optimal feedrate profile. However, they did not consider the lookahead length and the numerical integration issues.

2.5.4 The PVT interpolation

The PVT interpolation applied on some industrial CNC systems is actually a special case of cubic polynomial curve interpolation. Users should specify the exact position and velocity at the boundaries of each segment, as well as the total travel time for the segment. Suppose that the time is normalized to $[0, 1]$, a PVT move is given by

$$C(t) = \begin{bmatrix} 1 & t & t^2 & t^3 \end{bmatrix} \begin{bmatrix} 1 & 0 & 0 & 0 \\ 0 & 1 & 0 & 0 \\ -3 & -2 & -1 & 3 \\ 2 & 1 & 1 & -2 \end{bmatrix} \begin{bmatrix} P(0) \\ \dot{P}(0) \\ \dot{P}(1) \\ P(1) \end{bmatrix} = \sum_{i=0}^{3} a_i t^i \qquad 2\text{-}9$$

where $P(0)$ and $P(1)$ are the start and end points of the segment, $\dot{P}(0)$ and $\dot{P}(1)$ are the corresponding velocities, $\{a_i\}$ are the coefficients determined by the given positions, velocities and the time interval. The PVT interpolator uses cubic polynomial curves to approximate the freeform surface, the velocities at the join points are continuous, which is a huge improvement to the linear interpolator. However, the acceleration is not continuous at the join points. The PVT interpolator can be used as a benchmark for the proposed general parametric interpolator.

2.5.5 Summary of the review of parametric interpolation

The interpolation of parametric curves is an optimization problem, for which it is extremely difficult to get the time-optimal solution. The arc length parametrization approach has the disadvantage in computational efficiency. The recursive Taylor's expansion approach is capable of interpolating the general parametric curve efficiently without accumulating error. However, the feedrate scheduling is problematic. The lookahead technique is the promising approach to get the near time-optimal solution for the parametric interpolation problem. The PVT interpolation is a special case of cubic polynomial curve interpolation. It uses cubic polynomial curves to approximate the freeform surface, and avoids the velocity discontinuity problem encountered in the linear interpolation.

In summary, the challenges of existing parametric interpolation approaches lie in:

(1) There is no parametric interpolator for general parametric curves. The current approaches were designed for a single type of curve, while the 3D micro-products can be designed with various curves, such as polynomial, NURBS, and trigonometric etc.

(2) The interpolation accuracy and efficiency are still not satisfactory due to the complexity of the optimization problem that exists in the interpolation of parametric curves.

2.6 Review of toolpath smoothing

2.6.1 Classifications of toolpath smoothing approaches

Many toolpath smoothing methods have been developed in both industry and academia, as the linear segmented toolpath is increasingly becoming the bottleneck for high-speed high-accuracy machining of the 3D micro-products. These methods can be classified into local smoothing and global smoothing according to the

smoothing scope. Local smoothing works with two adjacent segments, while global smoothing can act on a group of segments. These methods can also be classified into curve-based smoothing and velocity blending smoothing according to the smoothing mechanism. Curve-based smoothing is a two-step solution. Firstly, a parametric curve is used either to connect two segments at the corner or to approximate a group of segments. Then, the specially designed parametric interpolator is used to interpolate the parametric curve. By contrast, the velocity blending method is a one-step solution, which schedules the velocity profile of each axis directly at the corner and creates a smooth transition. Table 2-2 summarizes the recently developed linear segmented toolpath smoothing methods.

Table 2-2 Summary of the linear segmented toolpath smoothing methods

Local corner rounding	Global curve approximation	Local velocity blending	Global velocity blending
SIEMENS [61]	FANUC [73]	Delta Tau [78]	S. Tajima, 2016 [30]
Aerotech [62]	SIEMENS [61]	S. Tajima, 2016 [79]	
J. Huang, 2018 [63]	Z. Yang, 2015 [74]		
J. Yang, 2017 [64]	W. Fan, 2015 [75]	B. Sencer, 2015 [80]	
S. Sun, 2016 [65]	Y. Wang, 2014 [76]		
J. Shi, 2015 [66]	A. Yuen, 2013 [77]		
Q. Bi, 2015 [67]			
S. Tulsyan, 2015 [68]			
B. Sencer, 2014 [69]			
H. Zhao, 2013 [70]			
X. Beudaert, 2013 [71]			
V. Pateloup, 2010 [72]			

2.6.2 Local corner rounding approach

Table 2-2 shows that the majority of researchers focused on the local corner rounding approach. As illustrated in Figure 2-9, a quintic B-Spline is inserted at the corner of the toolpath to achieve a smooth transition. This kind of approaches can solve the corner transition problem in an analytical way, which minimizes the computation load for real-time CNC systems. SIEMENS SINUMERIK 840D sl [61] implements its continuous-path mode (G641 etc.) by inserting a spline at the corner. Aerotech A3200 controller [62] inserts a circular arc (ROUNDING ON) for the corner transition, this measure can only achieve G^1 continuity which means that the acceleration is not continuous at the join points. High order parametric curves are required to guarantee smooth motion profiles at the corner. Cubic B-spline was used by [63], [65], [70]–[72], while quintic B-spline was adopted by [64], [68], [69]. Shi et al. [66] developed their five-axis corner rounding method with a pair of quintic PH curves. Bi et al. [67] realized the same purpose with dual cubic Bézier curves. However, such approaches have severe limitation when smoothing high density of short segments, which are very common in the finish machining of 3D micro-products with freeform surfaces, for the following reasons: 1) The adjacent corner transition path may overlap with each other and makes the subsequent interpolation impossible, the linear segments may be too short to accommodate a transition curve. As a consequence, the SIEMENS controller will automatically turn off the corner rounding when the linear segments are too short; 2) Alternatively, the length of the transition curve is constrained which leads to high curvature, the feedrate must slow down to avoid shock.
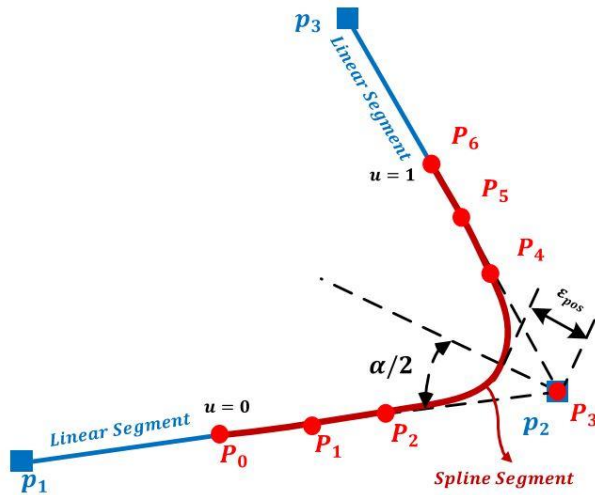
Figure 2-9 Local corner rounding with quintic B-Spline [68]

2.6.3 Global curve approximation approach

Global curve approximation approach can overcome the limitation of the local smoothing approach. As illustrated in Figure 2-10, the segmented toolpath is approximated by an Akima curve and a NURBS, respectively. However, this kind of approaches suffers from the difficulty in controlling the approximation deviation. Piegl and Tiller [26] have carried out some fundamental work on the B-spline approximation. They proposed an iterative way to approximate a set of points and using the least squares technique to calculate the unknown control points. They pointed out that the approximation process was computational intensive, wiggles tended to exist in the final curve. Moreover, their method only considered controlling the deviation between the points and the curve. For high-accuracy freeform machining, the deviation of the whole segments should be controlled, i.e., the Hausdorff distance between the original toolpath and the approximation curve [74]. This imposes considerable extra computation burden on the CNC system. SIEMENS SINUMERIK 840D sl [61] implements its NC block compression function (COMPCAD) by approximating consecutive linear segments with 5th degree NURBS. Users are warned that it is very processor and memory-intensive, and should be considered as the last resort when other measures are not satisfactory. FANUC Series 30i-LB [73] implements its smooth interpolation function (G05.1) by

fitting linear points using cubic splines [81]. Fan, Lee and Chen [75] developed the global smoothing method using mixed linear and quartic Bézier segments, the mixture will make the subsequent interpolation complicated. Wang, Yang and Liu [76] used the Akima curve to fit the linear toolpath, only C^1 continuity was achieved. Yuen, Zhang and Altintas [77] developed a five-axis linear toolpath smoothing method using quintic B-spline, the curve fitting algorithm was based on the Piegl and Tiller's method without considering the Hausdorff distance.
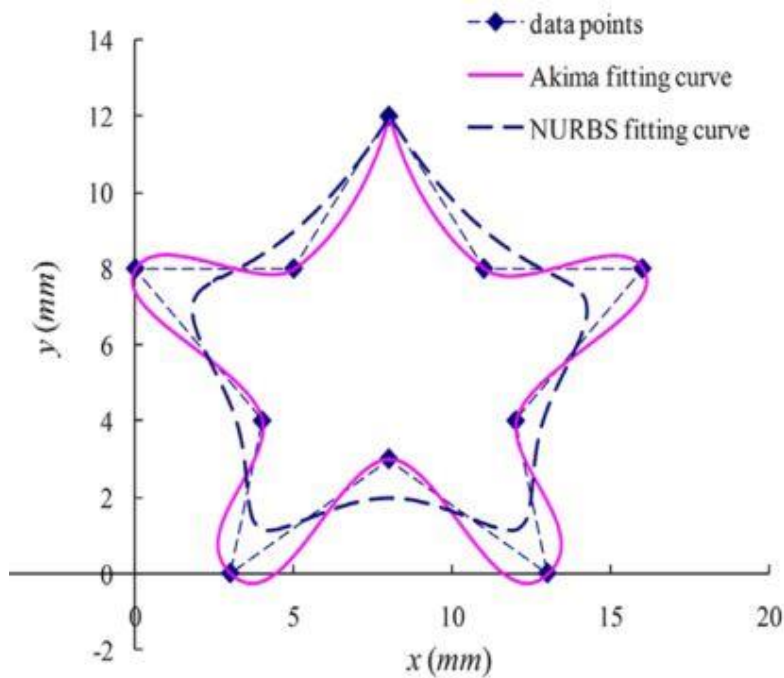
Figure 2-10 Global curve approximation of a star toolpath with a Akima curve and a NURBS curve [76]

2.6.4 Velocity blending approach

Velocity blending based smoothing approaches can achieve higher efficiency than curve-based smoothing approaches by eliminating the curve planning process. The one-step solution detects the corner and schedules axes velocities in the lookahead operation. As illustrated in Figure 2-11, the axes velocities are scheduled directly for a smooth transition instead of a full stop at the corner. However, this kind of approaches also has the same limitation as the local corner rounding methods. The

Delta Tau Power PMAC controller [78] achieves fixed-error corner blending by calculating the blending time based on the motional speeds and change in angle at the corner. The blending starts and ends at the blending-time-dependent distance from the corner, the actual blending length will be very limited if the original linear segments are short, thus the feedrate must slow down to avoid saturating the drives. This approach will be used as a benchmark in this thesis. Sencer, Ishizaki and Shamoto [80] developed a method using FIR (Finite Impulse Response) to filter the discontinuous axes velocities at the corner to achieve a smooth transition, the tolerance was controlled by selecting the overlapping time. However, the actual shape of the blended path was unclear, which is concerned in some high-accuracy machining cases. Tajima and Sencer [79] proposed the velocity blending method based on jerk limited acceleration profile (JLAP). Later they realized the limitation, and developed the Look-Ahead Windowing (LAW) technique [30] to overcome the overlapping problem at adjacent corners. However, coupling with the corner transition makes the interpolator less flexible in terms of adding new constraints.
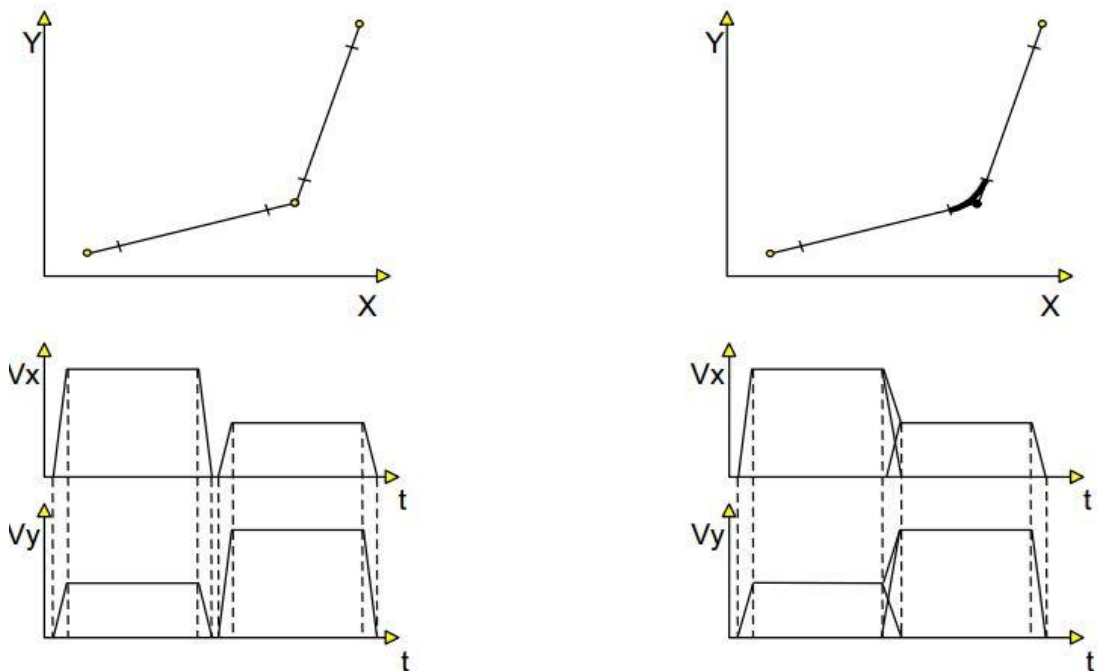
Figure 2-11 Comparision of corner transition without and with velocity blending [78]

2.6.5 Summary of the review of toolpath smoothing

Current toolpath smoothing methods can be classified into local smoothing and global smoothing according to the scope of smoothing. These methods can also be classified into curve-based smoothing and velocity blending smoothing according to the smoothing mechanism. Challenges still remain in toolpath smoothing:

(1) Severe limitation exists in the local smoothing method when dealing with high density of short segments, which are very common in the finish machining of freeform surfaces. The limitation is found in 1) The adjacent corner transition path may overlap with each other and makes the subsequent interpolation impossible; 2) Alternatively, the length of the transition path is constrained which leads to high curvature, the feedrate must slow down to avoid shock.

(2) It is still computationally inefficient to control the deviation between the approximation curve and the toolpath for global curve approximation method, which restricts its application in real-time CNC systems.

2.7 Summary of the literature review

Hybrid micro-machining has emerged as a solution to tackle the manufacturing challenges for high value-added 3D micro-products. The combination of micro-manufacturing processes for the hybrid process is largely determined by the characteristics of the application, such as material and geometry requirements. Various hybrid processes have been established for specific 3D micro-products, and more hybrid processes will be developed to achieve high-efficiency high-accuracy machining of future 3D micro-products.

This chapter identifies three CNC system requirements for hybrid micro-machines with the consideration of the characteristics of the machine and the 3D micro-product:

- The flexibility that allows easy integration of multiple modules.

- Parametric interpolator for high-speed high-accuracy machining of freeform surfaces.
- Built-in toolpath smoothing approaches to bridge the gap in toolpath representation.

Current commercial CNC systems are surveyed, and the literature on parametric interpolation and toolpath smoothing are reviewed. It concludes that:

(1) PC-based CNC systems are preferable for hybrid micro-machines, as PC has unprecedented I/O capabilities to exchange data with various communication interfaces used by different module vendors, and has reconfigurable software to interpret different data protocols. A generic control architecture for hybrid micro-machines is invaluable to accelerate the integration process.

(2) Parametric interpolator is highly desirable for high-speed high-accuracy machining of freeform surfaces. The interpolation of parametric curves is an optimization problem, and it is extremely difficult to get the time-optimal solution. The recursive Taylor's expansion and the lookahead technique are essential for a near time-optimal solution.

(3) Severe limitation exists in the local smoothing approach when dealing with high density of short segments. The adjacent corner transition path may overlap with each other and makes the subsequent interpolation impossible, or the length of the transition path is constrained which leads to high curvature. Moreover, it is still computationally inefficient to control the deviation between the approximation curve and the toolpath for global curve approximation approach.

Chapter 3   A generic control architecture for hybrid micro-machines

3.1   Introduction

As concluded in Chapter 2, integrating a new hybrid micro-machine requires high standard expertise and is very time-consuming due to the lack of plug-and-play solutions for the broad range of functional modules. A generic control architecture will not only be able to save the substantial development cost, but also improve the flexibility and reliability of the whole CNC system. The basic task of the control architecture is to manage a wide range of hardware, regulate data flow, and provide intelligent control algorithms to achieve the desired hybrid machining process.

This chapter proposes a novel control architecture for hybrid micro-machines, which consists of three layers, i.e. supervisory layer, coordination layer and process layer. The essential functions at each layer are encapsulated into individual software components. Thus the control architecture can be built with a set of components. The effectiveness of the control architecture will be demonstrated through the integration of a six-axis hybrid micro-machine, which is capable of laser machining, laser-assisted micro-milling and laser-assisted micro-grinding operations. The machine also incorporates a nano-second pulse laser, a high-power continuous laser, a dispersed reference interferometry (DRI) sensor and a material handling system.

3.2   Review of control architectures for CNC machines

In recent years, a lot of attentions are paid to the reconfigurable manufacturing system (RMS). Various architectures and frameworks have been developed [82], [83] to enhance the flexibility of RMS for the increasing customisation requirement in products. Those architectures and frameworks tend to take the advantage of the information and communication technology (ICT), as well as the cyber-physical system (CPS) [84], [85]. However, those architectures and frameworks are at the

factory level, while the control architecture for CNC machines is at the machine level, which requires much higher real-time performance.

Classic CNC system architecture focuses on regulating a single process, the compatible hardware modules should be specially designed. Nor and Cheng [86] divided the control system for ultraprecision machine tools into three subsystems, as shown in Figure 3-1. However, the coordination among the subsystems and the flexibility in integrating new modules were not specified.
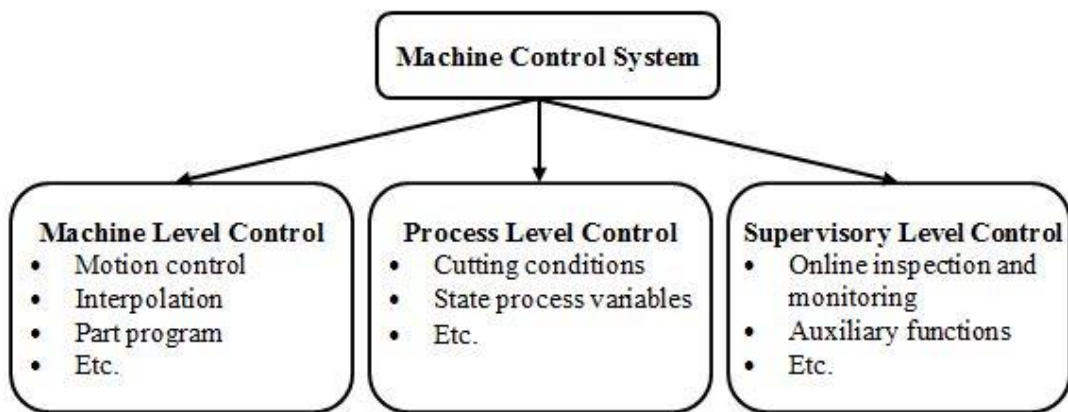
Figure 3-1 Ultraprecision machine tool control system elements [86]

The aforementioned OAC consortiums have presented some open control architectures toward the accommodation of a broad range of functional modules, which provide the inspiration of the development of the proposed control architecture. OMAC developed the OMAC API framework that provided a standard way for software components to collaborate, as shown in Figure 3-2. The OSACA aimed at developing a system platform for open control systems, which hides the actual implementation of the platform services. Therefore, users can focus on the development of application modules (so-called AOs), as shown in Figure 3-3. To achieve the goal of OMAC or OSACA, all the involved functional module vendors should follow the standards to provide the vendor-neutral software components. Unfortunately, these guidelines have not been followed in the industry yet.
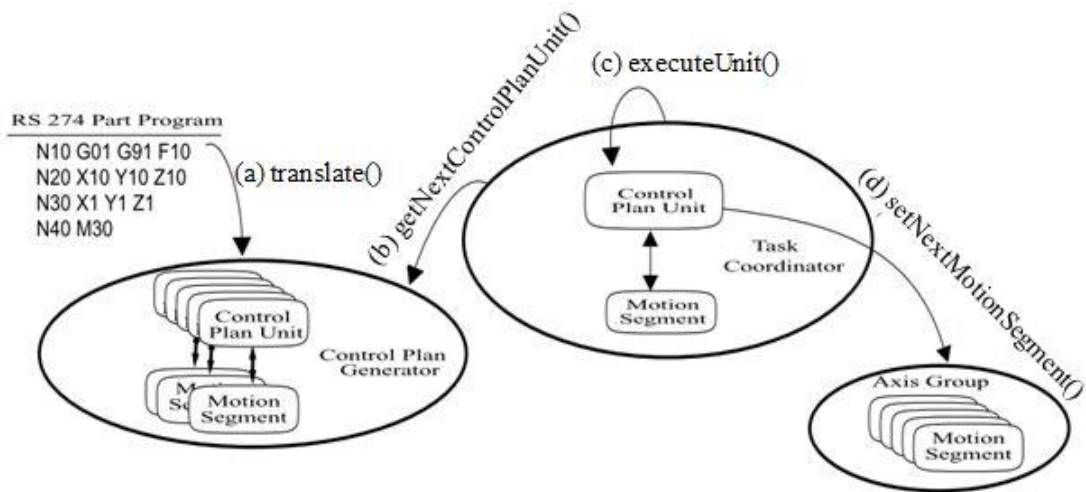
Figure 3-2 OMAC API framework collaboration model [19]

AO : architecture object (module of application software)
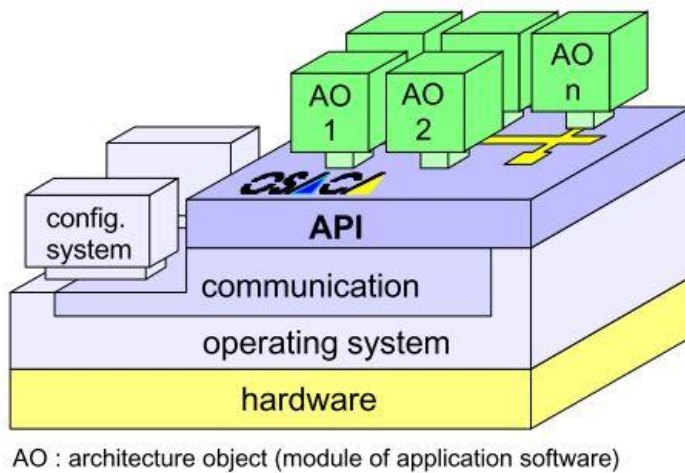
Figure 3-3 OSACA system platform for open control systems [87]

3.3   A novel control architecture

A novel control architecture for hybrid micro-machines proposed in this thesis is divided into three layers, as shown in Figure 3-4. The functions in the three layers are implemented on PC for on-line control. The off-line product data is transferred to the production via the supervisory layer, while the coordination layer synchronises all the modules on the machine, and the process layer deals with the low level control algorithms. The purpose of this design is to decouple the software from the hardware,

so the change of hardware modules will have minimum effect on the whole system. The essential functions at each layer are encapsulated into individual software components. Each software component maintains the specific interface. Thus, the data flow between components is standardised. The software components can be easily rebuilt and replaced. The system flexibility is therefore increased dramatically. Furthermore, those software components that have no direct links to the hardware can be reused, which helps reduce the amount of work when the machine is reconfigured.
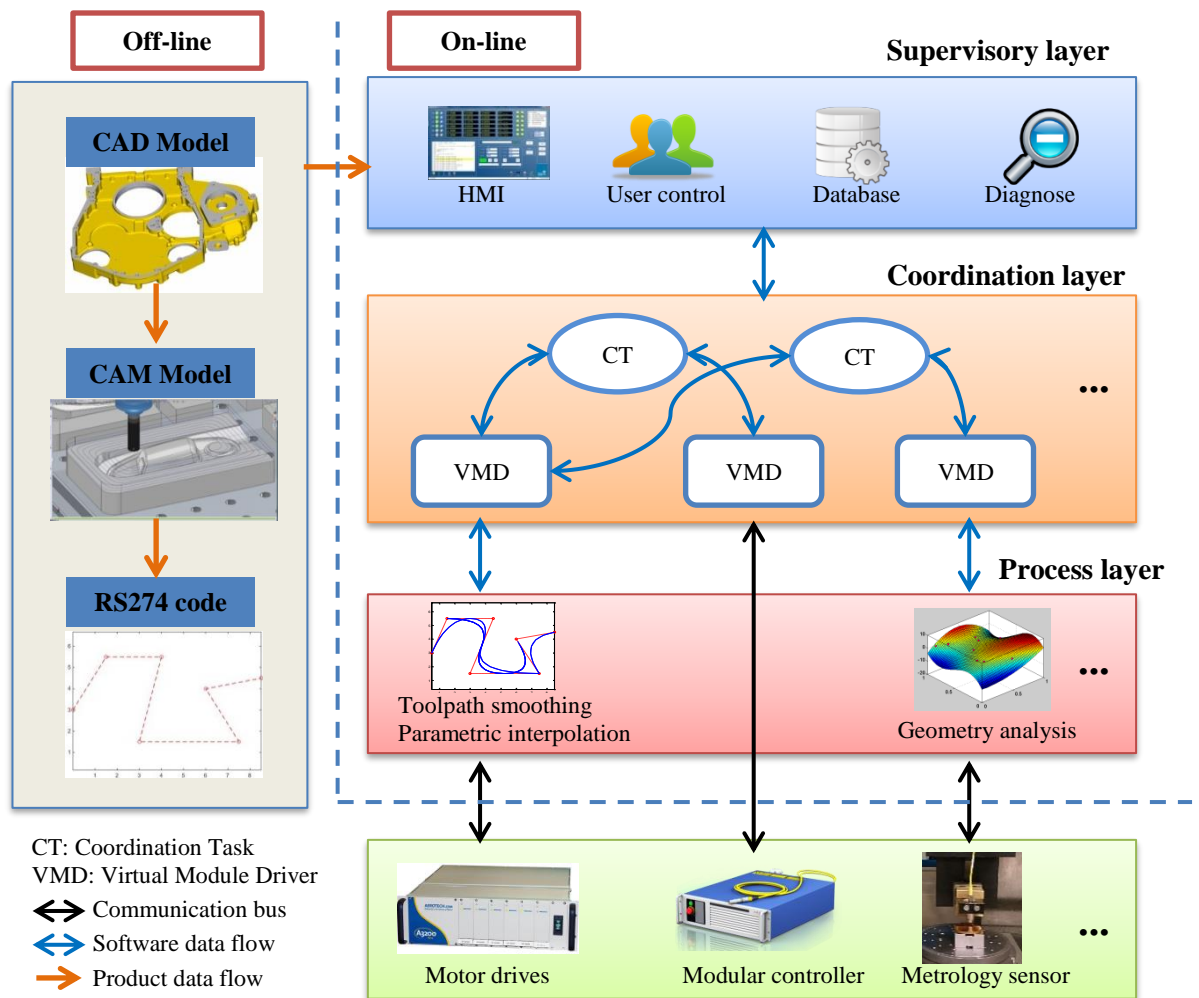
Figure 3-4 Proposed control architecture for hybrid micro-machines

3.3.1 Supervisory layer

The supervisory layer consists of four software components, i.e. HMI, user control, database and diagnostic. The HMI provides interface for users to interact with the machine directly, the RS274 machining code generated from the product data can be downloaded to the interpolator through the HMI. The user control component divides machine users into two categories, i.e. administrator and guest, which have different access right to change the machine configurations stored in the built-in database. The configurations will be used to initialize the software components at the coordination layer. Data exchange between the supervisory layer and the coordination layer is performed through the predefined APIs, which are hardware independent. Data is collected periodically for on-line inspection and diagnose.

3.3.2 Coordination layer

The coordination layer performs complex data regulation in order to coordinate all the functional modules to achieve the desired hybrid process. The virtual module driver (VMD) is innovatively proposed, it is a software component that can interpret the data of a specific functional module. Therefore, the device-specific read/write operations are converted to generic read/write operations. This abstraction encapsulates the differences in data protocol and communication interface used by different vendors. Therefore, the consistent interaction with a functional module is achieved. For example, the VMD maintains the following laser manipulation methods for any laser controllers, while the implementation of those methods is device-specific:

- public void LaserEnable(bool): Enable or disable the laser controller.
- public void LaserEmission(bool): Start or stop the laser emission.
- public void LaserPower(int): Set the laser output power.
- public void LaserFrequency(int): Set the laser output frequency.

The coordination task (CT) is the software component developed for the data exchange and synchronisation between specified functional modules. Because the data has been interpreted in the VMD, the CT can concentrate on the synchronisation logic, which is hardware independent. The coordination tasks should be executed in the real-time environment or in the normal desktop environment with high priority to guarantee the highest data throughput and the lowest delay. Process specified adaptive control algorithms can also be implemented in the CT, e.g. laser power adjustment after analysing the surface results from the metrology module.

The coordination layer makes the proposed control architecture fundamentally different from the classic control architectures. It can enhance the system's flexibility enormously as discussed in the following cases:

(1) When a functional module is upgraded, only the corresponding VMD component should be adapted for the new data protocol and communication interface, but maintains the original interface. The whole system can work seamlessly without modifying any other software components.

(2) If a new functional module is to be added, a corresponding VMD component should be developed. If it needs to interact with other functional modules, a new CT should be developed by invoking the given interfaces provided by the related VMDs. The other part of the system will not be affected.

3.3.3 Process layer

The process layer executes intelligent algorithms in real-time for the related functional modules. Motion control module is one of the basic modules for a hybrid micro-machine. It mainly consists of two parts, i.e. the interpolator and the servo, as shown in Figure 3-5. The interpolator interprets the RS274 code and converts the segmented toolpath to parametric curves with the built-in toolpath smoothing algorithm, then the parametric interpolator generates reference positions for the servo system. The servo system generally consists of the three cascaded control loops in order to follow the position commands. The communication between the interpolator

and the servo is usually achieved by high-speed deterministic buses, such as EtherCAT (Ethernet for Control Automation Technology), which was originally developed by Beckhoff Automation [88], and the FireWire used by Aerotech [35]. This design allows distributed hardware control. The servo part can be closer to the actual motor and feedback sensors.
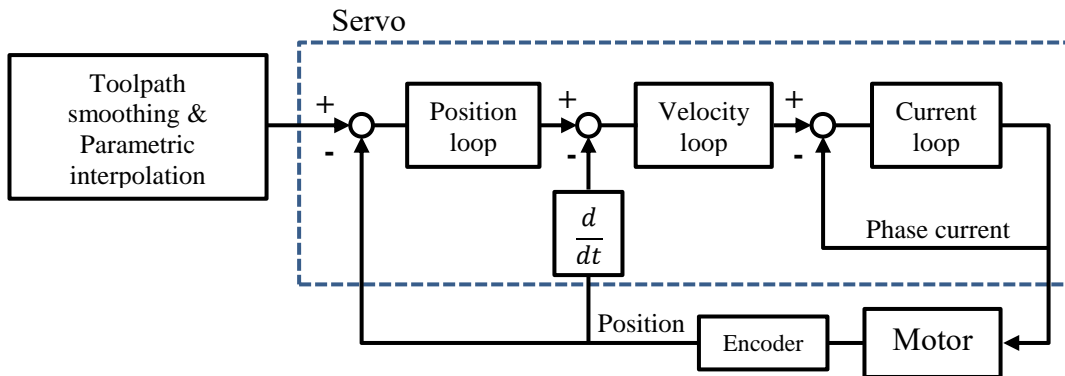
Figure 3-5 Motion control module structure

Sensor data processing algorithms are executed in this layer as well. The functional modules that do not require intelligent algorithms are connected directly to the coordination layer. For example, for the laser process, some simple laser manipulation logics are enough.

3.4   Component-based technology

A number of software components are used to encapsulate the functions at each layer of the proposed control architecture, in order to simplify the implementation of the control architecture and to increase its flexibility. From the perspective of software engineering, the component-based technology was developed with the inspiration of using components as building blocks for complex system software. An individual software component is a software package, or a module that encapsulates a set of related functions or data [89]. The component communicates with each other through interfaces, as shown in Figure 3-6. The interface defines a set of actions which are understood by both the original component and the target component [90]. Interfaces

are defined either by an Interface Definition Language (IDL) or by an objected-oriented programming language. In the latter case, a component is expressed as a class, while an interface is defined as a set of methods and attributes [90].
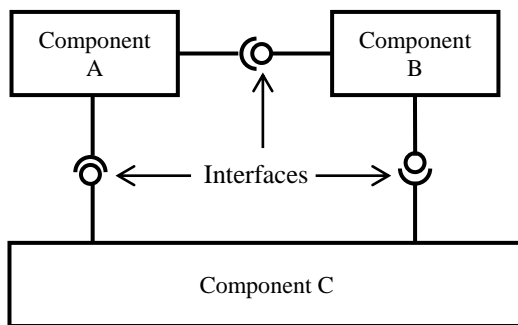
Figure 3-6 Software components and interfaces

Building systems from components has seen its wide applications in the industry control domain. For example, many component-based software frameworks have been created for the robotics systems to support the development and reuse of "large grained" pieces of robotics software [91]. The AUTomotive Open System ARchitecture (AUTOSAR) [92] maintains standardised architecture and architecture components for automotive applications. The OPC Foundation [93] has developed and maintained a specification that defines standard interfaces for process automation with the component-based technology.

The major benefits to use software components include:

- Software component is reusable. Component provides service to the system via its interface, the data structure and algorithms are encapsulated. If two components have the compatible provided interface and required interface, they can replace each other without breaking the system. The development of the system is therefore accelerated.
- The system scalability and flexibility are increased. Components are treated as the building blocks of the CNC system. Various control architectures can be constructed by combining the necessary components.

- The system maintainability is improved. An upgraded component can replace the old component, while the other components in the system are not affected. The component is linked dynamically at run-time. There is no need to re-compile other components.

Software components are composed by component models. Many component models have been proposed for different applications. Table 3-1 summarises the leading component models developed by three organizations.

Table 3-1 Leading component models

OMG (Object Management Group)	Microsoft	Sun Microsystems
CORBA (Common Object Request Broker Architecture) [94] CCM (CORBA Component Model) [95]	COM (Component Object Model) [96] .NET [97]	JavaBeans [98] Enterprise JavaBeans (EJB) [99]

The proposed control architecture in this thesis will be implemented on Microsoft Windows desktop environment. Microsoft has deemphasized COM for .NET. As a result, the software components for the control architecture will be developed with .NET technology. Specifically, the object-oriented programming language C# is adopted. The software components are implemented with classes in dynamic link libraries (DLLs) or in executable files.

3.5 System integration of a six-axis hybrid micro-machine

The proposed control architecture is applied in the integration of a six-axis hybrid micro-machine, as shown in Figure 3-7.
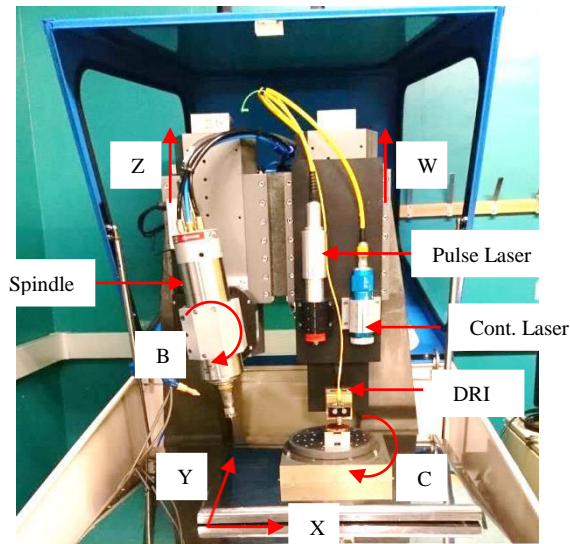
Figure 3-7 The configuration of the six-axis hybrid micro-machine

3.5.1 Integration of motion controller

The motion controller is in charge of the movement of the six motional axes and the spindle. The linear axes (X, Y, Z, W) are driven by linear motors and supported by micro recessed air bearings, so that the friction and backlash can be eliminated, which leads to better positioning accuracy and higher attainable acceleration. Easy maintenance is also achieved due to that no lubrication is required. Each linear axis uses a linear encoder with 20 μm pitch as the position and velocity feedback sensor for the servo system. The feedback resolution can achieve nanometre level with up to 65536 encoder multiplier.

Workpieces are fixed on the rotary C table, which is mounted on the top of the stacked X Y axes. The C axis is driven by a brushless DC motor with air bearing. A rotary encoder with 15,744 lines is used as the feedback sensor. The rotary B axis is mounted on the vertical Z axis. It is driven by the worm-gear mechanism, which offers high structural stiffness and long-term stability for the spindle that is fixed on the B axis. This design can improve the machined surface finish noticeably as the vibration of B axis will be enlarged by the long distance from the tool tip to the B

axis rotary centre. The heavy-duty spindle can reach up to 50,000 rpm with liquid cooling.

The Aerotech A3200 motion controller is chosen as the motion control module in the proposed control architecture in Figure 3-4. The A3200 interpolator is implemented in the INtime® for Windows [100] real-time kernel. The synchronised motion is achieved by sending the reference positions to the drive of each axis with the high-speed deterministic FireWire bus. However, the A3200 interpolator is not open to the user, the toolpath smoothing algorithm and the parametric interpolation algorithm will be implemented and verified in an in-house developed microcontroller.

The VMD for the A3200 interpolator is provided by Aerotech in the form of .NET components, as shown in Figure 3-8 [101]. The Controller Class encapsulates many classes, such as the Task Class that allows the interpolator to run programs, and the Information Class that provides monitoring information about the interpolator, etc. Therefore, the Controller Class offers centralized interface to interact with the interpolator for the coordination tasks at the coordination layer and the HMI in the supervisor layer. Figure 3-9 shows a code snippet that downloads a RS274 program file to the interpolator. Through the interface provided by the Controller Class, the HMI module can acquire the information of axes easily, as shown in Figure 3-10.
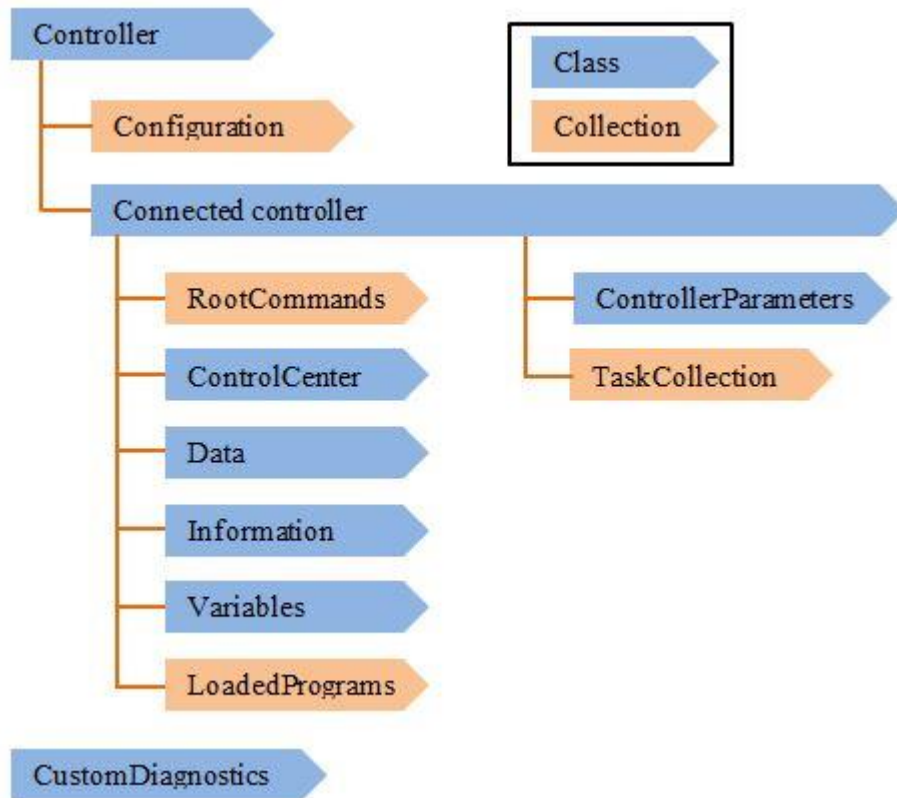
Figure 3-8 The A3200 components hierarchy

```
// Establish communication with the interpolator in the real-time process layer
Controller controller = Controller.Connect();
// Download and start executing the RS274 program
controller.Tasks[TaskId.T01].Program.Run("C:\\program.pgm");
```

Figure 3-9 Code snippet showing the use of the Controller Class

Figure 3-10 The customised HMI component

3.5.2 Integration of laser controllers

Two laser systems are integrated on the hybrid micro-machine. A nano-second pulse laser is used to manufacture micro structures or remove micro burrs that are generated by micro-milling process. The maximum power of the pulse laser is 20 W, and the spot size is 15 μm in diameter. The continuous laser is used to assist the micro-milling and micro-grinding process by pre-heating the workpiece, as shown in Figure 3-11. The maximum power of the continuous laser is 200 W, and the spot size is 4 mm in diameter.
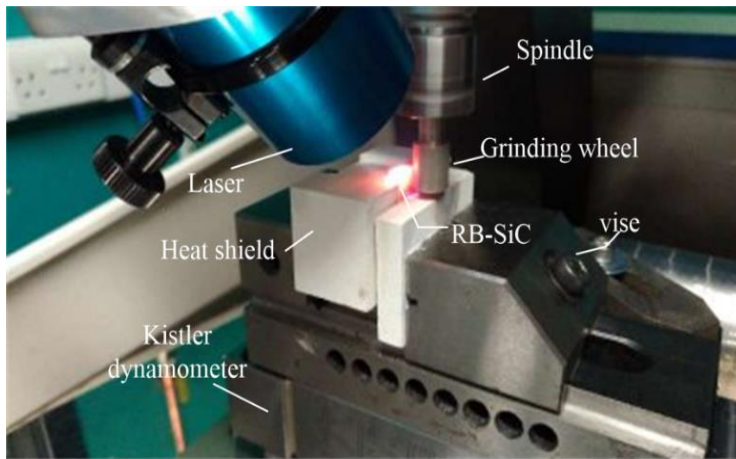
Figure 3-11 Laser-assisted micro-grinding process

Both laser controllers use RS232 to communicate with the PC. The RS232 settings for both laser controllers are given in Table 3-2. The laser controllers are connected to the coordination layer in the proposed control architecture, as no real-time algorithms are required to process their data. Although the laser controllers use identical communication method, the data protocols are different. Two VMD components should be developed separately to convert the generic laser operations to the device-specific operations. The laser operation methods provided by the VMD components and the encapsulated underlying device-specific operations are summarised in Table 3-3.

Table 3-2 Laser RS232 settings

Parameter	Value
Baud rate	57,600
Data bits	8
Stop bits	1
Parity	None
Flow control	None

Table 3-3 Laser VDM component implementation

Laser VMD interface methods	Meaning	Pulse laser operations	Continuous laser operations
void LaserEnable(true)	Enable the laser controller	1. Open the RS232 port 2. Write "$42;\r" to the port.	Open the RS232 port
void LaserEnable(false)	Disable the laser controller	1. Write "$43;\r" to the port 2. Close the RS232 port	Close the RS232 port
void LaserEmission(true)	Start the laser emission	Write "$30;\r" to the port	Write "EMON\r" to the port
void LaserEmission(false)	Stop the laser emission	Write "$31;\r" to the port	Write "EMOFF\r" to the port
void LaserPower(int percent)	Set the laser output power in percentage of the maximum power	Write "$32;" + percent +'\r' to the port	Write "SDC" + percent +'\r' to the port
void LaserFrequency(int freq)	Set the laser output frequency in kHz	Write "$28;" + freq + '\r' to the port	Not implemented

The best practice to achieve the aforementioned laser assisted hybrid process is to embed the laser control logics in the RS274 program, so that the users have the flexibility to manipulate the laser at any location of the program to satisfy the requirement of the hybrid process. However, it is impossible for the interpolator to use the laser VMD interface directly from the real-time environment, which is separated from the normal desktop environment. Therefore, a coordination task should be developed to synchronise interpolator commands and actual laser operations. For the interpolator, all the laser control logics are implemented as preprocessors or macros, which are similar to the conventional M codes in RS274 standard. An example of the laser hybrid machining code is shown in Figure 3-12.

Each preprocessor or macro actually changes the value of a particular interpolator global variable. The coordination task continuously reads the values of those variables through the interpolator VMD as mentioned in Section 3.5.1. If a value change is monitored, the coordination task will invoke the corresponding laser VMD interface method (as shown in Table 3-3) to finish the laser manipulation. The whole coordination algorithm is illustrated in Figure 3-13.

```
// Enable the pulse laser
PUL_LASER_ENABLE
// Set the laser power to 50%
PUL_LASER_POWER(50)
// Set the laser frequency to 20 kHz
PUL_LASER_FREQ(20)
// Turn on the laser radiation
PUL_LASER_ON
// Machining with linear move
G01 X10 Y20
// Turn off the laser
PUL_LASER_OFF
X0 Y0
// Disable the laser when machining is finished
PUL_LASER_DISABLE
```

Figure 3-12 An example of the laser hybrid machining code
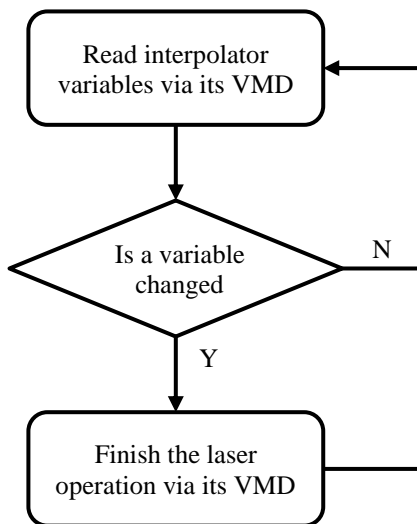
Figure 3-13 Laser interpolator coordination task flow chart

3.5.3 Integration of dispersed reference interferometry (DRI) in-line metrology system

The DRI is a single point variant of white light interferometry. It can achieve in-line non-contact metrology, which is capable of scanning the profiles and measuring the surface topography of workpiece. The vertical resolution of DRI is 5 nm, the measurement range is 600 μm. The raw interferogram signal is transmitted to the PC using Ethernet. Complex signal processing algorithms have been implemented in an executable component, which should run at the process layer in real-time. However, the INtime® for Windows real-time kernel is not open for the third party other than the A3200 interpolator. Therefore, it runs in the normal desktop environment with high priority in this application.

The DRI signal processing component only gives the current distance from the probe to the workpiece surface. The measurement height and the workpiece position should be synchronised to achieve the 3D position. A surface profile is achieved with many equally spaced scanned positions along a particular scanning direction. The surface topography is composed of many profiles. Figure 3-14 shows the measured surface profile as a result of the coordination task through reading the workpiece position and DRI measurement height simultaneously via their VMD interfaces.
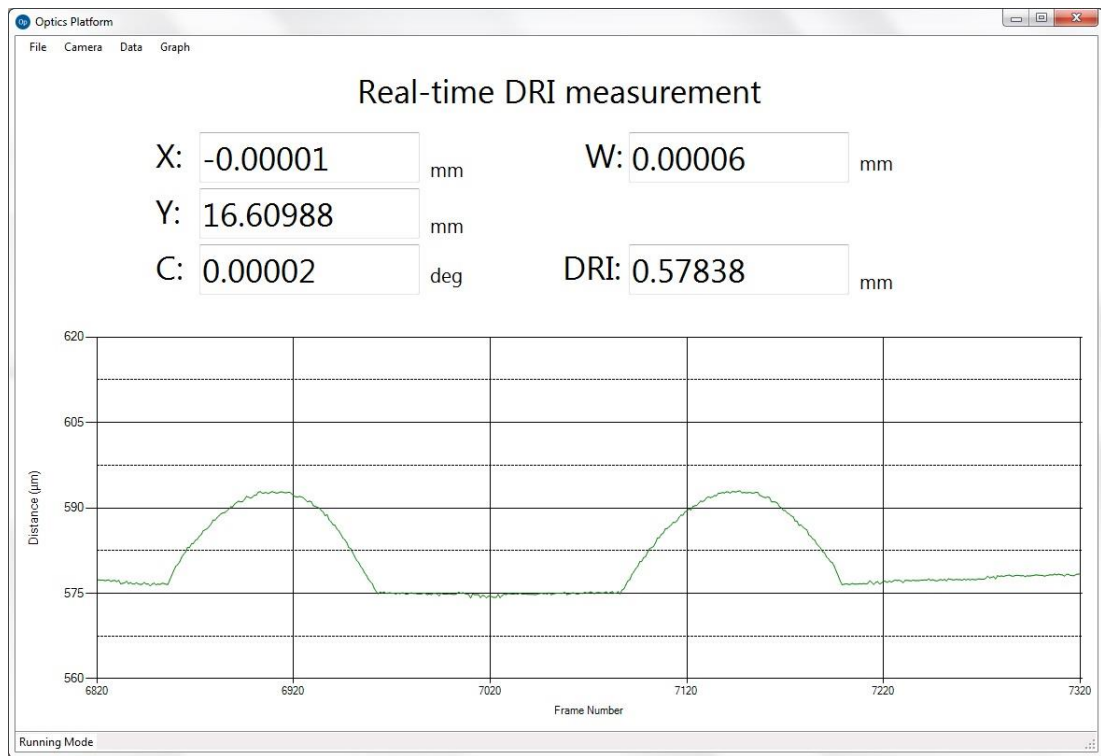
Figure 3-14 The DRI measurement coordination task

3.5.4 Integration of a material handling system

A complete material handling system, consisting of a SCARA (Selective Compliance Assembly Robot Arm) robot, a two finger gripper and a vision system, as shown in Figure 3-15, is also required to be integrated on this hybrid micro-machine. The maximum reach of the material handling system is 650 mm with a repeatability of 30 μm. The maximum payload is 5 kg and the gripping force range is 5-50 N. To avoid the high-degree interconnection between the material handling system and the hybrid micro-machine as well as to simplify the reconfiguration of the hardware platforms, the controllers of the material handling system are integrated on a standalone PC. The communication between the two control systems is via Ethernet.

A typical communication cycle between the two control systems includes command/data from one side and acknowledgement from the other side. The simplified communication protocol is shown in Table 3-4 for the material loading /unloading process. Like the VMD for the laser controller, the VMD for the material

handling system encapsulates the low level Ethernet read/write operations and the predefined communication protocol. The coordination task continuously monitors the status the A3200 interpolator and the material handling system, and performs corresponding actions. For example, when the interpolator finishes running all the machining code, the coordination task will send the complete command to the material handling system to initiate the material unloading process.
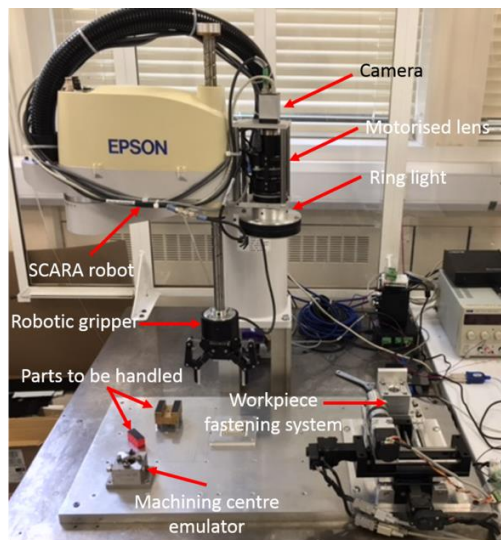
Figure 3-15 The material handling system

Table 3-4 Communication protocol for material loading /unloading process

Step No.	Process	Machine to Handling system	Handling system to Machine
1	Send ready command		✓
2	Send acknowledgement	✓	
3	Send three-dimensional part and material data	✓	
4	Send Acknowledgement		✓
5	Send activate command	✓	
6	Send acknowledgement		✓
	The material handling system conducts loading/unloading process		
7	Send complete command		✓
8	Send acknowledgement	✓	
	The machine conducts machining process		

3.6 Summary

This chapter presents a novel control architecture for hybrid micro-machines, which is made up of the following three layers:

- Supervisory layer: It is in charge of the human machine interaction and monitoring.
- Coordination layer: It provides abstraction for each functional module, and hosts the coordination tasks.
- Process layer: It executes the intelligent algorithms in real-time for related functional modules.

The essential functions at each layer are encapsulated into individual software components. The component-based technology contributes to the structured development of the proposed control architecture.

The proposed control architecture enhances the flexibility of the CNC system to accommodate a broad range of functional modules. The component design also improves the scalability and maintainability of the whole system. The effectiveness of the proposed control architecture has been successfully verified through the integration of a six-axis hybrid micro-machine. Thus it provides invaluable guidelines for the development of next generation CNC systems for hybrid micro-machines.

Chapter 4   Experimental test-bed for real-time algorithms

4.1   Introduction

As identified in the literature review, the parametric interpolation algorithm and the toolpath smoothing algorithm are essential for high-speed high-accuracy machining of 3D micro-products with complex freeform surfaces. Those algorithms are fit in the real-time process layer of the novel control architecture, as described in Chapter 3. However, the Aerotech A3200 interpolator used on the hybrid micro-machine is not open for the implementation of user specified algorithms. Moreover, the linear motors used on the six-axis hybrid micro-machine require closed-loop control, while different CNC systems have implemented different servo algorithms, which will interfere the benchmarking of the proposed algorithms. Therefore, this chapter develops an experimental test-bed for the implementation and verification of the proposed algorithms.

The test-bed consists of the following devices and software:

- A three-axis micro-milling machine that can carry out freeform machining experiments.
- A microcontroller that can implement the algorithms and control the movement of the micro-milling machine.
- A simple HMI that can exchange data with the microcontroller for machining trials.

4.2   Minitech three-axis micro-milling machine

A three-axis micro-milling machine, developed by Minitech Machinery Corporation, is selected as the machining trial platform, as shown in Figure 4-1. It has a stacked X and Y axes to carry the workpiece. A high-speed spindle (SF3060-ST32) is mounted

on the vertical Z axis. The maximum speed of the spindle is 60,000 rpm with air cooling. The travel ranges for the X, Y, Z axes are 254 mm, 127 mm, 200 mm, respectively. The linear axes are driven by stepper motors with acme screws. Each axis is equipped with dual ball bearing guideways.
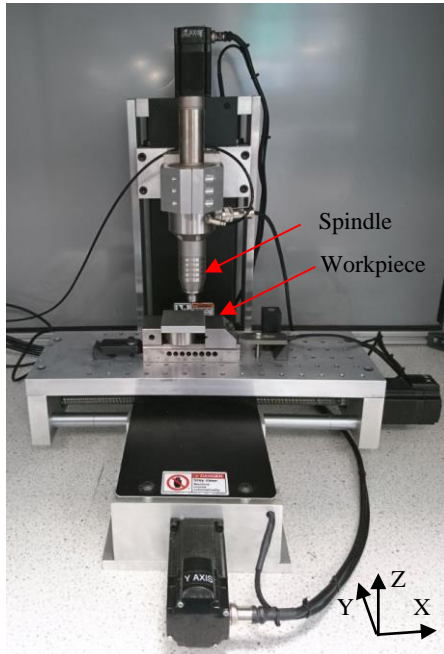
Figure 4-1 The layout of the three-axis micro-milling machine

There are no position feedback sensors for the machine axes, which are controlled in the open loop manner. Therefore, the influence of the servo algorithm on the performance of the interpolation algorithm and toolpath smoothing algorithm is eliminated. Each machine axis has a home switch, which is used to determine the home position. The full step angle of those stepper motors is 1.8°, they are driven by the KL-8056D drive with 50 micro-steps for a full step, i.e. the stepper motor needs to move 10,000 steps for a revolution. The helical pitch of the acme screw is 5 mm, so the nominal resolution of each axis is 0.5 µm.

The stepper motor drive accepts three optically isolated logic inputs to control the movement of the motor, as shown in Figure 4-2. The PUL pins are for pulse signal input. The stepper motor moves a micro-step at the rising edge of the pulse signal. The DIR pins are for direction signal input. The stepper motor rotates in clockwise

when the direction signal is in high level. Otherwise the motor rotates in counter clockwise. The ENA pins are for enable signal input. The drive is enabled if the enable signal is in high level or unconnected, otherwise the drive is disabled.
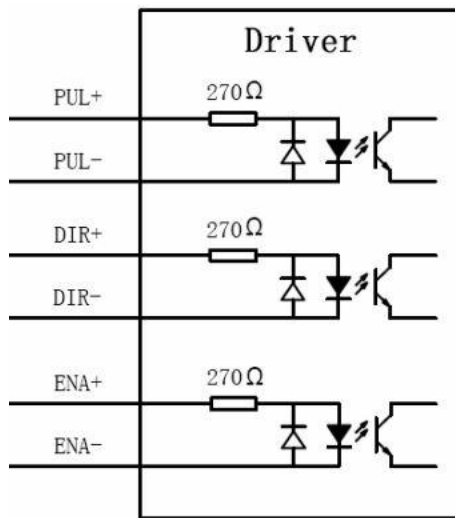
Figure 4-2 Stepper motor drive control logic inputs [102]

The work spindle is driven by the CSF600 drive. It requires a 0-10V analog input as the speed reference, three control logic inputs as the start signal, direction signal, and error reset signal, respectively. It also outputs an alarm signal, which indicates whether an error has arisen, such as spindle over current.

A system emergency stop input is also required. The overall system connection diagram is shown in Figure 4-3.
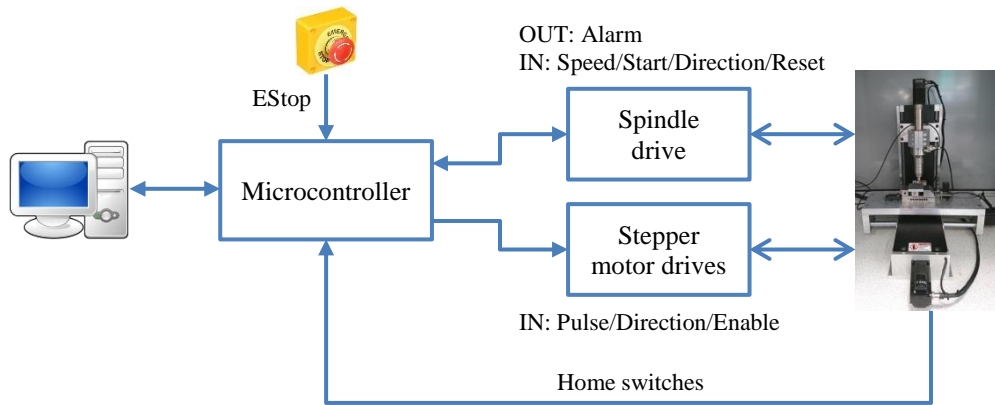
Figure 4-3 System connection of the micro-milling machine

4.3 The microcontroller

A cost-effective customised microcontroller is developed to seamlessly control the micro-milling machine and to allow the implementation of the proposed algorithms. The complete microcontroller is shown in Figure 4-4. It consists of two stacked printed circuit boards (PCBs), i.e. the interface board and the CPU board.
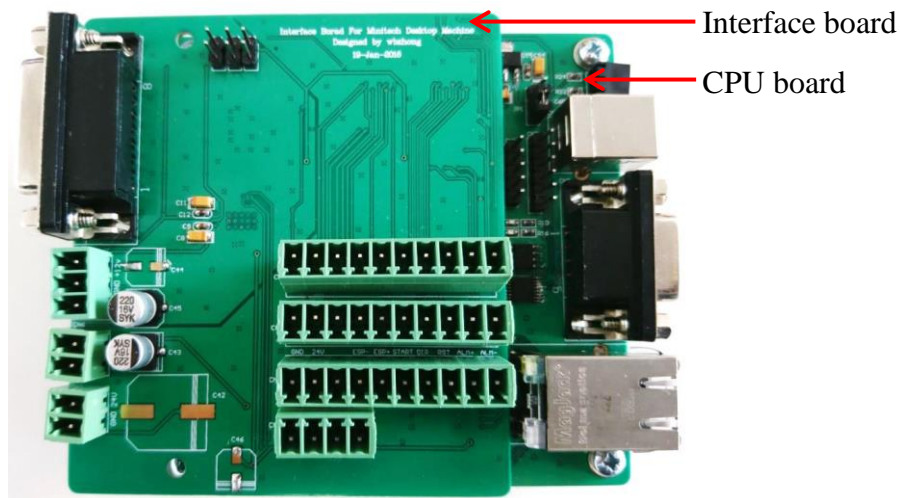
Figure 4-4 The microcontroller for the micro-milling machine

4.3.1 Hardware development

4.3.1.1 The CPU board

The CPU board is in charge of the execution of algorithms and the management of peripherals. The layout of the CPU board is shown in Figure 4-5. An ARM Cortex-M7 chip (STM32F746ZGT6 [103]) is adopted as the main CPU. The 32-bit core features 6-stage superscalar pipeline with branch prediction and built-in data and instruction caches. It also includes a single floating point unit (SFPU), a full set of digital signal processing (DSP) instructions and a memory protection unit (MPU). This architecture makes it ideal for a variety of high-performance control applications, such as audio processing, automotive, industrial automation and drone [104]. The operation frequency of the chip can reach 216 MHz.
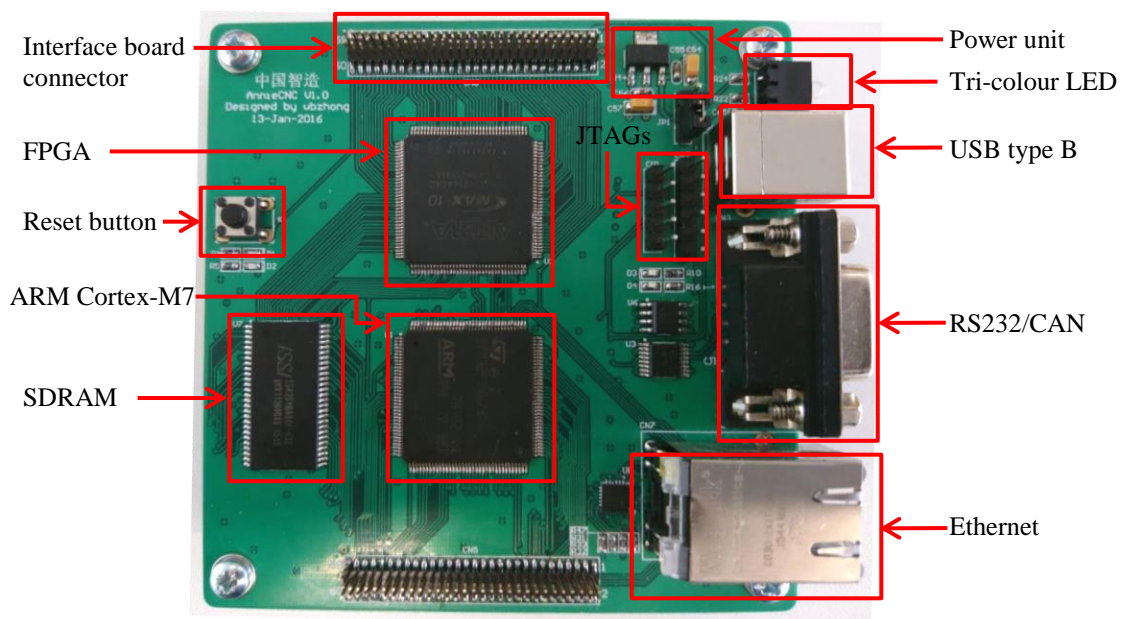
Figure 4-5 The layout of the CPU board

The ARM CPU also provides very flexible communication interfaces. It has an on-chip 10/100 Ethernet MAC (Media Access Controller), the Ethernet PHY (Physical Layer) is implemented with a third-party chip (LAN8742A-CZ). The RMII (Reduced Media-Independent Interface) is used as the data interface between the MAC and

PHY. The on-chip USB 2.0 full-speed PHY enables direct link between the chip and PC. A RS232 bus and a CAN (Controller Area Network) bus are also implemented to further enhance the connectivity of the microcontroller. The MAX3232 and MCP2562 are used as the transceivers for the two buses, respectively.

An external 16 MB SDRAM (Synchronous Dynamic Random Access Memory, IS42S16800F) is connected to the CPU to extend its ability to handle large data buffers for the algorithms. A FPGA (Field Programmable Gate Array, 10M02SCE144C8G) is integrated to generate control logics for external devices, such as the pulse and direction signals to the stepper motor drives, ADCs (Analog-to-digital Converters), and DACs (Digital-to-analog Converters) etc. FPGA has the advantage in parallel execution and hardware reconfigurability over ASIC (Application Specific Integrated Circuit), thus it can increase the data throughput and accelerate the design significantly. Both the SDRAM and FPGA are connected to the CPU via its external memory bus. They are mapped to two memory space regions of the CPU. The whole CPU board interconnection is shown in Figure 4-6.
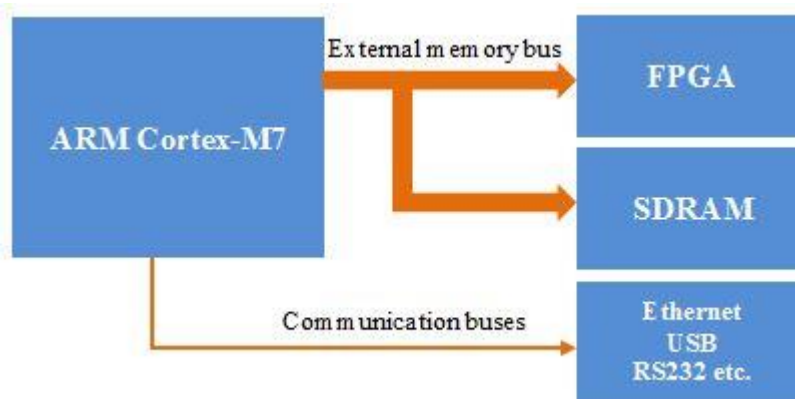
Figure 4-6 The interconnection of the CPU board

The JTAG (Joint Test Action Group) interfaces of the CPU and FPGA have been connected to two headers, which offer debug and programming interfaces for the two chips. The CPU uses the ST-LINK/V2 [105] as the debug tool, while the USB-Blaster [106] is used for the FPGA. The CPU board requires 5 V and 3.3 V voltages as the power supply. The 5 V voltage source can be from the USB port or the

interface board, while the 3.3 V voltage is generated by a power regulator (TLV1117-33) from 5 V.

The CPU board uses four layers design, as shown in Figure 4-7. The top layer is used to solder the main components and connectors. The passive components, like decoupling capacitors and resistors, are soldered at the bottom layer. The inner layers are allocated to the 3.3V power and signal ground. The inner layer pair offers solid power planes for all the components, thus the signal integrity is improved. The power planes can also isolate the electromagnetic interference between the top and bottom routing layers. Furthermore, the PCB routing is simplified dramatically because the power and ground can be easily connected using a hole with the shortest distance. The material of the PCB is FR-4.
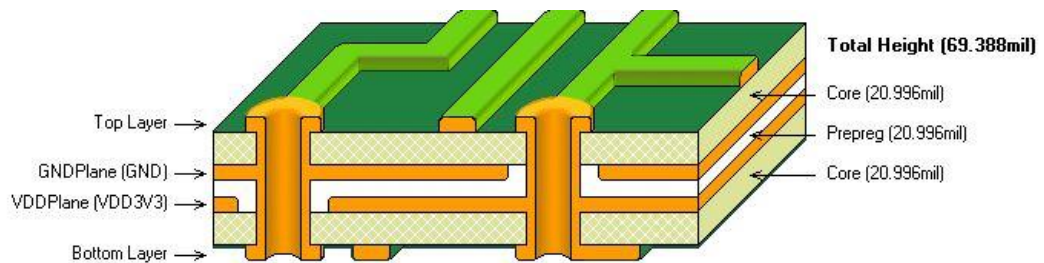
Figure 4-7 The CPU board layer stack configuration

4.3.1.2 The interface board

The CPU board can be re-used for general purpose control applications. The interface board is developed to provide the specific connection interfaces to the micro-milling machine. The layout of the interface board is shown in Figure 4-8.
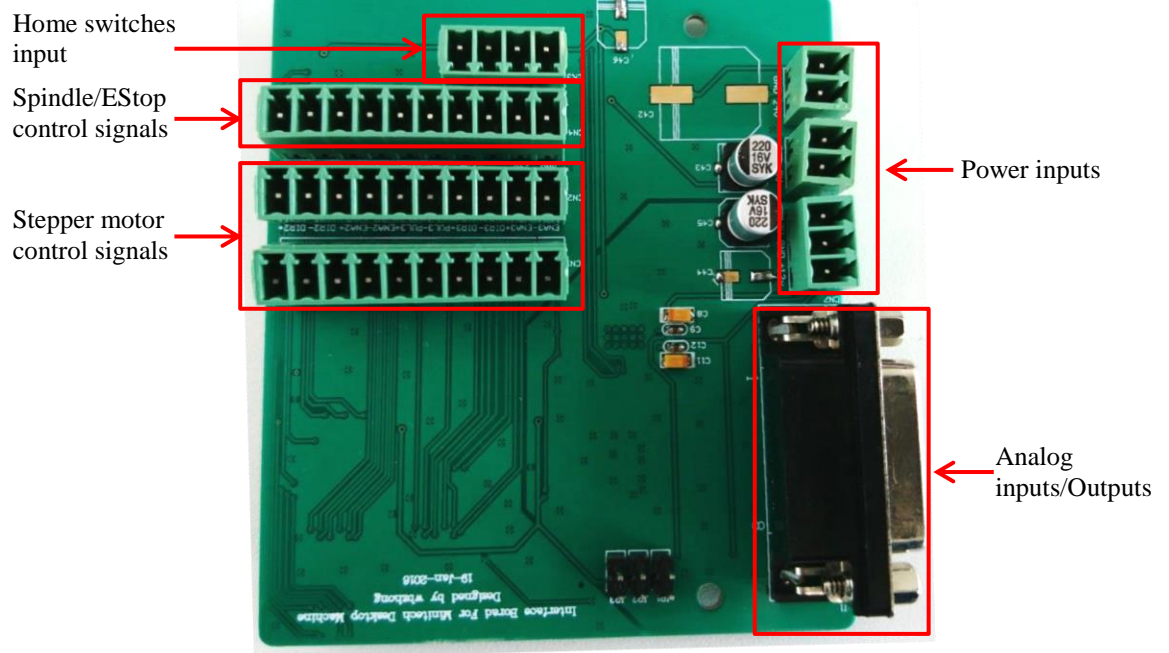
Figure 4-8 The layout of the interface board

Instead of using the common-cathode or common-anode connection method, this thesis adopts the differential line driver (SN75ALS192) to connect the control logic pairs of the stepper motor drive, as shown in Figure 4-9. The differential signal offers better noise immunity especially when the signal distance is long. The differential line driver can convert the single-ended 3.3 V FPGA I/O output to differential signal pair and provides enough current to drive the optocoupler of the motor drive.
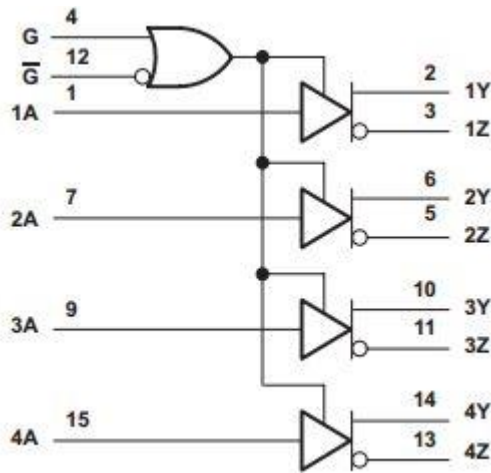
Figure 4-9 The quadruple differential line driver for stepper motor control [107]

The spindle drive control logic inputs and outputs use 24 V level voltage, while the FPGA I/O voltage is 3.3 V and the input and output current is very limited. This thesis uses an optocoupler (ACPL-247) to isolate the microcontroller from the spindle drive, meanwhile, it matches the voltage and current requirements, as illustrated in Figure 4-10. The spindle speed reference voltage is generated by a 16-bit DAC (AD5752R). The DAC connects to the FPGA via a serial interface that operates at clock rates up to 30 MHz, which allows fast voltage output update.
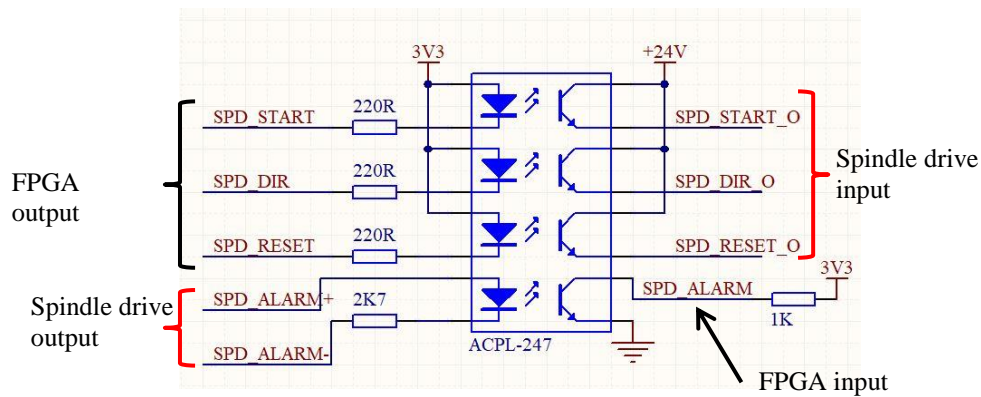
Figure 4-10 Spindle drive control logic connection

The EStop input is used to monitor the state of the emergency stop button. If the EStop input is high, i.e. the button is pressed down, the FPGA will disable the spindle drive and all the stepper motor drives. A high-speed optocoupler (6N137) is

used to isolate the EStop input and convert the 24 V EStop signal to 3.3 V. The optocoupler has a typical delay of 40 ns, which guarantees fast response to the emergency stop event. The home switches are connected similar to the EStop input. They are usually used to determine the home position of each axis when the machine is powered on.

The interface board uses the cost-effective two layers design due to the low density of the components.

4.3.2 Software development

The software development of the microcontroller includes the embedded development of the ARM CPU and the FPGA. The CPU embedded development is carried out using C programming language on an ARM complier, while the FPGA embedded development is performed on an EDA (Electronic Design Automation) software package with Verilog HDL (Hardware Description Language).

4.3.2.1 The CPU embedded development

The complete CPU software includes the user bootloader program and the user firmware program, which are saved in the first and second section of the internal flash memory of the CPU, respectively. The user bootloader replaces the cumbersome JTAG method for upgrading the user firmware, while the user firmware implements the proposed control algorithms. The algorithms are usually developed by numerous trial and error iterations. The user bootloader can significantly accelerate the process to deploy the updated algorithm on the CPU. The CPU has a built-in system bootloader, which can be used for the same purpose. However, the CPU only jumps to the system bootloader at reset with the boot pin at the specific level, while the boot pin is difficult to access when the microcontroller is installed in the cabinet.

The CPU starts executing the user bootloader program by default at power on or after system reset. If no firmware upgrade flag is detected, it will jump to the user

firmware program. Otherwise, the bootloader clears the flag and enters bootloader mode. The user firmware can jump to the user bootloader by setting the firmware upgrade flag in the backup registers and then initiating a software system reset. The contents in the backup registers will not be cleared during system reset.

This thesis uses USB as the communication interface between the microcontroller and PC, because USB has sufficient bandwidth (full-speed: 12Mbs) for this application and provides a 5 V power supply to the CPU board. The bootloader and firmware implement the standard USB Device Firmware Upgrade Class (DFU) and Communications Devices Class (CDC) [108], respectively. The microcontroller is enumerated as different USB devices in bootloader mode and firmware mode, as shown in Figure 4-11. In the bootloader mode, the binary file of the control algorithms generated by the complier can be programmed to the second section of the flash memory. In the firmware mode, the Windows operating system provides standard APIs to read and write the USB device.
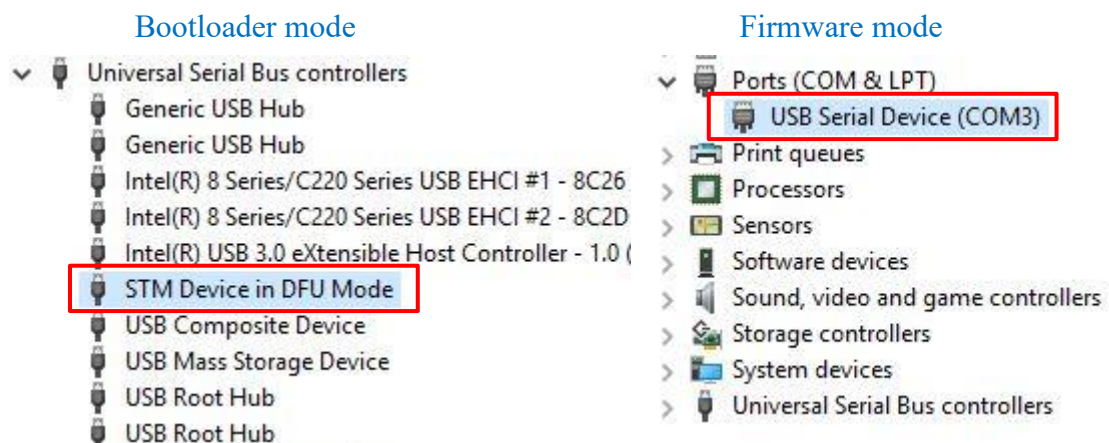
Figure 4-11 The microcontoller USB enumeration in bootloader and firmware mode

The user firmware consists of motion control task and some housekeeping tasks. The motion control task executes the proposed algorithms and feeds the commands to the FPGA, which has the direct control of the spindle drive and stepper motor drives. Housekeeping tasks include system monitoring task and USB communication task. The system monitoring task collects the machine status and microcontroller information, such as command positions, CPU and memory usage etc. The USB

Communication task interprets the data received from PC, coordinates the data transmission to PC, and handles the communication error.

To guarantee the highest real-time performance, all the data will be transmitted to PC asynchronously. For example, the motion task generates some algorithm run-time information that should be sent to PC. It does not need to wait for the transmission to be completed, instead it hands the data block to the USB communication task and continues executing algorithms immediately. The USB communication task has implemented a first-in-first-out (FIFO) structure to coordinate all the data to be sent, as shown in Figure 4-12. The new data will be saved in front of the head of the circular buffer, and the head pointer will then point to the new data. The old data will be extracted from the tail of the buffer to be put on the USB bus when the bus is free, and the tail pointer will move a step forward. If the head caches the tail, it indicates that the buffer is full, and no new data will be accepted. If the tail catches the head, it means the buffer is empty now. A proper buffer size should be set according to the amount of data generated by the tasks.
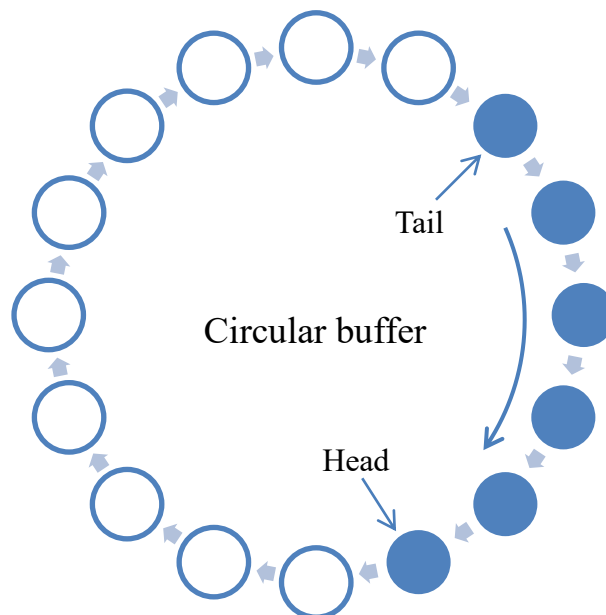
Figure 4-12 FIFO implemented as circular buffer

4.3.2.2 The FPGA embedded development

The CPU treats the FPGA as an external memory, the read and write operations initiated by the CPU will be transformed into waveforms of the external memory bus signals, as shown in Figure 4-13. It is important to configure the memory space, where the FPGA is mapped, non-cacheable and non-bufferable. So that all the commands will be written to the FPGA immediately instead of being stored in the cache, and all the data will be read from the FPGA directly instead of from the buffered data. The FPGA shares the external memory bus with the SDRAM, and the bus operation should be performed very carefully to avoid corrupting data.
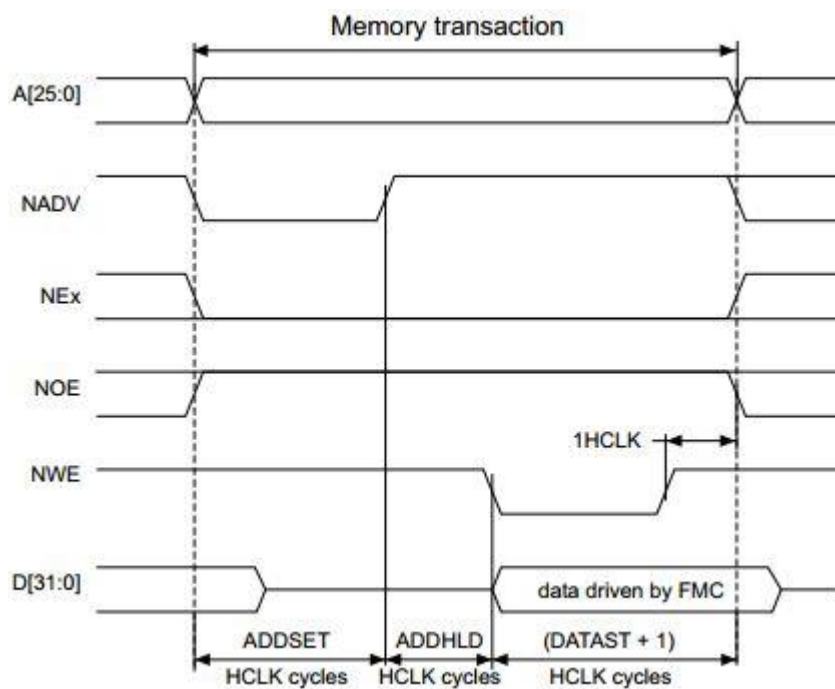
Figure 4-13 The signals waveform when CPU writes data to FPGA [109]

All the signals in Figure 4-13 are inputs for the FPGA, except for the data signals (D[31:0]). The FPGA pins connected with the data signals have three states, as show in Table 4-1. Those pins should be set to input mode during CPU write operations, and output mode during CPU read operations. Otherwise, they are in high impedance.

Table 4-1 External memory bus decoding

	Chip enable input (NEx)	Output enable input (NOE)	Write enable input (NWE)	Data bus (D[31:0])
CPU Write operation	Low	High	Low	Input mode
CPU Read operation	Low	Low	High	Output mode
Idle	High	x	x	High impedance

A communication module is developed to fulfil the CPU read and write operations. It interprets the bus address and dispatches the received data to the corresponding modules or puts the requested data from other modules on the bus. For example, each axis motion control module accepts pulse frequency, direction, and enable commands, and outputs the actual pulse count. A unique address is allocated to each of the data, which ensures correct and efficient data flow.

4.4   The HMI

A simplified HMI is developed for the experiments, as shown in Figure 4-14. A worker thread is running at the background to interpret the received data and format the outgoing data according to the predefine data protocol. The Windows operating system has provided the low level USB communication devices read/write APIs.

The HMI displays the program positions and absolute positions, which are related to the workpiece and the machine coordinates, respectively. The offset values of the workpiece coordinate can be set according the machining requirement. The axes can be jogged using the on-screen buttons in free run mode or distance mode. The parametric curves or linear segments can be added to the microcontroller as the toolpath. When the algorithms start executing those toolpaths, the run-time information of the algorithms will be displayed to assist the analysis of the performance of the algorithms, such as the interpolation lookahead data and toolpath

smoothing errors, etc. When the algorithms are updated, the HMI will command the microcontroller to enter the bootloader mode.
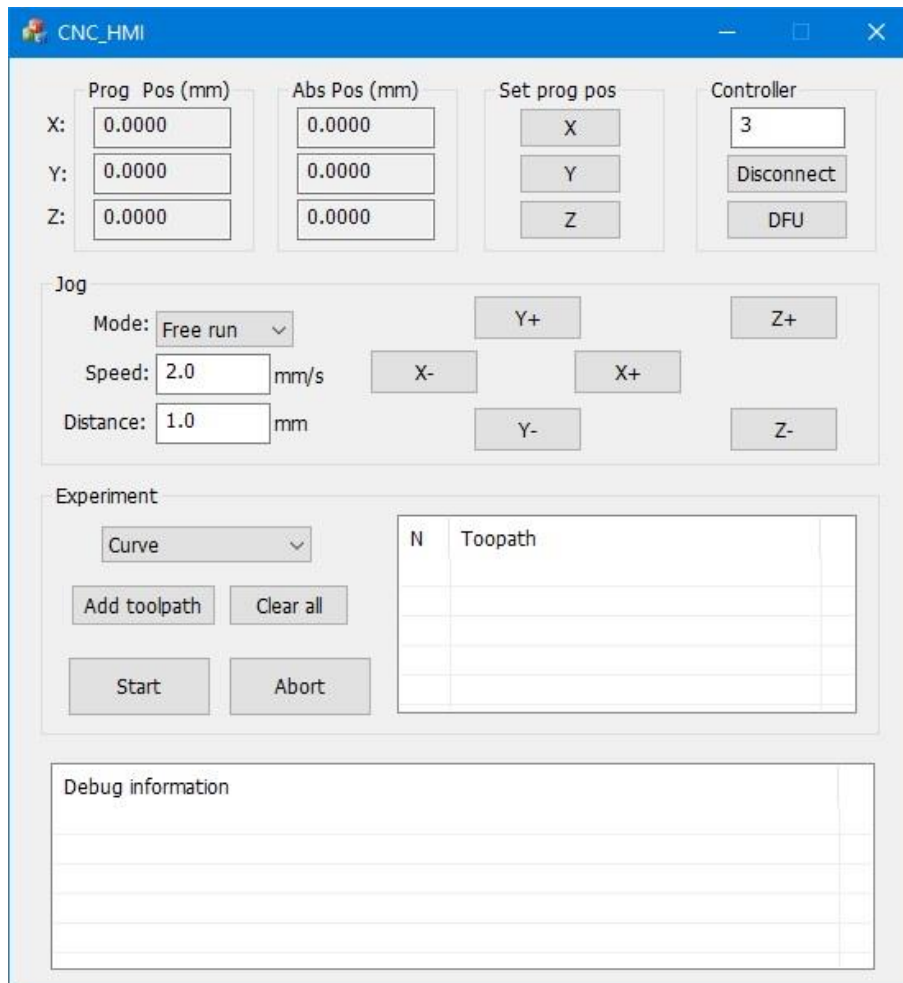
Figure 4-14 The HMI for the experiments

4.5 Summary

This chapter prepares the experimental test-bed for the parametric interpolation algorithm and the toolpath smoothing algorithm, which have been identified as important control approaches for the hybrid micro-machining of 3D micro-products. Those algorithms are fit in the real-time process layer of the proposed novel control architecture, however, the six-axis hybrid machine, which has been integrated, is not open enough to implement those algorithms.

The developed experimental test-bed includes: (1) a three-axis micro-milling machine, which can carry out the freeform machining trials. The open loop control of the machine makes it ideal for the benchmarking of the proposed algorithms. (2) a microcontroller, which can implement the proposed algorithms and control the micro-milling machine to finish the machining trials. The microcontroller consists of a CPU board and an interface board. Extensive embedded development is required for the ARM and FPGA chips on the CPU board. (3) a HMI, which can exchange data with the microcontroller. It helps set up the experiment and analyse the performance of the algorithms.

Chapter 5   Real-time interpolator for parametric curves

5.1   Introduction

This chapter develops the proposed RTIPC which is applicable to not only NURBS but also general parametric curves. The interpolator will fully take into consideration of constraints from machine dynamics (axial velocities, axial accelerations and jerk) and contour error while maintaining the feedrate as high as possible. As concluded in Chapter 2, this thesis will adopt the recursive Taylor's expansion and the lookahead techniques for the development of the RTIPC. However, new techniques such as dynamic lookahead length, the numerical integration error compensation, the multi-cases design for feedrate lookahead and intelligent activation of the acceleration lookahead, are introduced for the first time, which greatly enhance the interpolation efficiency and accuracy.

The numerical simulation is performed to demonstrate the effectiveness of the RTIPC. The real-time performance of the RTIPC is tested on the microcontroller developed in Chapter 4, which shows satisfactory efficiency. Finally, machining trials are carried out in comparison with the industrial standard linear interpolator and the state-of-the-art PVT interpolator.

5.2   Algorithm development

Figure 5-1 shows the overall design of the RTIPC. The parametric curve $C(u)$ is transferred to the RTIPC with proprietary G-code. The lookahead length is calculated as the time of deceleration to a full stop. The feedrate lookahead module checks feedrate limits along the curve. Intermediate results are saved in a buffer to avoid repeated calculation. New data is added when lookahead length exceeds the buffered length, while outdated data is removed. The initial feedrate modification decisions are made by comparing the current and lookahead motion states. Decisions can be

categorized into multi-cases, among which some special cases will bypass future lookahead operations for certain periods of time. Then, the acceleration lookahead module validates the initial decision by checking it against acceleration and jerk limits. The decision will be changed if the limits are to be violated. The acceleration lookahead will be intelligently activated when it is necessary. The final decision is fed to the module that generates servo reference points. A succession of reference points are generated without lookahead operations for special cases.
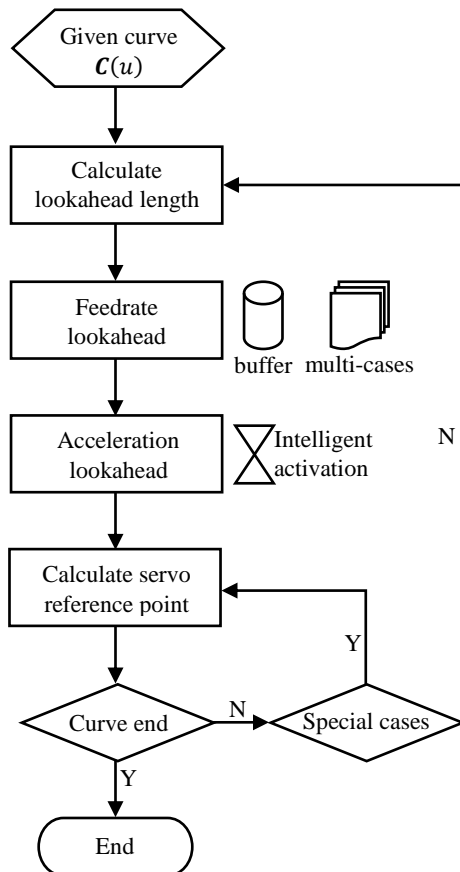
Figure 5-1 Overall design of the RTIPC

5.2.1 Dynamic lookahead length

The lookahead length should be long enough to scan possible feedrate abrupt changing points ahead, so that the interpolator has sufficient distance to schedule a deceleration profile without violating any constraints. However, excessive length results in unnecessary computation load. In the worst case, a full stop is required, e.g.

curve end. So the dynamic lookahead length is calculated as the time required for a full stop. It guarantees reliable response of the RTIPC to any circumstances of the curve, as well as confidence of maintaining high feedrate. Meanwhile, it decreases computation load dramatically compared with constant lookahead length.

Given the current motion state (feedrate F_0 and tangent acceleration $a_{t,0}$), the deceleration profile for a full stop is determined. The conservative tangent deceleration A_t^{csv} is set to the minimum value among axial acceleration limits, it is used as the maximum deceleration value and results in the conservative lookahead length. It can be deduced that if the inequality 5-1 is satisfied, the deceleration profile is a trapezoidal one, as shown in Figure 5-2. Otherwise, the triangular deceleration profile is resulted, as shown in Figure 5-3.

$$\frac{2A_t^{csv\,2} - a_{t,0}{}^2}{2J} < F_0 \qquad\qquad 5\text{-}1$$
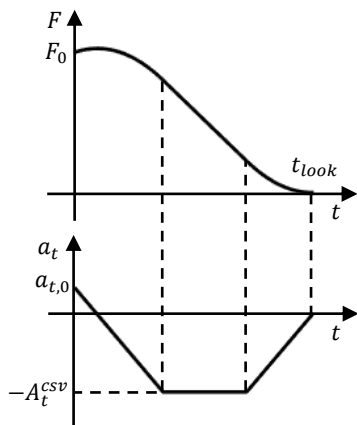
Figure 5-2 Trapezoidal deceleration profile
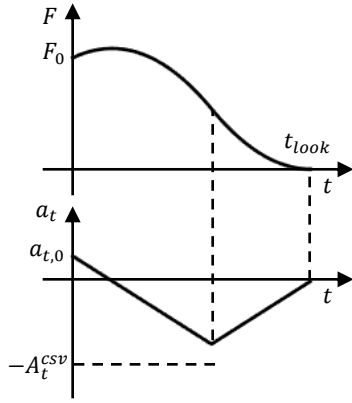
Figure 5-3 Triangular deceleration profile

The tangent acceleration is a piecewise linear function with respect to time, while feedrate is the integral of tangent acceleration over time. In case of the trapezoidal profile, the lookahead length is calculated by

$$t_{look} = \frac{F_0}{A_t^{csv}} + \frac{a_{t,0} + A_t^{csv}}{J} + \frac{a_{t,0}^2}{2A_t^{csv}J}$$

5-2

In case of the triangular profile, the lookahead length is given by

$$t_{look} = \frac{a_{t,0} + \sqrt{4F_0 J + 2a_{t,0}^2}}{J}$$

5-3

The number of lookahead points is the quotient of t_{look} divided by T.

5.2.2 Feedrate limit

The feedrate limit module has considered the command feedrate, the maximum axial velocity limits, contour error tolerance, and centripetal acceleration limit. Moreover, it has the flexibility to add other constraints.

Firstly, the feedrate should not exceed the command feedrate, as the command feedrate is specified by the user with the consideration of the process.

$$F_{lmt,1} = F_{cmd}$$

5-4

where $F_{lmt,i}$ denotes the ith feedrate limit, and F_{cmd} is the command feedrate specified by the user.

The second constraint on feedrate is the maximum axial velocity.

$$F_{lmt,2} = \min\left[\frac{V_x}{|\alpha|} \quad \frac{V_y}{|\beta|}\right] \qquad 5\text{-}5$$

where $\min[\ ]$ denotes the minimum value in the square bracket, V_i is the maximum velocity of axis i, α and β are the first derivative factors given by

$$\begin{cases} \alpha = \dfrac{\dot{x}(u)}{\|\dot{C}(u)\|} \\ \beta = \dfrac{\dot{y}(u)}{\|\dot{C}(u)\|} \end{cases} \qquad 5\text{-}6$$

Figure 2-8 gives the third constraint which is the contour accuracy.

$$F_{lmt,3} = \frac{2}{T}\sqrt{2\rho\varepsilon - \varepsilon^2} \qquad 5\text{-}7$$

where ρ is the radius of curvature, it can be calculate by the curvature formula with the first and second derivatives of the curve. Since centripetal acceleration is proportional to the square of feedrate, limiting feedrate helps to reduce the risk of acceleration saturation. Representing axial accelerations with tangent acceleration a_t and centripetal acceleration a_n yields

$$\begin{cases} a_x = \alpha a_t - \beta a_n \\ a_y = \beta a_t + \alpha a_n \end{cases} \qquad 5\text{-}8$$

The acceleration values in Eq. 5-8 are signed scalars. Positive a_x and a_y indicate accelerations toward positive axis directions, while a positive a_t means feedrate is increasing. Particularly, a_n has the same sign as the signed curvature. Apply triangle inequality rule to Eq. 5-8 yields

$$\begin{cases} |a_x| \le |\alpha a_t| + |\beta a_n| \le A_x \\ |a_y| \le |\beta a_t| + |\alpha a_n| \le A_y \end{cases} \qquad 5\text{-}9$$

Where A_i is the maximum acceleration of axis i. From Eq. 5-9 the limit of a_n can be given by

$$\begin{cases} |\beta a_n| \leq \lambda A_x \\ |\alpha a_n| \leq \lambda A_y \end{cases} \quad \lambda \in (0,1) \qquad 5\text{-}10$$

where λ is a safety factor, the lower λ is, the lower centripetal acceleration will be. Considering the relationship between a_n and F, the fourth feedrate limitation is given by

$$F_{lmt,4} = min\left[\sqrt{\frac{\lambda \rho A_x}{|\beta|}} \quad \sqrt{\frac{\lambda \rho A_y}{|\alpha|}} \right] \qquad 5\text{-}11$$

Combining all the limits together, the final limit of feedrate for a point on the curve is given by

$$F_{lmt} = min[F_{lmt,1} \quad F_{lmt,2} \quad F_{lmt,3} \quad F_{lmt,4}] \qquad 5\text{-}12$$

F_{lmt} will be used in the feedrate lookahead module. It is simple to achieve other features, such as cutting force limit, by adding the extra constraints in Eq. 5-12. As the cutting force is closely related to the actual feedrate.

5.2.3 Acceleration limit

Tangent acceleration is usually used to schedule the feedrate and confine axial accelerations. Transform Eq. 5-8 yields the representation of a_t

$$\begin{cases} a_t = \dfrac{a_x}{\alpha} + \dfrac{\beta}{\alpha} a_n \\ a_t = \dfrac{a_y}{\beta} - \dfrac{\alpha}{\beta} a_n \end{cases} \qquad 5\text{-}13$$

In Eq. 5-13, a_n is determined by the expected feedrate and the radius of curvature at one point on the curve. a_t reaches its limit when one of the axes saturates in acceleration, the maximum tangent acceleration is given by

$$A_t^{max} = min\left[\frac{A_x}{|\alpha|} + \frac{\beta}{\alpha}a_n \quad \frac{A_y}{|\beta|} - \frac{\alpha}{\beta}a_n\right]$$ 5-14

And the minimum tangent deceleration is given by

$$A_t^{min} = max\left[-\frac{A_x}{|\alpha|} + \frac{\beta}{\alpha}a_n \quad -\frac{A_y}{|\beta|} - \frac{\alpha}{\beta}a_n\right]$$ 5-15

Where $max[\,]$ denotes the maximum value in the square bracket. Particularly, A_t^{min} is set to $-A_t^{csv}$ when it is higher than the later, this is to guarantee that feedrate can be decreased fast enough to avoid violating feedrate limits in rare cases. A_t^{max} and A_t^{min} will be used in the acceleration lookahead module.

5.2.4 Numerical integration error

Integration plays an important role in lookahead operations, as feedrate is the integral of tangent acceleration over time, while distance is the integral of feedrate over time. However, the numerical integration error used in the digital interpolator has always been ignored by existing works. According to the integral rules

$$\begin{cases} a_t = a_{t,0} \pm Jt \\ F = F_0 + \int_0^t a_t\,dt = F_0 + a_{t,0}t \pm \frac{1}{2}Jt^2 \\ S = \int_0^t F\,dt = F_0 t + \frac{1}{2}a_{t,0}t^2 \pm \frac{1}{6}Jt^3 \end{cases}$$ 5-16

where plus is used if a_t is to be increased, otherwise minus is used. However, for digital interpolators, those values are accumulated at each interpolation period

$$\begin{cases} a_{t,k} = a_{t,k-1} \pm JT \\ F_k = F_{k-1} + a_{t,k}T \\ \Delta S_k = F_k T \end{cases}$$ 5-17

where $a_{t,k}$, F_k and ΔS_k denote the tangent acceleration, feedrate and distance increment in the kth interpolation period, respectively. If Eq. 5-16 were adopted to estimate feedrate and distance-to-go in lookahead operations, the results would deviate from actual output values calculated by the interpolator. The error

80

accumulates with time, and will cause undesirable motion profiles due to incorrect lookahead outcome. One possible solution is to decrease the interpolation period further, so that the numerical integration error will accumulate more slowly. However, this solution imposes much more computation load on the interpolator. For the RTIPC, a new approach is developed, iterating Eq. 5-17 yields

$$\begin{cases} a_{t,N} = a_{t,0} \pm NJT \\ F_N = F_0 + Na_{t,0}T \pm \frac{1}{2}N(N+1)JT^2 \\ S_N = NF_0T + \frac{1}{2}N(N+1)a_{t,0}T^2 \pm \frac{1}{6}N(N+1)(N+2)JT^3 \end{cases} \qquad 5\text{-}18$$

where S_N is the total distance that will be travelled in N interpolation periods. The result of Eq. 5-18 will be identical to the output of the interpolator, which guarantees accurate and reliable lookahead operations.

5.2.5 Feedrate lookahead

The feedrate lookahead module with multi-cases design is introduced for the first time. The lookahead operation takes place at every interpolation period, but when special cases occur, it can be skipped for certain periods, which will increase the efficiency significantly. Figure 5-4 shows the algorithm of the feedrate lookahead module, three cases are resulted by comparing F_{lmt} at the lookahead point and F_0 at current point. Case A implies that the feedrate can be increased, Case B represents that the feedrate is supposed to be decreased, and Case C suggests that the feedrate keep constant. The feedrate lookahead loop ends when either one of the cases concludes an exit situation or the lookahead length reaches its end.
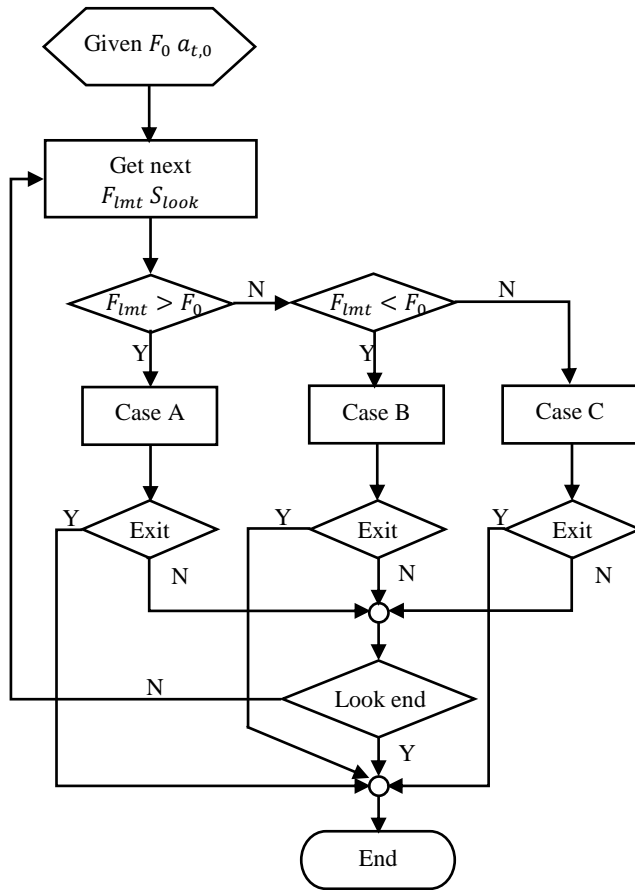
Figure 5-4 Algorithm for the feedrate lookahead module

5.2.5.1 Case A: Feedrate increases

Figure 5-5 illustrates the algorithm for Case A. If the current feedrate is increasing, it is vital to check whether the acceleration should be decreased immediately to avoid feedrate overshoot. Suppose that the feedrate reaches F_{lmt} after N interpolation periods, N becomes the independent variable in the second function of Eq. 5-18, which yields

$$\frac{JT^2}{2}N^2 + \left(\frac{JT^2}{2} - a_{t,0}T\right)N + F_{lmt} - F_0 = 0 \qquad 5\text{-}19$$

If the discriminant Δ is less than zero, it implies that the target feedrate cannot be reached, which results in Case A.1, where some distance is still available to increase the feedrate further. Otherwise, the target feedrate can be reached twice, as shown in Figure 5-6, the roots are N_1 and N_2 respectively. If the lookahead distance S_{look} falls

between distance-to-go S_{N1} and S_{N2}, the actual feedrate at the lookahead point will exceed F_{lmt}, which leads to Case A.2, where feedrate increasing rate must be lowered, the feedrate lookahead loop can exit in advance. Note that Case A.2 is a special case, the lookahead operations will be bypassed for $N1$ interpolation periods. If S_{look} falls outside the span, the actual feedrate at the lookahead point will be lower than F_{lmt}. Case A.3 deals with the situation that current feedrate is decreasing, the deceleration rate can be decreased to achieve a U-turn of tangent acceleration. Case A.4 deals with the situation that current feedrate is constant, it suggests initiating acceleration again.
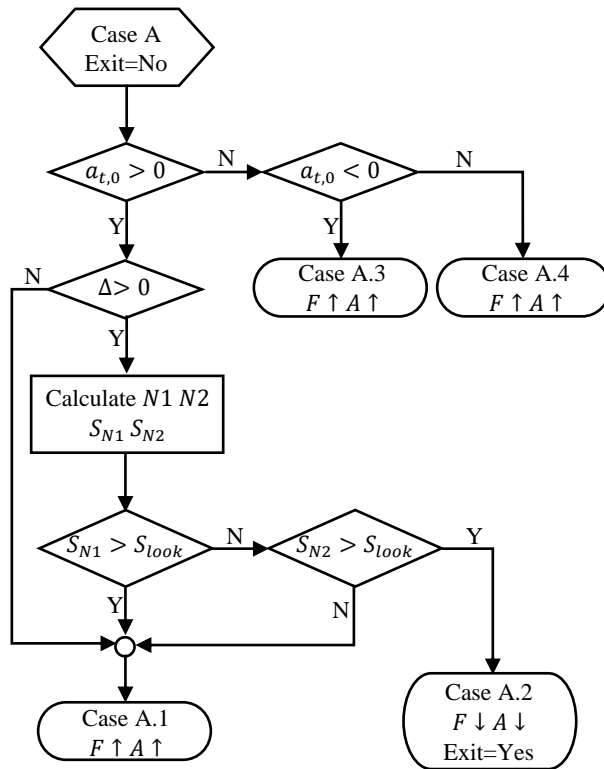
Figure 5-5 Algorithm for Case A
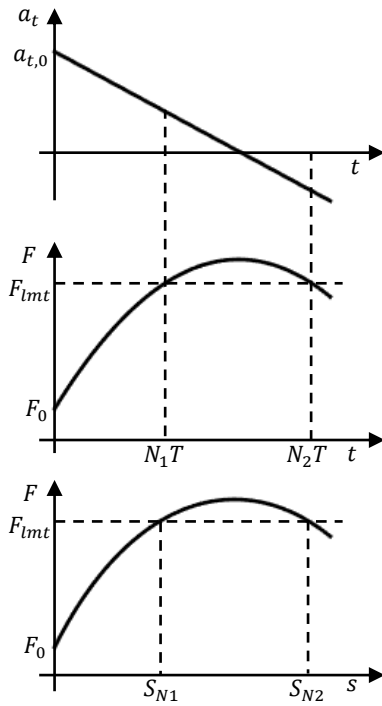
Figure 5-6 Increase feedrate while decreasing acceleration

5.2.5.2 Case B: Feedrate decreases

Figure 5-7 shows the algorithm for Case B. When the feedrate is expected to be lowered, it is of great importance to check whether the acceleration should keep decreasing to avoid possible violation. There is only one valid root for Eq. 5-19, as shown in Figure 5-8. If the planned deceleration distance is longer than S_{look}, the actual feedrate at the lookahead point will exceed F_{lmt}, which are Case B.1 and B.3, the acceleration must keep decreasing and the lookahead operation can exit now. Otherwise, there are some distance to boost the feedrate. Note that the allowable deceleration value varies with curvature, when the planned deceleration exceeds A_t^{csv}, there is a risk of saturating axes in acceleration. In this case, a simulation of the deceleration process is necessary to determine the distance-to-go accurately, i.e. calculate N' and $S_{N'}$. It usually happens when F_{lmt} is much lower than the current feedrate, e.g. curve end. Both Case B.1 and B.3 are special cases. Case B.1 can bypass N lookahead operations, while Case B.3 can bypass lookahead operations until the actual deceleration reaches A_t^{csv}.
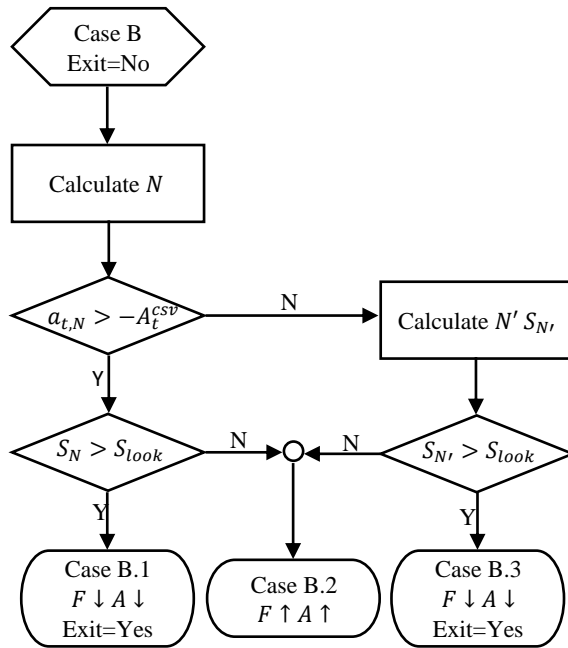
Figure 5-7 Algorithm for Case B
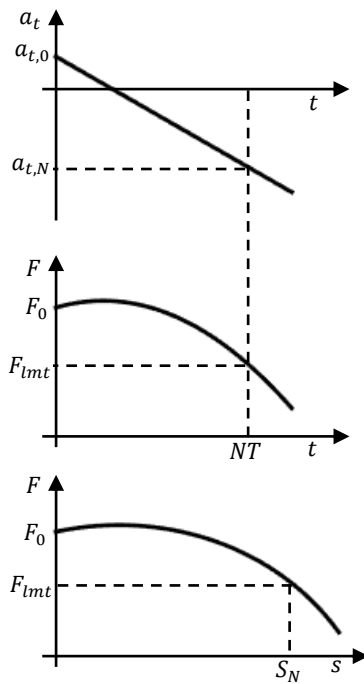
Figure 5-8 Decrease feedrate with decreasing acceleration

Particularly, a three-stage stop strategy is used when approaching the curve end. The interpolator will increase the jerk slightly in the first stage to decelerate to a low

feedrate, then keep the low feedrate in the second stage, and at last applying a triangular deceleration profile to a full stop. This strategy can avoid the situation that feedrate drops to an extremely low value before the end and takes long time to the end, or motion stops abruptly at the end with relatively high feedrate.

5.2.5.3 Case C: Feedrate is constant

When the feedrate is suggested to keep constant, the tangent acceleration should be scheduled toward zero. The concluded cases here are not mandatory. Particularly, if the lookahead operation reaches the end but no special case occurs, the predominant case will be issued to the next module.

5.2.6 Acceleration lookahead

Like the feedrate lookahead operation, it is not necessary to perform the acceleration lookahead at each interpolation period when there is no risk of violation of the acceleration or jerk limits. This measure can significantly reduce computational load. The acceleration lookahead module is only activated when one of the following feedrate modification decisions is issued:

(1) Increase feedrate with increasing acceleration, while the tangent acceleration is close to A_t^{max};

(2) Decrease feedrate with decreasing acceleration, while the deceleration value exceeds A_t^{csv}.

For other situations, this module is deactivated to decrease the computation burden. The curvature varies along the curve, so does the acceleration limits. Suppose that the acceleration is increasing, it is vital to check whether it is the time to decrease it to avoid possible saturation.

$$a_{t,0} - iJT > A_{t,i}^{max} \qquad 5\text{-}20$$

Where $A_{t,i}^{max}$ is the maximum acceleration at the ith lookahead point, which is given by Eq. 5-14. If this inequality is true, it means that even the acceleration is decreased from now, the limit at the lookahead point will be violated. The tangent acceleration should be reduced immediately in this case, otherwise the original decision can be kept. Similarly, suppose that the acceleration keeps decreasing, the below criterion is used to check possible violation.

$$a_{t,0} + iJT < A_{t,i}^{min} \qquad\qquad 5\text{-}21$$

The final lookahead result will be used to calculate the feedrate for the next interpolation period, and the servo reference point can be calculated with the feedrate value using the second-order approximation of the Taylor's expansion.

The feedrate lookahead and acceleration lookahead operations can be unstable at some noisy curve points with extremely high curvature. These points can be treated as curve end point, i.e. decelerating the feedrate to zero at these points and accelerating the feedrate again for the remaining path.

5.3   Numerical experiments

Demonstration software has been developed to implement the proposed RTIPC algorithm. The software open access information is in the Appendix A. Specifying the curve definition as input, the software will generate the actual servo reference point set, as well as internal feedrate lookahead and acceleration lookahead data. The numerical simulation is performed to study the characteristics of the scheduled motion profiles, and to show the effectiveness of the lookahead operations. The interpolator parameters are set as shown in Table 5-1, and the command feedrate is 20 mm/s.

Table 5-1 Interpolator parameters for the numerical experiments

X/Y velocity limit (mm/s)	X/Y acceleration limit (mm/s^2)	Jerk limit (mm/s^3)	Contour error tolerance (µm)

30	30	200	0.01

Two typical parametric curves are selected for both numerical simulation and experimental validation. The teardrop curve is an example of polynomial curves, which are usually used in curve fitting. The ribbon curve is an example of B-splines, which are used in geometric data exchange. The teardrop curve is given by

$$\begin{cases} x(u) = -150u + 450u^2 - 300u^3 \\ y(u) = -150u + 150u^2 \end{cases} \quad u \in [0,1] \qquad \text{5-22}$$

Figure 5-9 shows the interpolation results of the teardrop curve. The curvature reaches the maximum value for the first time at point A, as shown in Figure 5-9(a). The feedrate is limited to the lowest value at point A accordingly, as shown in Figure 5-9(c). The interpolator plans s-shaped feedrate profiles at the beginning and end of the curve, as shown in Figure 5-9(b). In contrast to the linear or circular interpolation, the tangent acceleration limit varies during the s-shaped profile planning, as shown in zone 1 and 7 of Figure 5-9(d), which makes it extremely difficult to decide when the tangent acceleration should be increased or decreased to avoid feedrate overshoot or undershoot. This problem is solved by the lookahead operations and the numerical integration technique. The three-stage stop strategy helps to achieve the accurate and smooth stop, as shown in zone 2 of Figure 5-9(b).

The feedrate is maintained as high as possible, and the fluctuation is minimized, as shown in Figure 5-9(c). The smoothness of the feedrate comes from the confined jerk, as shown in Figure 5-9(f). The tangent acceleration reaches limit when one of the axes saturates in acceleration, as shown in Figure 5-9(d) & (e). The acceleration of X axis exceeds the limit slightly in zone 6 of Figure 5-9(e), because the interpolator has a delay when reacting to the error, just like any other digital controller.

(a) Feedrate variation along the curve

(b) Velocity profile

(c) Feedrate lookahead

(d) Acceleration lookahead

(e) Acceleration profile

(f) Jerk profile
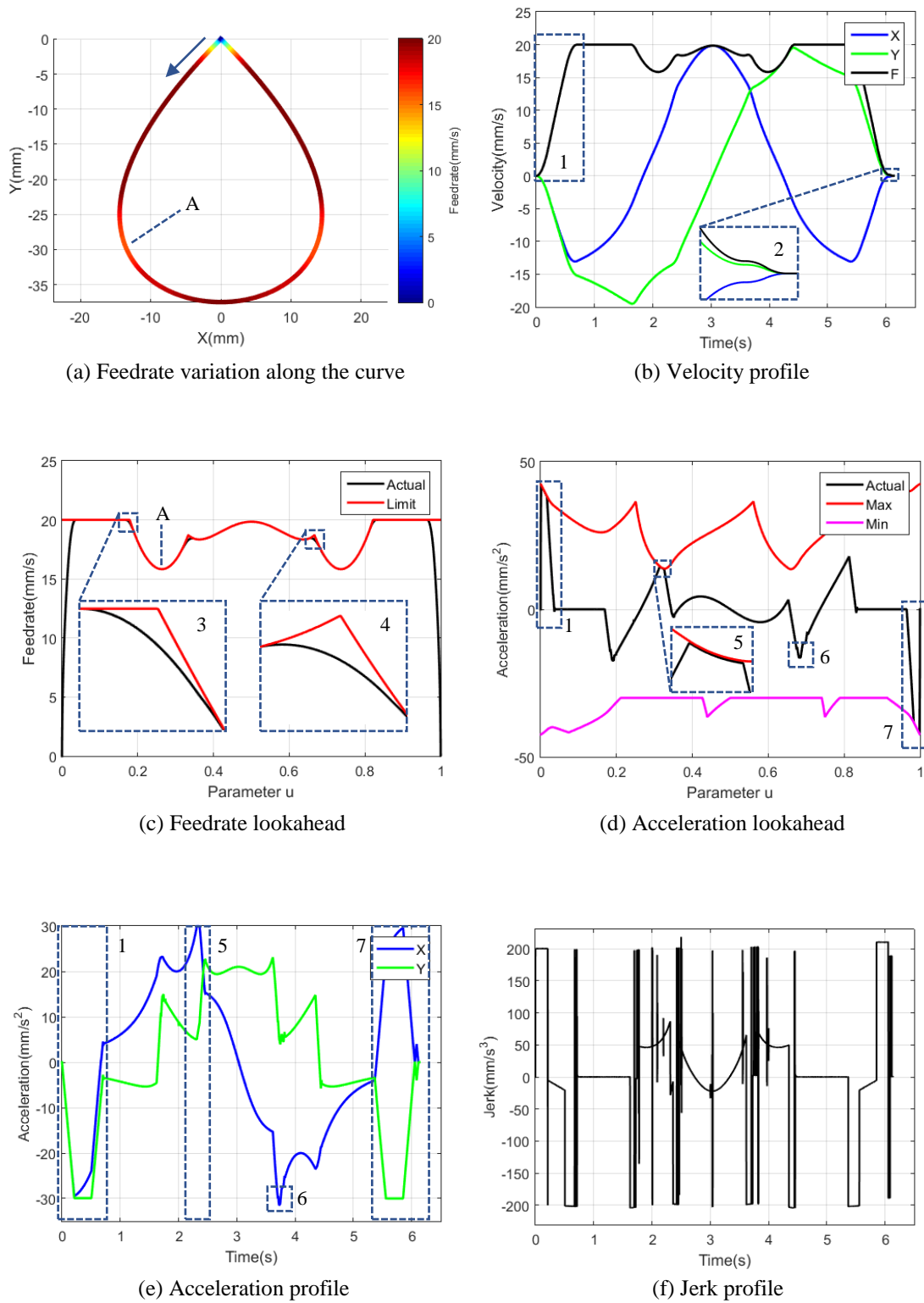
Figure 5-9 Interpolation results of the teardrop curve

The ribbon curve is constructed by a 3rd degree B-spline with control points

$$\{\boldsymbol{P_i}\} = \{(-15,0), (20,30), (0,50), (-20,30), (15,0)\}$$

and knot vector

$$U = \{0,0,0,0,0.5,1,1,1,1\}$$

Figure 5-10 shows the interpolation results of the ribbon curve. Both examples achieve smooth velocity profiles and confined axial accelerations and jerk profiles. Actually, the time-optimal solution of the interpolation for parametric curves is that at least one of the values reaches its limit at any time in the velocity, acceleration and jerk profiles, and the RTIPC achieves the near time-optimal solution, as shown in Figure 5-10 (b), (e) and (f).

(a) Feedrate variation along the curve   (b) Velocity profile

(c) Feedrate lookahead   (d) Acceleration lookahead

90
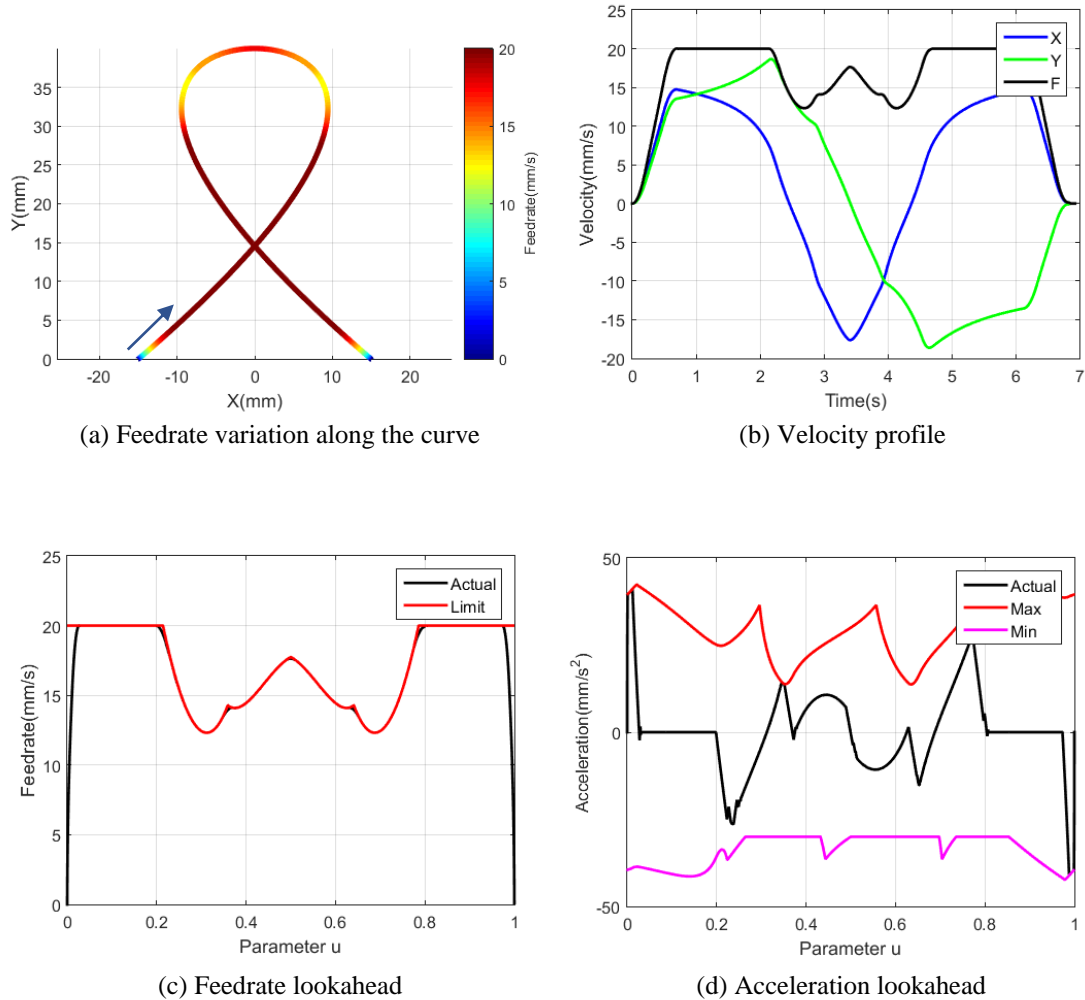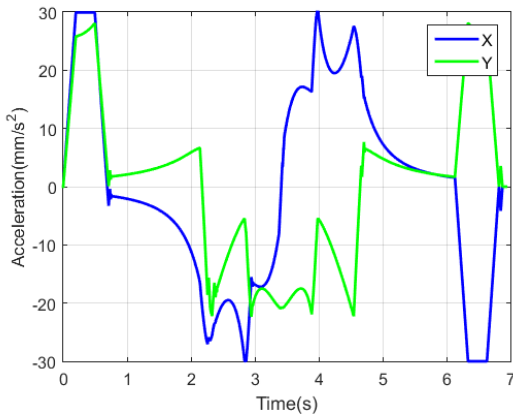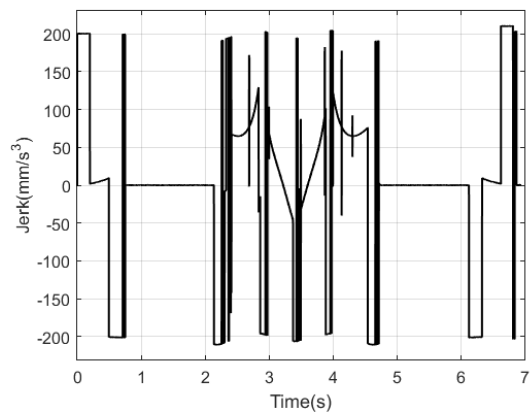
(e) Acceleration profile   (f) Jerk profile

Figure 5-10 Interpolation results of the ribbon curve

Figure 5-11 shows the contour error of the interpolation for both curves. The error is small at the beginning and end as the feedrate and curvature are small. The error increases with increasing feedrate and reaches the maximum value at the points with largest curvature. The maximum contour error for both curves is below 4 nm, which is within the tolerance (10 nm).
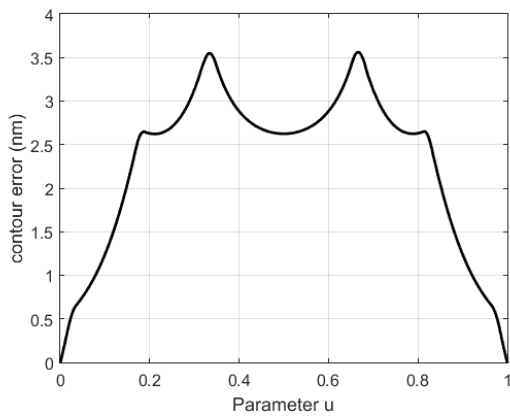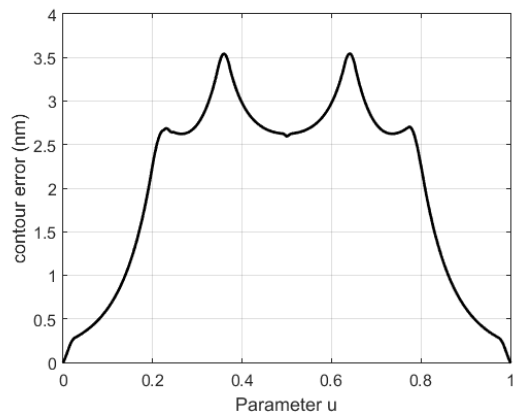
(a) Teardrop   (b) Ribbon

Figure 5-11 Contour error of the interpolation

5.4   Real-time performance test

The real-time performance test is performed to show how efficient the RTIPC is. The RTIPC has been implemented in the aforementioned microcontroller. The same interpolator parameters shown in Table 5-1 are used. The command feedrate is set as 2 mm/s. Table 5-2 shows the interpolation time for both curves using the controller. The average cycle time, i.e. the time to compute an interpolation point, for both curves is around 1 ms. Due to the complexity of B-spline evaluation, the ribbon curve consumes more cycle time. Note that the algorithm is implemented using double floating point arithmetic to ensure the best accuracy. However, the currently used microcontroller does not have a built-in double floating point unit, which can boost the algorithm execution by 7.2 times [110]. The real-time performance test on the current controller has demonstrated that the developed interpolator is efficient enough to achieve the real-time characteristic on a more advanced controller, such as the multi-core digital signal processor with built-in double floating point unit.

Table 5-2 The RTIPC real-time performance test

Curve	Teardrop	Ribbon
Total points	51176	55342
Total time (ms)	37236	62846
Max. cycle time (ms)	4	11
Average cycle time (ms)	0.728	1.136

5.5   Machining experiments

5.5.1 Machining trial setup

To further assess the performance of the RTIPC, a series of machining experiments are carried out on the experiment platform developed in Chapter 4. The machining results will be compared with the results obtained from the Delta Tau Power PMAC controller, which has the industrial standard linear interpolator and the state-of-the-art PVT interpolator.

In addition to the two parametric curves used in the numerical experiments, a cubic phase plate freeform surface, as shown in Figure 5-12, is also machined, which has wide applications in optics. The surface is defined by

$$z = 0.007(x^3 + y^3) \; x \in [-5, 5] \; y \in [-5, 5] \qquad 5\text{-}23$$

The profile of the surface in XZ plane is a polynomial curve, which is given by Eq. 5-24. The toolpath for the finish machining of the surface can be composed of a series of polynomial curves by spacing Y uniformly.

$$\begin{cases} x(u) = u \\ z(u) = 0.007y^3 + 0.007u^3 \end{cases} \; u \in [-5, 5] \qquad 5\text{-}24$$

(a) The cubic phase plate   (b) The surface profile at $y = 0$
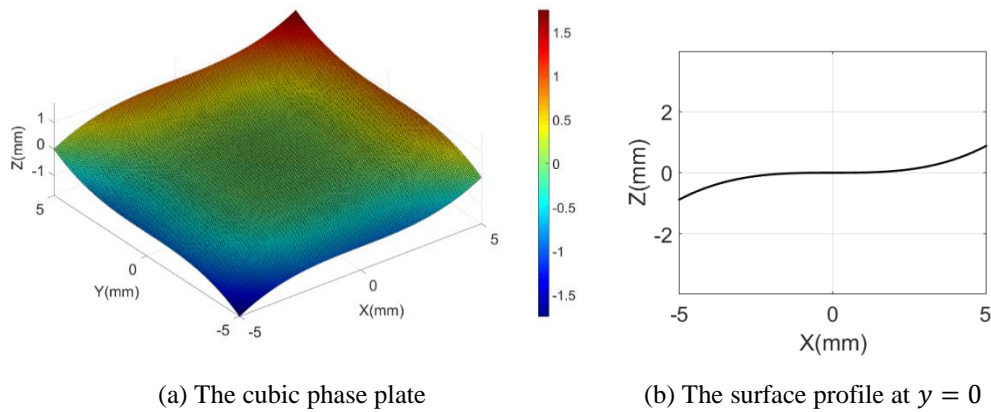
Figure 5-12 The cubic phase plate freeform surface

A command feedrate of 2 mm/s, a spindle speed of 12,000 rpm, a depth of cut of 0.1 mm, and a milling cutter with a diameter of 2 mm are used in the curve machining experiment. A 1 mm diameter ball end mill is used in the finish machining of the freeform surface, while the machining allowance and the cutting width along Y axis are 20 µm and 10 µm, respectively. The workpiece material is aluminum. In this thesis, proprietary G-codes are developed for the RTIPC. The CAM software – Pro/ENIGNEER Wildfire 4.0 is used to generate the linear interpolation code. As the CAM does not support PVT interpolator, a customized program is developed to generate PVT code for those curves and the surface.

5.5.2 Machining trial results

Table 5-3 - Table 5-5 list the machining codes and machining times for the specified curves and surface. The RTIPC can reduce the code size in three orders of magnitude compared with the linear interpolator and two orders of magnitude compared with the PVT interpolator. In addition, the RTIPC code is much more concise and readable. The RTIPC is as productive as the PVT interpolator, both can achieve up to ten times productivity increase over the linear interpolator. The machined workpieces are shown in Figure 5-13 - Figure 5-15.

Table 5-3 The teardrop curve interpolation comparison

	RTIPC	Linear	PVT
NC code	G06.1 X{-150*U+450*U^2-300*U^3} Y{-150*U+150*U^2} U[0 1] F2	G01 X-.066 Y-.066 F2 X-.133 Y-.133 X-.198 Y-.199 X-.264 Y-.265 ⋮	PVT200 X-0.2823:-1.4088 Y-0.2834:-1.4196 X-0.5635:-1.4033 Y-0.5678:-1.4250 X-0.8436:-1.3977 Y-0.8534:-1.4305 ⋮
Line count	1	2324	256
Machining time (s)	51.2	489.4	51

Table 5-4 The ribbon curve interpolation comparison

	RTIPC	Linear	PVT
NC code	G06.2 K0 X-15 Y0 F2	G01 X-14.902 Y.084 F2	PVT200
	K0 X20 Y30	X-14.815 Y.159	X-14.6965:1.5162
	K0 X0 Y50	X-14.721 Y.239	Y0.2606:1.3043
	K0 X-20 Y30	X-14.634 Y.315	X-14.3935:1.5138
	K0.5 X15 Y0	⋮	Y0.5217:1.3070
	K1		X-14.0910:1.5114
	K1		Y0.7834:1.3098
	K1		⋮
	K1		
Line count	9	2641	277
Machining time (s)	55.3	556.9	55.2

Table 5-5 The cubic phase plate interpolation comparison

	RTIPC	Linear	PVT
NC code	G06.1 X{U} Y{-0.875+0.007*U^3} U[-5 5] F2	G01 X4.7261 Z-.0219 F2	PVT100
	G01 Y-4.99 Z0.005 F2	X4.6657 Z-.0524	X-4.8216:1.7973
	G06.1 X{-U} Y{-0.87-0.007*U^3} U[-5 5] F2	X4.605 Z-.0822	Z-1.6596:0.8774
	⋮	X4.5441 Z-.1114	X-4.6406:1.8223
		⋮	Z-1.5746:0.8241
			X-4.4572:1.8458
			Z-1.4948:0.7701
			⋮
Line count	2001	122070	54068
Machining time (s)	5640	20820	5400

(a) RTIPC　　　　　　　(b) Linear　　　　　　　(c) PVT
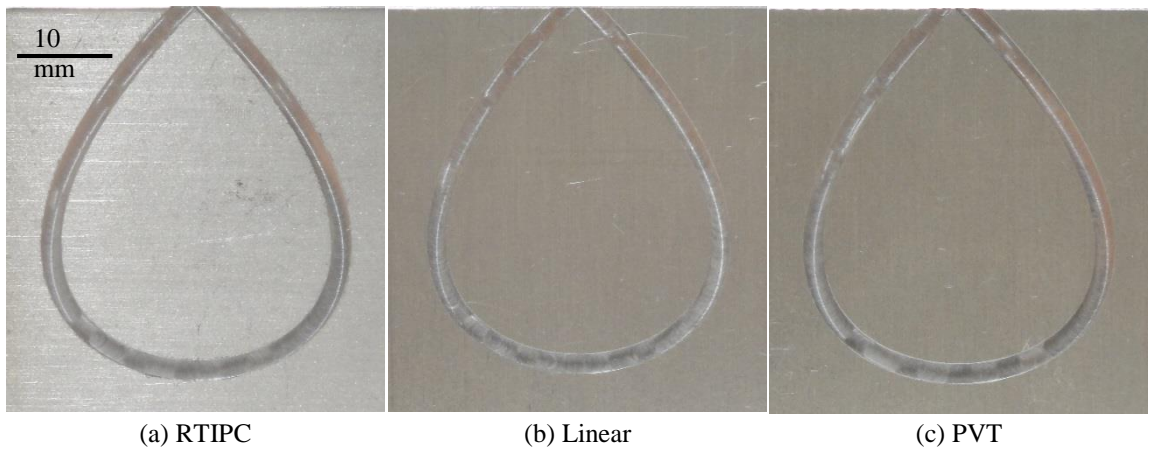
Figure 5-13 The teardrop curve machined workpieces

(a) RTIPC　　　　　　　(b) Linear　　　　　　　(c) PVT
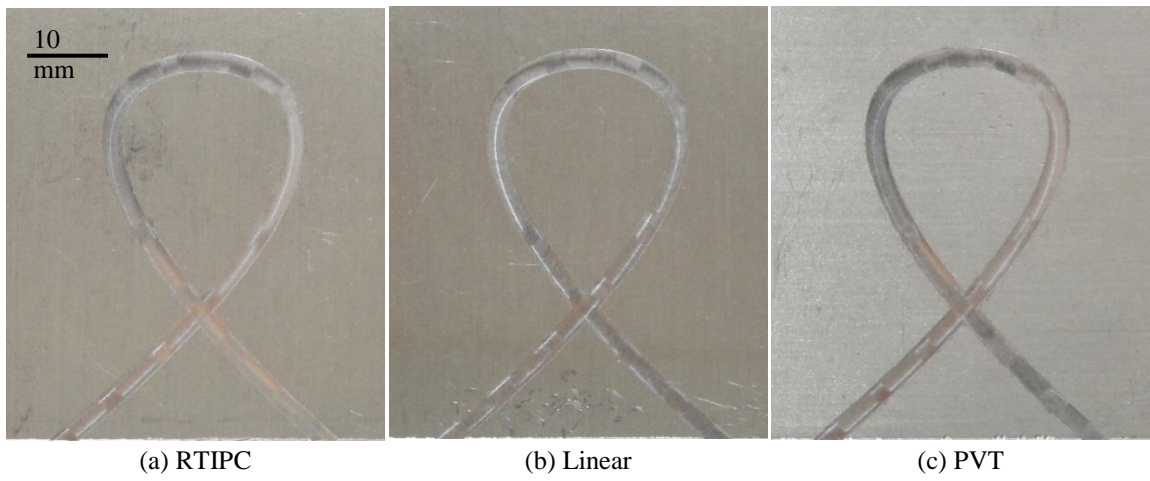
Figure 5-14 The ribbon curve machined workpieces

(a) RTIPC　　　　　　　(b) Linear　　　　　　　(c) PVT
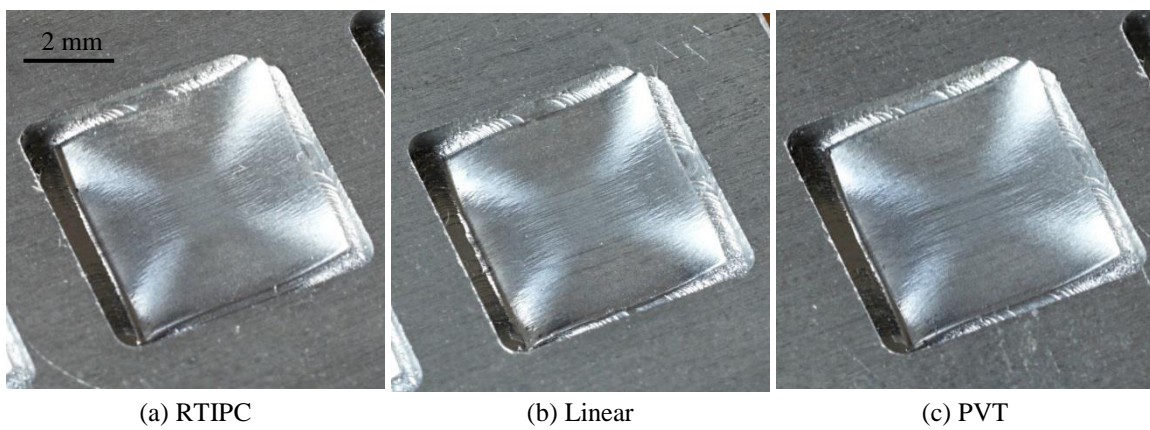
Figure 5-15 The cubic phase plate machined workpieces

5.5.3 Discussions

In addition to the code simplicity and machining efficiency, the RTIPC is also superior to the linear interpolation and PVT interpolation in terms of motion smoothness. Figure 5-16(a) shows the motion profiles of linear interpolation for the first segment of the teardrop curve. Triangular acceleration profile is observed as the segment is too short. The attainable feedrate is 0.933 mm/s which is much lower than the target value (2 mm/s). Moreover, such motion profiles occur in each segment, which decreases average feedrate and causes vibration.

The feedrate and acceleration profiles in each PVT segment are a quadratic polynomial and a linear function respectively, as can be deduced from Eq. 2-9. Although feedrate and acceleration are continuous within the segment, they are not necessarily continuous at the boundaries, as the coefficients in Eq. 2-9 vary for different segments. Figure 5-16(b) shows the motion profiles of PVT interpolation for the first two segments of the teardrop curve, each segment takes 0.2s. The feedrate is maintained to be higher than the linear interpolation, but it is not smooth at the boundaries, and overshoot is observed. Moreover, the discontinuity of acceleration leads to infinite jerk, which causes shock to the machine.

(a) Linear interpolator   (b) PVT interpolator
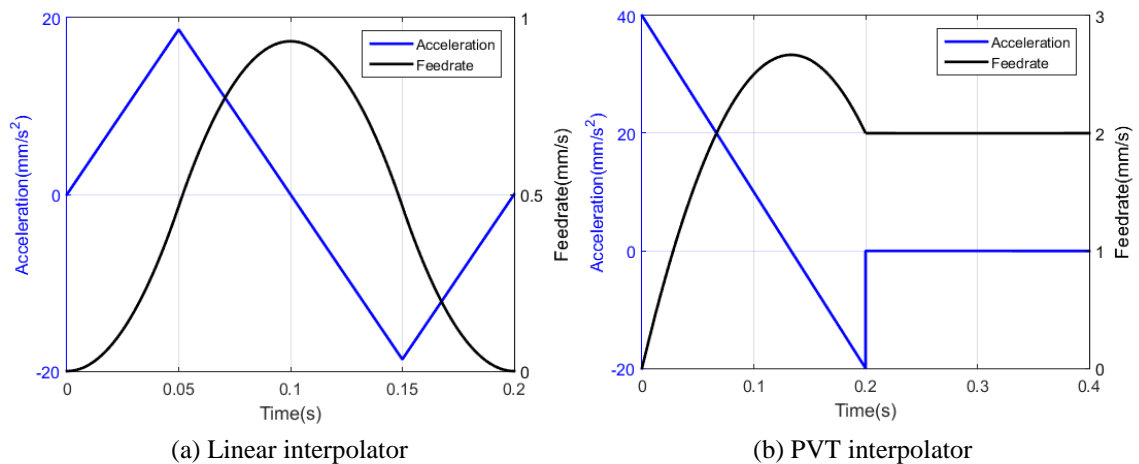
Figure 5-16 Feedrate and acceleration fluctuation of the linear and PVT interpolators

97

Figure 5-17 shows the surface topography at the center of the cubic phase plate measured by a white light interferometer (Zygo CP200 with 5x objective). The field of view is 1.45 mm x 1.08 mm. The surface profiles at $y = 0$ are extracted as shown in Figure 5-18. The maximum absolute form errors of the profile machined by linear interpolator, PVT and RTIPC are 2.45 µm, 6.82 µm and 2.33 µm, respectively. The standard deviations of the form error are 0.927 µm, 3.20 µm and 0.764 µm, respectively. It shows that the RTIPC achieves the best form accuracy. The result is related with the motion smoothness which is determined by the interpolator. Smoother motions make the stepper motors less likely to lose step. This is especially important when there are no axis feedbacks to be used to correct the motion.

(a) RTIPC   (b) Linear   (c) PVT
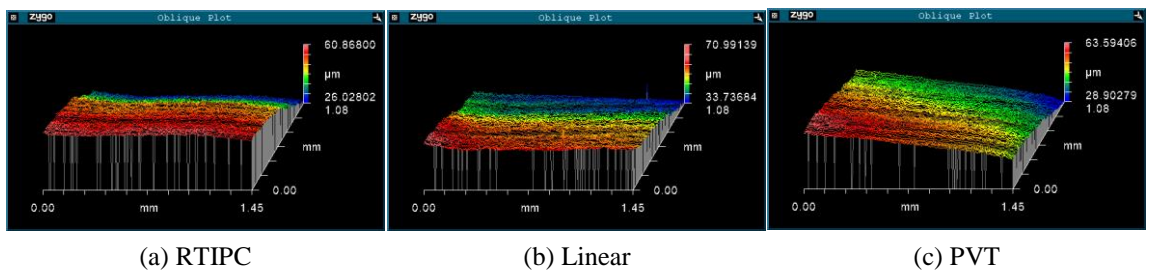
Figure 5-17 Surface topography at the center of the machined cubic phase plate workpieces
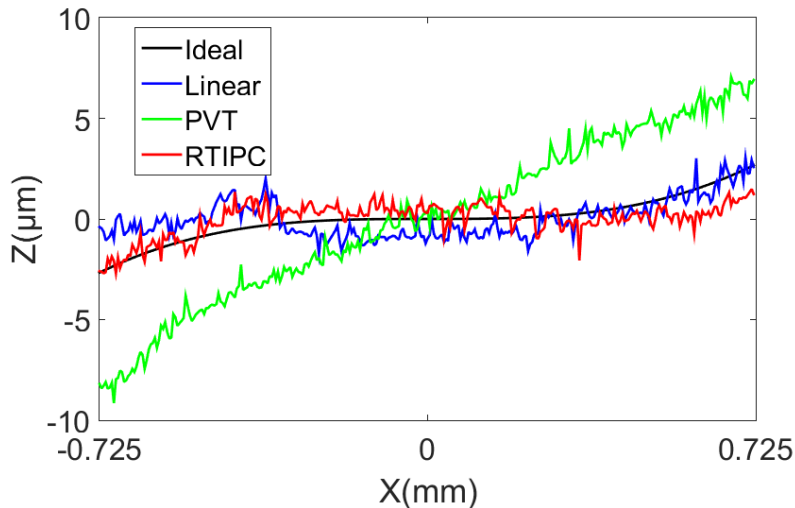
Figure 5-18 Surface profiles at the center of the machiend cubic phase plate workpieces

The advantage of the RTIPC is also found in the contour error limit. To achieve higher contour accuracy, the linear interpolator needs more segments to approximate to original surface, which pose huge burden for the CNC memory and decrease the average feedrate further. The PVT interpolator uses cubic polynomial curves to approximate the original surface. The end points of each segment are on the surface, but it is difficult to control the deviation between the polynomial curve and the surface. Moreover, the PVT interpolation is error-prone, as it requires to map the parameter of the parametric curve to time. Unsuitable mapping will result in undesirable motion profiles. For the RTIPC, the contour error is limited internally by the lookahead operations, the assistance of CAM is eliminated.

5.6   Summary

The linear interpolator has its intrinsic drawback in acceleration and feedrate fluctuation. The driven demand for the high-speed high-accuracy machining of 3D micro-products with freeform surfaces makes the interpolator for parametric curves highly desirable. This chapter proposes a novel solution to the interpolation of parametric curves using feedrate lookahead and acceleration lookahead operations. The experiments have shown that it can achieve the real-time feature. Moreover, it can not only simplify the coding significantly, but also achieve ten times productivity increase compared with the linear interpolator. The proposed interpolator can also achieve much smoother motion profiles than the state-of-the-art PVT interpolator and has the advantage in limiting contour error. The main advantages of this interpolator comparing with existing works can be summaries as follows:

(1) Its application is not limited to NURBS but general parametric curves with real-time feature;

(2) It limits both machine dynamics (axial velocities, axial accelerations and jerk) and contour error while maintaining the feedrate as high as possible with minimum fluctuation.

(3) The dynamic lookahead length technique, the numerical integration error consideration, the multi-cases design for feedrate lookahead and intelligent activation of the acceleration lookahead are introduced for the first time, which greatly enhance the interpolation efficiency and accuracy.

Chapter 6   Real-time global toolpath smoothing

6.1   Introduction

As identified in Chapter 2, a built-in toolpath smoothing algorithm is of great importance to bridge the gap in the toolpath representation for high-speed hybrid machining of 3D micro-products. However, many challenges still remain in current toolpath smoothing approaches, as concluded in Chapter 2.

This chapter presents a new real-time global toolpath smoothing algorithm, which uses a cubic B-spline to approximate a sequence of linear segments. Instead of calculating the unknown control points with the least squares approximation, this algorithm, for the first time, utilizes the original toolpath as the control polygon. The original toolpath is usually generated by CAM software. The approximation deviation is controlled by inserting and moving new control points on this control polygon. The effectiveness of the proposed algorithm will be demonstrated by the numerical experiments and freeform surface machining trials.

6.2   Preliminaries

6.2.1 B-spline representation of the toolpath

The mathematical representation of a *pth*-degree B-spline is given by

$$\boldsymbol{C}(u) = \sum_{i=0}^{n} N_{i,p}(u)\boldsymbol{P}_i \qquad \text{6-1}$$

where $\boldsymbol{P}_i$ are the specified n control points, control polygon is the polygon formed by the control points. $N_{i,p}(u)$ are the basis functions defined on the knot vector $U = \{u_0, \cdots, u_{n+p+1}\}$ as follow

$$N_{i,0}(u) = \begin{cases} 1 & if\ u_i \le u < u_{i+1} \\ 0 & otherwise \end{cases}$$

$$N_{i,p}(u) = \frac{u - u_i}{u_{i+p} - u_i} N_{i,p-1}(u) + \frac{u_{i+p+1} - u}{u_{i+p+1} - u_{i+1}} N_{i+1,p-1}(u)$$

<div align="right">6-2</div>

In Eq. 6-2, the convention $0/0 = 0$ is adopted. A variety of curves can be constructed by manipulating the control points and the knot vector. However, the continuity of the curve is of great importance, as it will determine the smoothness of the motion profiles scheduled by the interpolator. Piegl and Tiller [26] proved that if C^r continuity is desired for a B-spline curve, then the chosen degree k must satisfy

$$k \ge r + 1 \qquad\qquad 6\text{-}3$$

The precondition of Eq. 6-3 is that the multiplicities of interior knots are 1. For high-speed high-accuracy freeform machining, at least C^2 continuity is required, i.e., both the velocity and acceleration are continuous. Therefore, cubic B-spline is adopted to guarantee the continuity as well as to reduce the computation intensity compared with using higher order B-spline.

6.2.2 Local corner rounding with B-spline

Local corner rounding with B-spline gains its popularity among the industry and academia, as described in Section 2.6, since it can provide an analytical solution for the corner transition. Figure 6-1(a) depicts that a cubic B-spline curve is inserted between the linear segments $\boldsymbol{Q_0 Q_1}$ and $\boldsymbol{Q_1 Q_2}$. Five symmetric control points are positioned on the linear segments. The knot vector $\{0, 0, 0, 0, 0.5, 1, 1, 1, 1\}$ is usually used to create a symmetric B-spline curve. The maximum deviation can be calculated analytically as

$$\varepsilon = \|\boldsymbol{P_2} - \boldsymbol{C}(0.5)\| = \left\| \frac{1}{2}\boldsymbol{P_2} - \frac{1}{4}\boldsymbol{P_1} - \frac{1}{4}\boldsymbol{P_3} \right\| \qquad 6\text{-}4$$

The deviation can be easily controlled by carefully positioning $\boldsymbol{P_1}$ and $\boldsymbol{P_3}$. Since the first three and last three control points are collinear, the new toolpath is G^2 and curvature continuous at the connecting points $\boldsymbol{P_0}$ and $\boldsymbol{P_4}$. The smoothness can be

further improved if the second derivatives of the B-spline at both ends are zero, as shown in Eq. 6-5, which can be further simplified to Eq. 6-6, which gives the positions of P_0 and P_4.

$$\begin{cases} \ddot{C}(0) = 12P_2 - 36P_1 + 24P_0 = 0 \\ \ddot{C}(1) = 12P_2 - 36P_3 + 24P_4 = 0 \end{cases} \qquad \text{6-5}$$

$$\begin{cases} P_2 - P_1 = 2(P_1 - P_0) \\ P_2 - P_3 = 2(P_3 - P_4) \end{cases} \qquad \text{6-6}$$

It is obvious that this kind of approach is very restrictive if the toolpath is composed of high density of short linear segments, which are very common in the finish machining of freeform surfaces. The inserted B-spline will overlap with each other, which makes the subsequent interpolation impossible. Tulsyan and Altintas [68] proposed to restrict the length of the transition path to avoid the overlap problem, i.e., the maximum length of P_0P_2 and P_2P_4 are restricted to the minimum half-length of the connecting segments, as shown in Figure 6-1(b). However, this measure will lead to the over-constrained tolerance and much higher curvature, as shown in Figure 6-1(b). The Figure 6-1(c) compares the curvature of the resulted transition curves in (a) and (b). For the case (b), the feedrate must slow down to avoid shock at the corner. Therefore, the proposed new algorithm will seek a global approach to overcome this limitation.

(a) Unrestricted transition length   (b) Restricted transition length
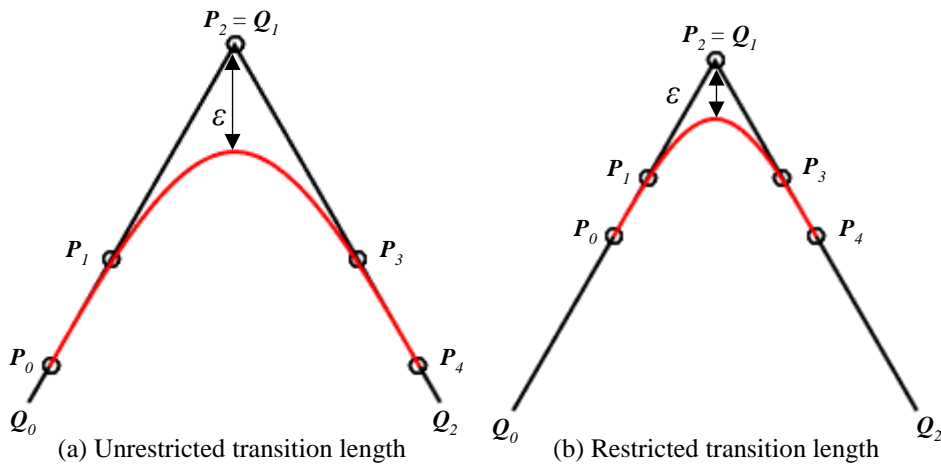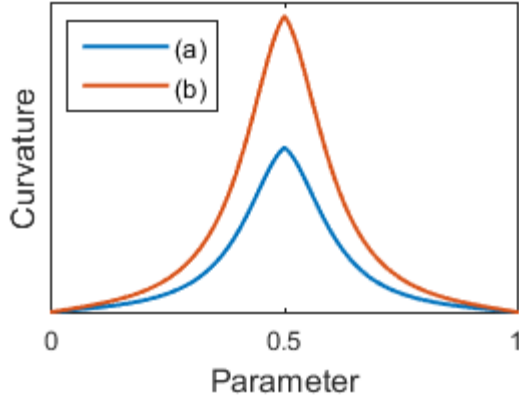
(c) Curvature comparison

Figure 6-1 Local corner rounding with B-spline

6.2.3 Global approximation with B-spline

The essential problem of approximating a given set of points $\{\boldsymbol{Q}_i, i = 0, \cdots, m\}$ by a B-spline curve is to find appropriate control points for the Eq. 6-1, so that the distance between $\boldsymbol{Q}_i$ and $\boldsymbol{C}(u)$ is minimum. The objective function can be expressed as

$$f = \sum_{i=0}^{m} [\boldsymbol{Q}_i - \boldsymbol{C}(\tilde{u}_i)]^2 \qquad \text{6-7}$$

where $\tilde{u}_i$ are the precomputed parameter values with a certain parametrization method. Piegl and Tiller [26] have developed an effective method to solve this least squares approximation problem. However, this kind of approach only considers controlling the deviation of the toolpath points. The deviation within each segment is very likely to be enormous. To avoid this undesirable problem for high-accuracy freeform machining, the Hausdorff distance between the approximation curve and the original toolpath should be used, which can be expressed as

$$H\big(\boldsymbol{C}(u), \boldsymbol{T}(v)\big) = max\{h(\boldsymbol{C}(u), \boldsymbol{T}(v)), h(\boldsymbol{T}(v), \boldsymbol{C}(u))\} \qquad \text{6-8}$$

where $\boldsymbol{T}(v)$ is the parametric representation of the original toolpath, $h(A, B) = max_{p \in A}\|p - B\|$ is the one-sided Hausdorff distance from A to B, as shown in

Figure 6-2. The evaluation of Hausdorff distance is exceptionally computation intensive [111], which makes it very restrictive for real-time CNCs. Therefore, the proposed new algorithm should address the global toolpath approximation problem in a completely novel way.
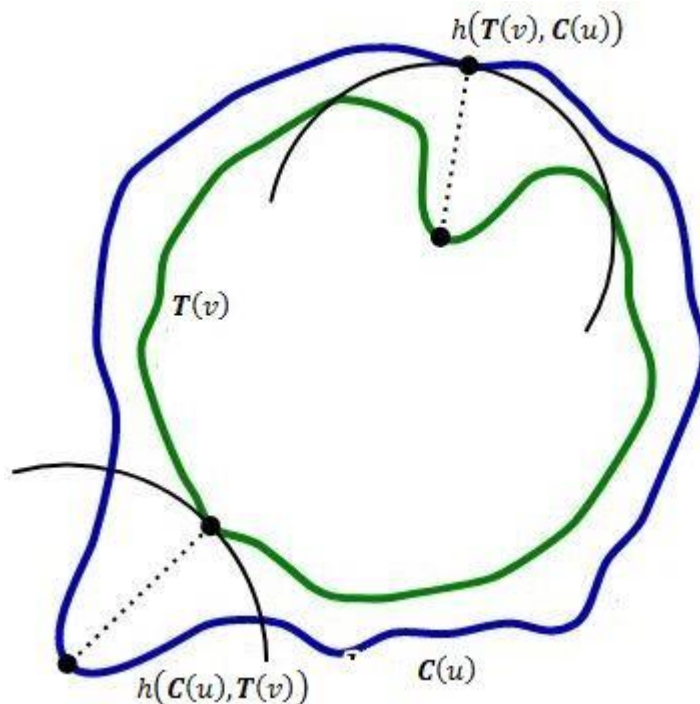
Figure 6-2 The Hausdorff distance calculation[112]

6.3 Algorithm development

6.3.1 Mechanism of the new algorithm

Control point plays a vital role in controlling the shape of the B-spline curve. Instead of calculating the unknown control points by using the least squares technique, this algorithm uses the original linear segmented toolpath as the control polygon. Figure 6-3(a) shows the initial B-spline curve constructed by the original points of a trapezoidal toolpath, which incorporates the obtuse angle, acute angle and right angle. To control the deviation between the curve and the linear segments, two extra control points are inserted on the control polygon near each corner. The curve is pulled

toward the linear segments dramatically by the newly inserted control points due to the strong convex hull property of B-spline, as shown in Figure 6-3(b). A part of the curve becomes straight line if four consecutive control points are collinear, where the curve coincides with the toolpath. This feature can guarantee that the deviation within each segment is minimized, so that the evaluation of the Hausdorff distance between the approximation curve and the original toolpath is eliminated. The curve will come closer to the toolpath if the newly inserted control points are moved toward the corner. In the extreme case, a cusp is generated if the three control points are coincident, as shown in Figure 6-3(c). The curve and the toolpath are coincident as well at the corner in this case.
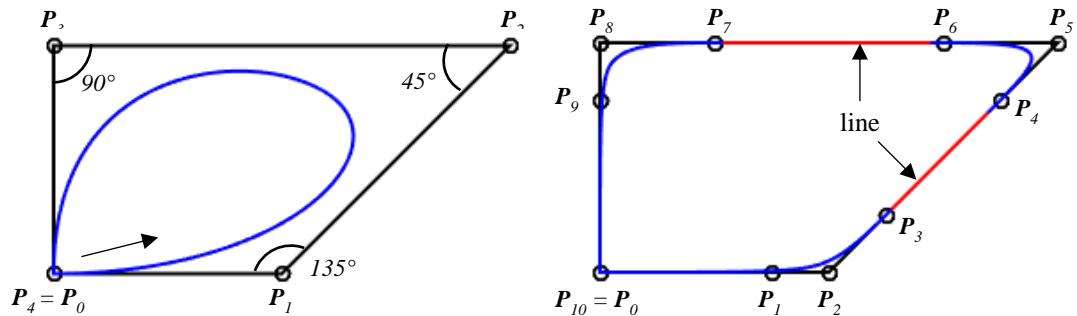
(a) Using original toolpath points as control points   (b) Inserting new control points near the corner
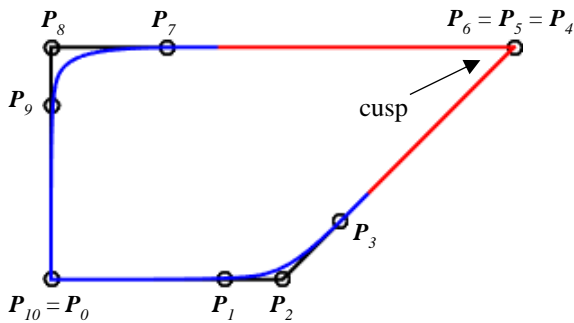
(c) Moving new control points toward the corner

Figure 6-3 Linear segmented toolpath approximated by cubic B-spline

Hence, the approximation of linear segmented toolpath using cubic B-spline can be achieved in a straightforward way, i.e., the linear segments are used as the control polygon and the deviation is controlled by inserting and moving two extra control

points near the corner. However, the problems of choosing the knot vector and determining positions of the new control points remain in order to finalize the B-spline curve. Even though the knot vector has relatively less effect on the shape of the curve, unsuitable knot vector may result in erratic shape. This thesis uses the parametrization method proposed by Hartley and Judd [113], which can achieve reasonable parametrization in all toolpath cases.

$$\begin{cases} u_0 = \cdots = u_p = 0 \\ u_i - u_{i-1} = \dfrac{\sum_{j=i-p}^{i-1} |P_j - P_{j-1}|}{\sum_{s=p+1}^{n+1} \sum_{j=s-p}^{s-1} |P_j - P_{j-1}|}, i = p+1, \cdots, n \\ u_{n+1} = \cdots = u_{n+p+1} = 1 \end{cases}$$
6-9

The knots determined by Eq. 6-9 reflect the relative lengths of the polygon arms, the multiplicities of interior knots are unlikely more than 1, thus the C^2 continuity is guaranteed. Furthermore, the knot interval (u_i, u_{i+1}) is only affected by control points $P_{i-p}, \cdots, P_i$, which is coincident with the local modification property of B-spline.

6.3.2 Approximation deviation control

When a new control point is inserted or repositioned, the knot vector will be changed according to Eq. 6-9. The change in either control points or the knot vector leads to the modification of the curve shape. As a result, the deviation control is a nonlinear problem which is extremely difficult to get the analytic solution. An iterative method is developed for this algorithm to obtain the desired deviation, as shown in Figure 6-4. The whole process contains four steps as described below:

(a). Use the given linear toolpath points (denoted as $\boldsymbol{Q}_i$) as the initial control points;

(b). Update the knot vector and the B-spline curve;

(c). Check the deviations between $\boldsymbol{Q}_i$ and the curve;

(d). If the deviation is not satisfied, insert or reposition the two extra control points (denoted as P^i_{left} and P^i_{right}, respectively) near Q_i, and go back to step (b); If all the deviations are satisfied, then exit.
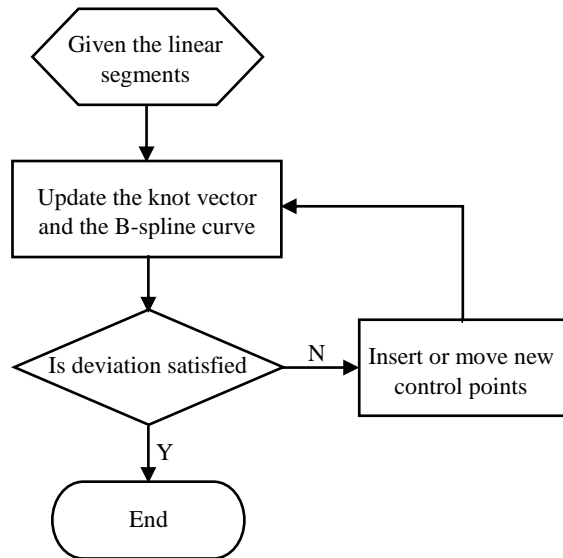
Figure 6-4 Flow chart of the new global toolpath smoothing algorithm

Due to the strong convex hull property of B-spline, the maximum deviations between the curve and the linear segments lie in the corner points. Therefore, instead of evaluating the Hausdorff distance between the original toolpath and the curve, only the deviations of Q_i are evaluated in step (c), which significantly reduces the computation load. If a point on the curve has the minimum distance to Q_i, then it will satisfy

$$\dot{C}(u)(C(u) - Q_i) = 0 \qquad \qquad 6\text{-}10$$

Eq. 6-10 is a non-linear function, which can be solved by the Newton-Raphson iteration. Note that control point P_j, which is corresponding to Q_i, only affects the curve at interval $[u_j, u_{j+p+1})$, the start value for the Newton-Raphson iteration is chosen as the parameter whose corresponding curve point is closest to Q_i among several equally spaced parameters in that interval. The number of the candidate parameters in that interval is chosen dynamically according to the length of the

interval. This guarantees fast and reliable convergence of the Newton-Raphson iteration.

In step (d), there is a trade-off between the algorithm convergence rate and the smoothness of the curve. If $\boldsymbol{P}_{left}^i$ and $\boldsymbol{P}_{right}^i$ are moved rapidly toward $\boldsymbol{Q}_i$, the deviation decreases fast, but there is a risk of over constraint, which creates a relatively sharper transition at the corner. In this algorithm, the following control points reposition method is developed:

$$\begin{cases} \boldsymbol{P}_{left}^i = \boldsymbol{Q}_i + \dfrac{1}{2k}(\boldsymbol{Q}_{i-1} - \boldsymbol{Q}_i) \\ \boldsymbol{P}_{right}^i = \boldsymbol{Q}_i + \dfrac{1}{2k}(\boldsymbol{Q}_{i+1} - \boldsymbol{Q}_i) \end{cases} \qquad 6\text{-}11$$

where k denotes the algorithm iteration number. Eq. 6-11 can achieve good balance between the convergence rate and the smoothness of the curve in the experiments. Figure 6-5 gives a good visualization of the approximation process of the trapezoidal toolpath after the first, second and third iteration of the algorithm. The maximum approximation deviation happens at $\boldsymbol{Q}_2$ for all the three iterations, it is 0.517, 0.258 and 0.172, respectively.
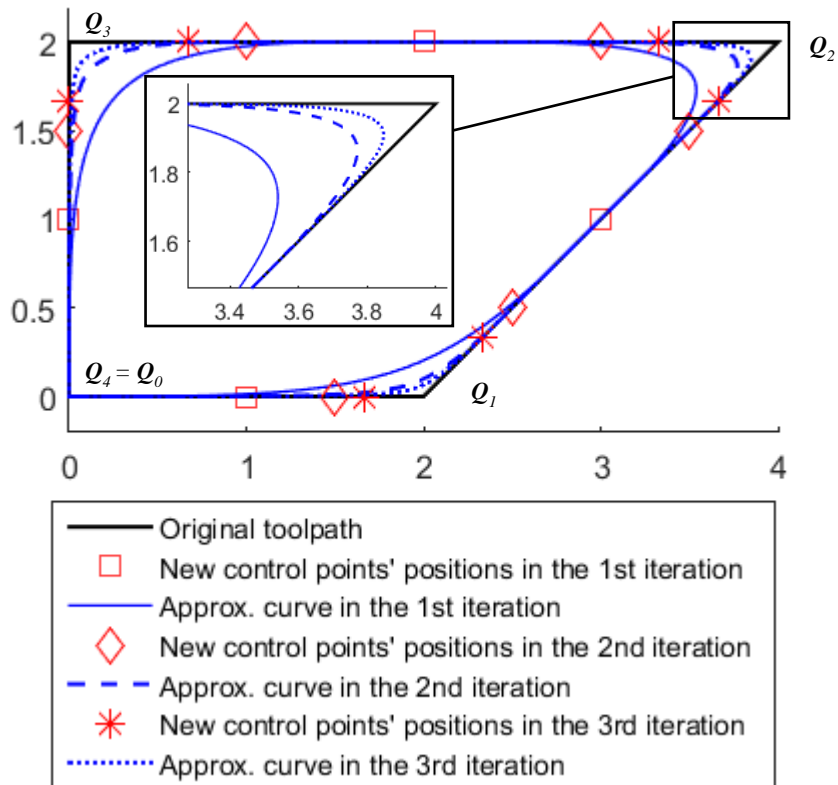
Figure 6-5 Approximation process visualization of the trapezoidal toolpath in three iterations

6.3.3 Comparison with Piegl and Tiller's global approximation algorithm

Piegl and Tiller's global approximation algorithm [26] has been widely used in the current global toolpath smoothing methods. Their algorithm is extremely useful in computer aided geometric design (CAGD), but its application in the toolpath approximation is unsatisfactory, as the Hausdorff distance between the approximation curve and the original toolpath is not considered. Figure 6-6 illustrates the trapezoidal toolpath approximated by the proposed algorithm and the Piegl and Tiller's algorithm, respectively. The specified deviation is 0.1. P_i are the control points used by the proposed algorithm, which are determined after the fifth iteration.

While P'_i are the control points used by the Piegl and Tiller's algorithm, which are calculated using the least squares technique.

Both curves can control the deviations of the toolpath points, as shown in Figure 6-7. The maximum deviations of the curve generated by the proposed algorithm at the three corners are 0.093, 0.091 and 0.098, respectively. The curve, which is generated by the Piegl and Tiller's algorithm, goes through those toolpath points exactly when the number of control points and toolpath points are the same. However, the first curve keeps closely to each linear segment due to the strong convex hull property of B-spline, two parts of the curve have a deviation of zero, the average deviation is minimized. In contrast, the deviations within each linear segment are enormous for the second curve, which is highly undesirable for the high-accuracy freeform machining.
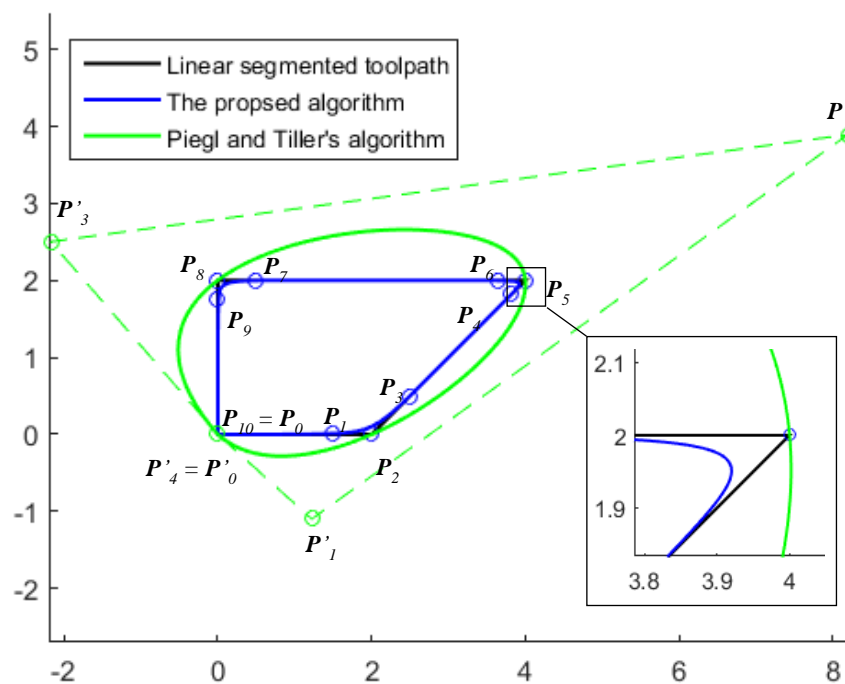
Figure 6-6 Toolpath approximation comparison between the proposed algorithm and Piegl and Tiller's algorithm
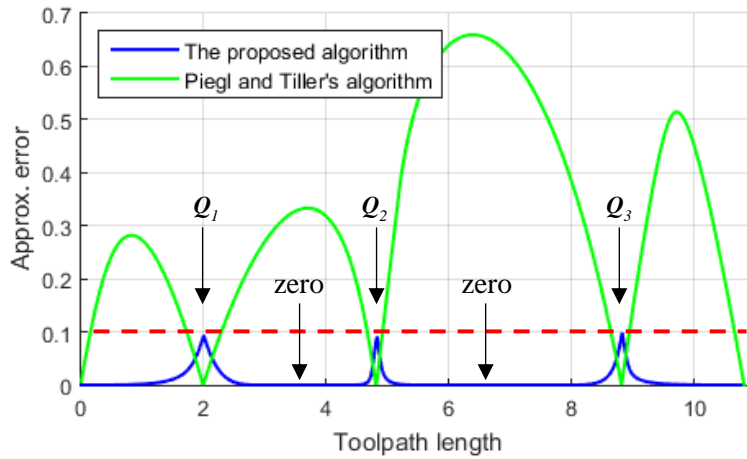
Figure 6-7 Approximation error map of the trapezoidal toolpath

6.4 Numerical experiments

The proposed smoothing algorithm has been implemented in open accessed software, the access information is in Appendix B. Numerical experiments can be performed with the software. In order to demonstrate its effectiveness, it is applied to process two typical toolpaths with the parametric interpolation algorithm, which is detailed in Chapter 5. The interpolator parameters are shown in Table 6-1, the command feedrate is 2 mm/s.

Table 6-1 Interpolator parameters for the toolpath smoothing experiments

X/Y velocity limit (mm/s)	X/Y acceleration limit (mm/s^2)	Jerk limit (mm/s^3)	Contour error tolerance (μm)
100	100	1000	0.1

Figure 6-8(a) shows the global smoothing result of the character "G" toolpath, which consists of 7 linear segments with an average length of 1.05 mm. It is an example of the toolpath used for rough machining. The specified deviation is 20 μm, the actual maximum deviation happens at corner A with a value of 19.45 μm after the sixth iteration of the smoothing algorithm. This proves that the algorithm can limit the deviation accurately without over constraint. The feedrate is only decreased at corner

A and B due to the relatively higher curvature, as shown in Figure 6-8(b). The acceleration and jerk are well confined, as shown in Figure 6-8(c) and (d).

(a) Global smoothing

(b) Velocity profile

(c) Acceleration profile

(d) Jerk profile
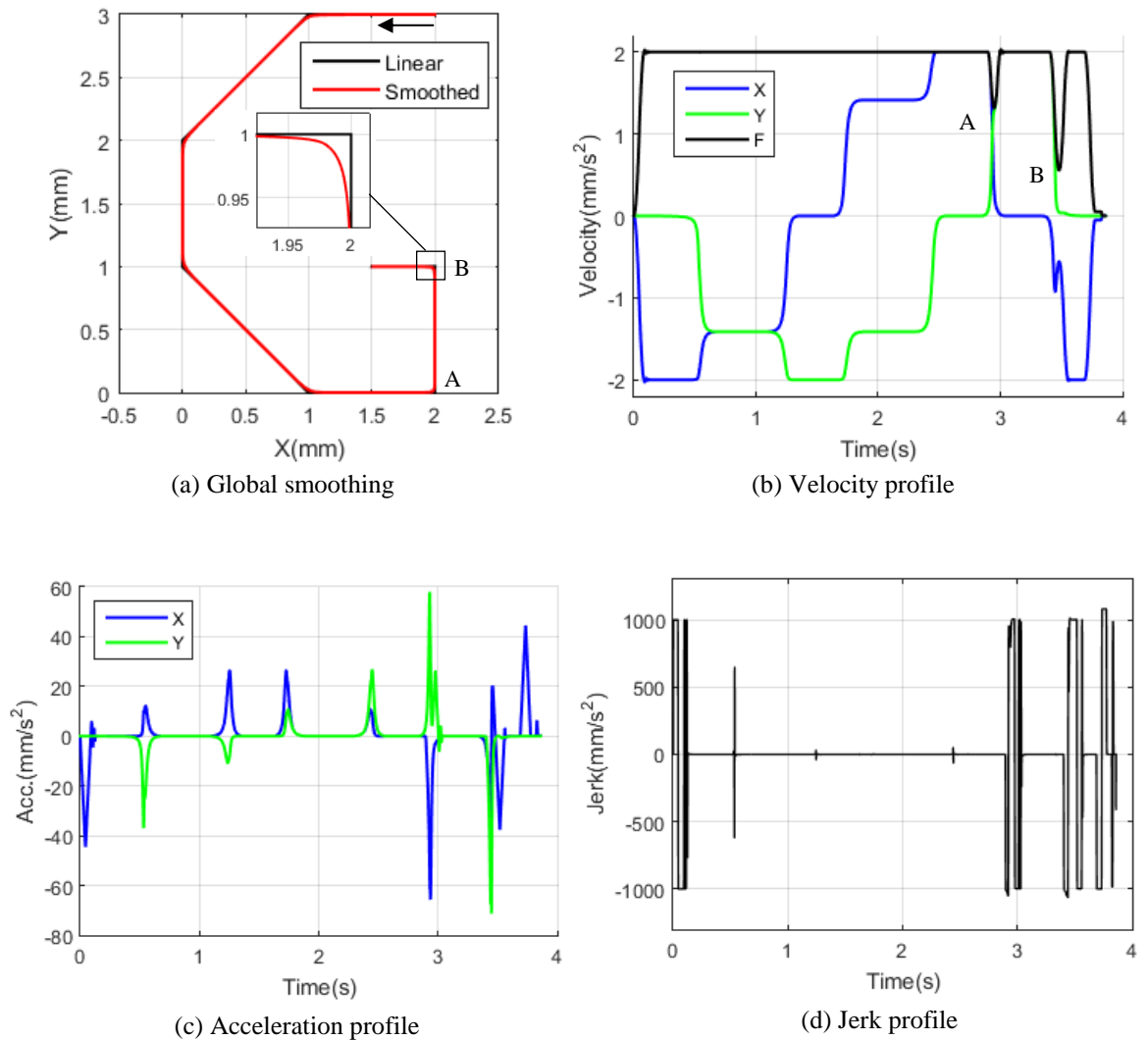
Figure 6-8 Smoothing and interpolation results of the character "G" toolpath

In Figure 6-9(a), a wavy linear toolpath is smoothed with the specified deviation of 2 μm. It is composed of 54 linear segments with an average length of 0.105 mm. It is one of the offset parallel toolpath for the finish machining of the freeform wavy surface, as shown in Figure 6-10(d). The maximum deviation of the smoothing operation is 1.63 μm, which is achieved without inserting any new control points, i.e., the iteration number is zero. Actually, if the toolpath points are spaced closely, the initial approximation curve is generally adequate. Therefore, the proposed smoothing

algorithm is especially suitable for the finish machining of freeform surfaces, which usually accounts for the largest part of the machining time. The fluctuation of the feedrate is kept to a minimum, thanks to the smooth curved toolpath, as shown in Figure 6-9(b). The acceleration and jerk are also maintained within the limits, as shown in Figure 6-9(c) and (d).

(a) Global smoothing

(b) Velocity profile

(c) Acceleration profile

(d) Jerk profile
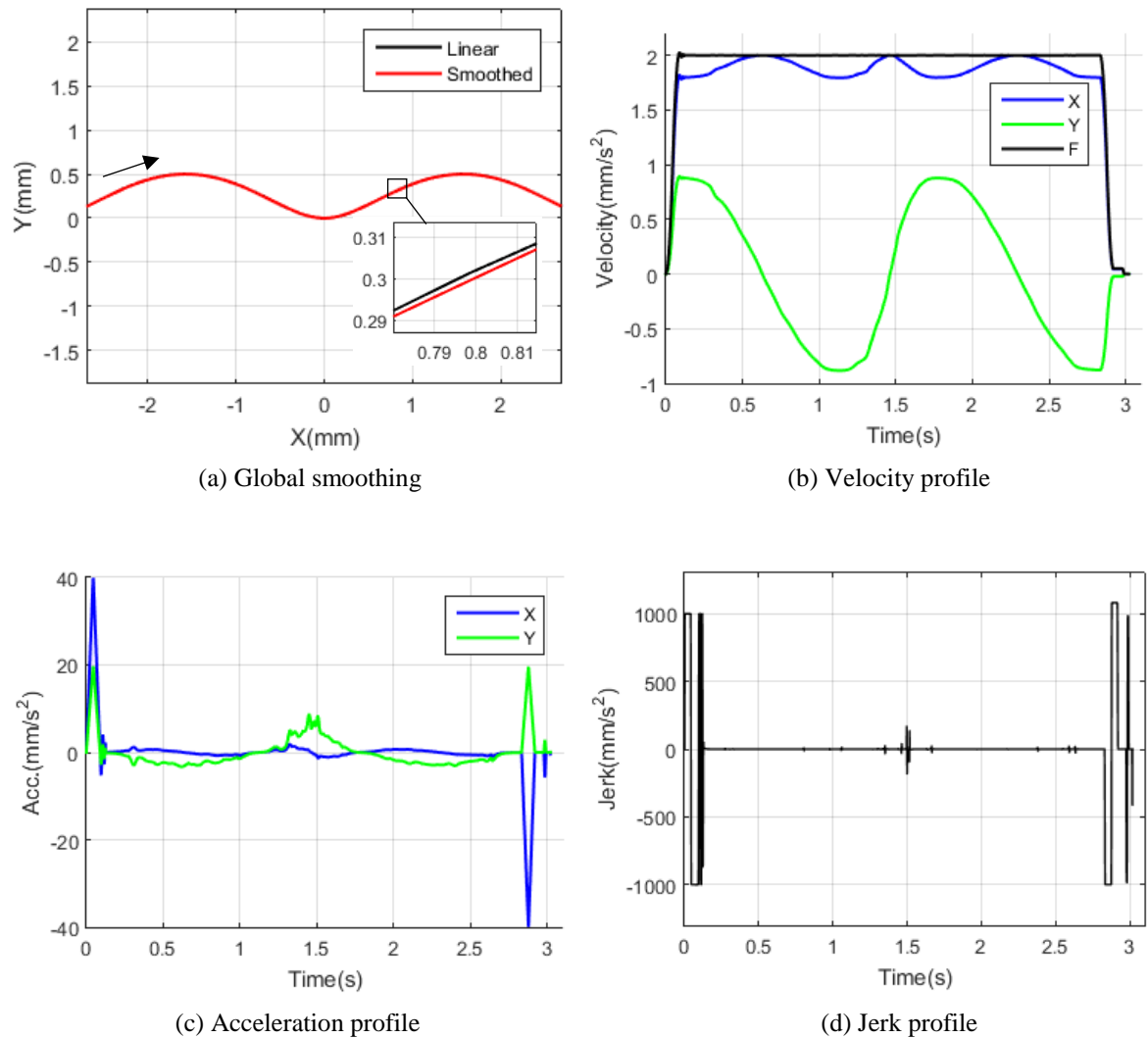
Figure 6-9 Smoothing and interpolation results of the wavy toolpath

6.5   Real-time performance test

The real-time performance test of the proposed algorithm is carried out on a digital signal processor (TMS320C6748), which runs at 456 MHz. The proposed smoothing

algorithm takes 2.63 ms to obtain the specified deviation for the character "G" toolpath, while the wavy toolpath takes 3.44 ms. The CNC interpolation period is usually in millisecond level (1 ms in the thesis), the toolpath can be prepared by the smoothing algorithm within several interpolation periods. Actually, the algorithm spends most of the time on the evaluation of the deviation for each corner, however, each evaluation can be completed in μs level, thanks to the aforementioned optimization measures. Furthermore, the toolpath smoothing algorithm and interpolation algorithm can be run in parallel using the real-time operating system (RTOS). This demonstrates that the proposed smoothing algorithm is efficient enough for real-time CNC systems. However, it is necessary to limit the number of linear segments for each smoothing operation to avoid unacceptable smoothing time if the corner is sharp while the specified tolerance is very small.

6.6 Machining experiments

6.6.1 Machining trial setup

To further assess the performance of the proposed smoothing algorithm, the machining experiments of a freeform wavy surface are carried out on the experiment platform developed in Chapter 4. The Delta Tau Power PMAC controller is used as the benchmark to assess the performance of the proposed global smoothing algorithm. The Delta Tau Power PMAC controller is equipped with the standard toolpath traversing algorithm and the state-of-the-art local corner blending algorithm. The local corner blending algorithm is a one-step solution, it schedules the velocity profile of each axis directly at the corner and creates a smooth transition, the curve planning process is eliminated. As a result, it is highly efficient. The overall blending time T_b is decided by the current moving speed V and the angle of the corner, its detailed calculation method is, however, not disclosed to the public. The corner blending starts and ends at a distance $VT_b/2$ from the corner point.

A 0.8 mm ball end mill is used in the finish machining of the freeform wavy surface, the cutting width is 20 μm along Y axis. The linear segmented toolpath is generated

by Pro/ENGINEERING Wildfire 4.0, which contains over 14,000 lines of code. The specified smoothing deviation is 2 μm, the command feedrate is 2 mm/s and the spindle speed is 15,000 rpm. The workpiece material is aluminum. Both controllers use the same interpolator parameters shown in Table 6-1.

6.6.2 Machining trial results

Figure 6-10(a) – (c) show the workpieces machined by the three different algorithms. Figure 6-11 shows the machining time of the freeform wavy surface with the three different algorithms. It takes 836.5 s for the microcontroller with the proposed algorithm to finish the machining, while the machining is completed in 2891.9 s and 1437.7 s for the Power PMAC controller with the standard toolpath traversing algorithm and the corner blending algorithm, respectively. The proposed algorithm has achieved more than three times productivity compared with the standard toolpath traversing algorithm, while it increases the productivity by more than 40% compared with the state-of-the-art corner blending algorithm.
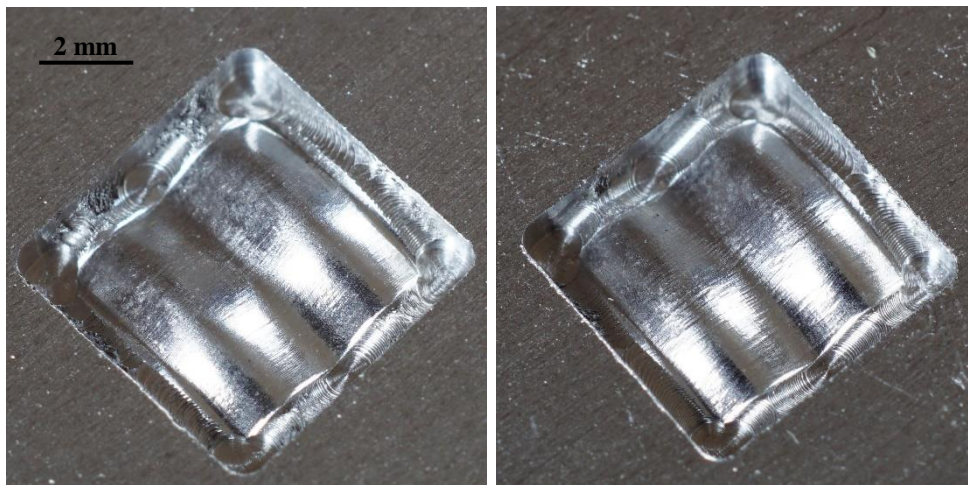
(a) Machined with the proposed algorithm   (b) Machined with the standard algorithm
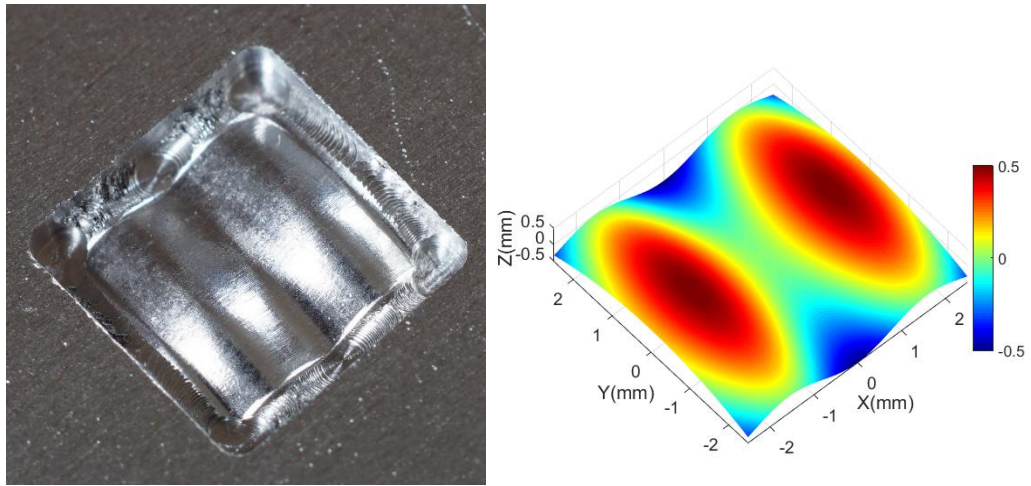
(c) Machined with the corner blending algorithm   (d) The 3D model of the surface

Figure 6-10 The machined freeform wavy workpieces and the 3D surface model
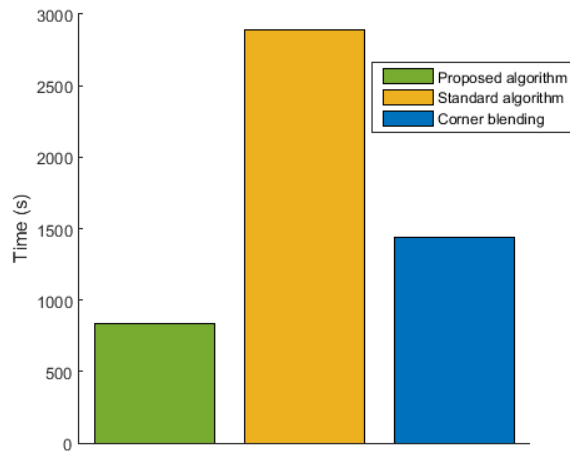
Figure 6-11 Freeform wavy surface machining time comparison

6.6.3 Discussions

It is not surprising that the proposed smoothing algorithm can achieve such outstanding productivity. The standard toolpath traversing algorithm solves the toolpath discontinuity problem by decelerating to a full stop at the end of each segment and accelerating again at the beginning of the next segment. The feedrate fluctuation significantly decreases the productivity. The corner blending algorithm can alleviate the feedrate fluctuation problem to some extent. However, it suffers from the limitation of local smoothing methods, i.e., it is difficult to plan a corner

transition when the segments are short, for the following reasons: 1) The adjacent corner transition path may overlap with each other, which makes the subsequent interpolation impossible; 2) Alternatively, the length of the transition path is constrained which leads to high curvature, the feedrate must slow down to avoid shock. The superiority of the proposed algorithm will become even more obvious with high density of short linear segments.

A white light interferometer (Zygo CP200 with 10x objective) is used to evaluate the surface finish of these workpieces. In Figure 6-10(d), the two peaks at $y = 0$ (denoted as peak1 and peak2 from left to right) and the valley between them are measured. The field of view of each measurement is 0.72 mm x 0.54 mm. Figure 6-12 - Figure 6-14 show two measurement results of each workpiece. Table 6-2 gives the surface roughness Ra of these measurements after applying remove cylinder function. Both the proposed algorithm and the corner blending algorithm achieve distinct improvement in surface finish compared with the standard toolpath traversing algorithm. Moreover, the standard toolpath traversing algorithm leaves some undesirable toolpath marks on the surface, as can be observed in Figure 6-13.

(a) The peak1   (b) The valley
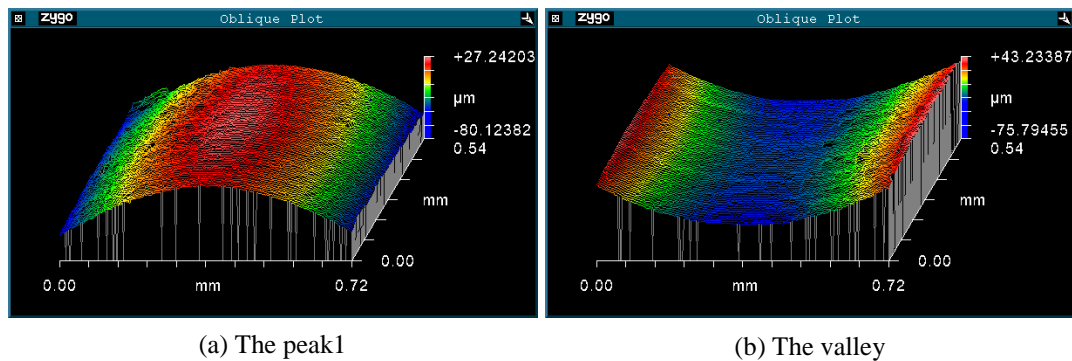
Figure 6-12 Surface topography of the workpiece machined by the proposed algorithm

(a) The peak1   (b) The valley
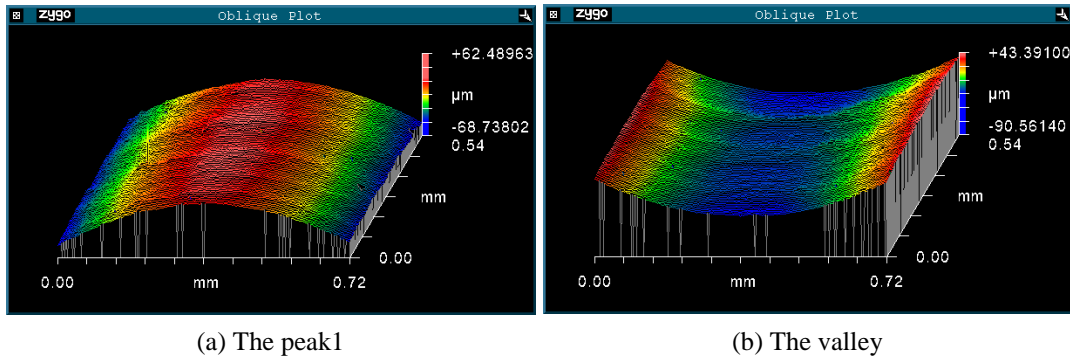
Figure 6-13 Surface topography of the workpiece machined by the standard algorithm

(a) The peak1   (b) The valley
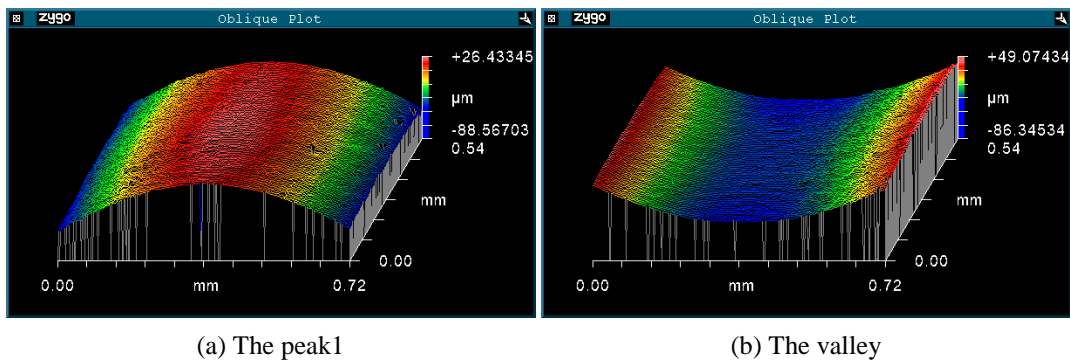
Figure 6-14 Surface topography of the workpiece machined by the corner blending algorithm

Table 6-2 Surface roughness Ra (µm) of freeform wavy surface workpieces

	The proposed algorithm	The standard algorithm	The corner blending algorithm
Peak1	0.89	1.04	0.83
Valley	0.84	1.31	0.79
Peak2	0.78	1.08	0.76

The high-frequency machine resonance excited by the frequent acceleration oscillation of the standard toolpath traversing algorithm adversely affects the surface finish. Thus, toolpath smoothing is an effective way to improve the surface finish for high-accuracy machining of the freeform surfaces. The Power PMAC corner blending algorithm achieves slightly better surface finish than the proposed algorithm, this is because that although the proposed algorithm can achieve much

smoother feedrate and acceleration profiles, the rapid back and forth machining is more likely to cause vibration due to the considerable higher average feedrate. However, this kind of low-frequency vibration can be easily eliminated on a more rigid machine.

6.7 Summary

The toolpath for 3D micro-product machining is usually composed of a large number of linear segments, the discontinuity along the toolpath leads to high-frequency fluctuation of feedrate and acceleration, which will decrease the productivity and the surface finish. This chapter proposes a new global toolpath smoothing algorithm to bridge the gap in toolpath representation. It can address the challenges remained in current toolpath smoothing approaches:

(1) It overcomes the severe limitation of the local smoothing methods when smoothing high density of short linear segments, which are very common in the finish machining of freeform surfaces. The limitation is found in 1) The adjacent corner transition path may overlap with each other and makes the subsequent interpolation impossible; 2) Alternatively, the length of the transition path is constrained which leads to high curvature, the feedrate must slow down to avoid shock.

(2) For the first time, it adopts the original toolpath as the control polygon and controls the deviation by inserting and moving control points on this control polygon. Computational efficiency is significantly improved by avoiding the least squares approximation and Hausdorff distance evaluation. The smoothing accuracy is greatly increased as well.

The effectiveness of the new algorithm is well demonstrated by the numerical experiments. The machining experiments have shown that the new algorithm is efficient enough for real-time CNCs, and it can increase the productivity by more

than three times than the standard toolpath traversing algorithm and 40% than the state-of-the-art corner blending algorithm, while achieving excellent surface finish.

Chapter 7   Conclusions and future work

7.1   Summary of research contributions

This research aims to provide novel control approaches to overcome the major challenges within CNC system of hybrid micro-machines. With this aim, this thesis first provides a thorough review on current state-of-the-art commercial hybrid machines and their CNC systems, as well as the existing literature. The system integration, parametric interpolation and toolpath smoothing are identified as the three major challenges. A generic control architecture is then proposed to enhance the system flexibility to accommodate a wide range of functional modules. The effectiveness of the control architecture has been demonstrated through the integration of a six-axis hybrid micro-machine. An experimental test-bed is then developed to implement and verify the proposed control algorithms. Finally, the real-time parametric interpolation algorithm and the global toolpath smoothing algorithm are successfully developed and implemented on the test-bed. The benchmarking experiments have demonstrated their advantages over existing approaches.   The novelty and contribution arising from this research include:

- The development of a new flexible control architecture for hybrid micro-machine, which can greatly enhance the efficiency of the system integration to accommodate a wide range of functional modules.
- The research, development, implementation and evaluation of a novel real-time interpolator for parametric curves are performed, which can provide near time-optimal solution to the parametric interpolation problem. The proposed interpolator can overcome the drawbacks of conventional linear or circular interpolator, which lead to large amount of machining codes and high-frequency fluctuation of feedrate and acceleration. The proposed interpolator is promising to provide a unified machining method for 3D micro-products.
- The research, development, implementation and evaluation of a novel real-time global toolpath smoothing algorithm are performed, which can overcome the

limitations of current toolpath smoothing approaches. It will bridge the gap in toolpath representation and fulfil the potential of the novel parametric interpolator.

7.2   Conclusions of the research

The research has identified three major challenges within the CNC system of hybrid micro-machines, i.e. system integration, parametric interpolation and toolpath smoothing. The remarkable findings resulting from this research can be summarised as follows:

 (1) The lack of plug-and-play solutions leads to tremendous difficulty in system integration of hybrid micro-machines. PC-based CNC systems are preferable to hybrid micro-machines, as PC has unprecedented I/O capabilities to accommodate various hardware and software interfaces used by different vendors.

(2) The proposed control architecture can enhance the flexibility of the CNC system to accommodate a broad range of functional modules. The component design also improves the scalability and maintainability of the whole CNC system. The successful integration of a six-axis hybrid micro-machine has verified the effectiveness of those approaches.

(3) The conventional machining approach, which uses small segments to approximate the freeform surfaces of the 3D micro-products, leads to large amount of machining codes and high-frequency fluctuation of feedrate and acceleration, which will decrease the productivity and machined surface finish.

(4) Parametric curve is an optimal toolpath representation method. However, the interpolation of parametric curves is an optimization problem, which is extremely difficult to get the time-optimal solution. The recursive Taylor's expansion and the lookahead technique are essential for a near time-optimal solution.

(5) The proposed parametric interpolator can be applied to general parametric curves with real-time feature. The machining experiments shows that it has significant advantages in coding, machining efficiency and motion smoothness over the industrial standard linear interpolator and the state-of-the-art PVT interpolator.

(6) The linear segmented toolpath is still dominantly used on the factory floor. Current local smoothing approaches have severe limitation in dealing with the high density of short segments, while global smoothing approaches suffer from high computational load.

(7) The proposed global toolpath smoothing approach can avoid those limitations. The machining experiments show that it can increase the productivity by more than three times than the standard toolpath traversing algorithm and 40% than the state-of-the-art corner blending algorithm, while achieving excellent surface finish.

7.3   Recommendation of future work

This research opens discussions on the CNC system for hybrid micro-machines, which are still in the immature development stage. Three major challenges within the CNC system are identified and the corresponding control approaches are developed, which provides a solid foundation for the development of next generation CNC system for hybrid micro-machines. However, many challenges still remain in this new domain. The following researches for the improvement of the CNC system in the future are suggested:

(1) High efficiency adaptive cutting force control algorithm. The small-sized tools used in hybrid micro-machining are extremely sensitive to the cutting force. Due to the lack of scientific tool to estimate the cutting force, conservative feedrate is usually used to prevent tools from excessive wear, which will decrease the productivity. A dynamometer can be used for online cutting force feedback to address this problem. It is straightforward to fit the dynamometer into the proposed control architecture. A coordination task should be developed in the future to develop

and implement an adaptive cutting force control algorithm to adjust the feedrate override dynamically in order to improve the machining efficiency.

(2) On-line machining control algorithm. An adaptive algorithm should be developed in the future to adjust the machining parameters during machining for better results with the support of in-line measurement system. The adaptive algorithm can be implemented in the coordination task of the proposed control architecture.

(3) Industry 4.0 system. The trend for smart factory requires machines to have the capability to be integrated into the industry 4.0 system. The control architecture should be further enhanced to satisfy this requirement.

(4) Freeform surface integrity. The relationship between the smoothness of motion profiles and the freeform surface integrity should be investigated in order to develop better motion scheduling strategies.

(5) Influence of motion profiles on the hybrid process. How the axes motion profiles affects the hybrid process, such as ultrasonic assisted, laser assisted etc., is still unclear.

(6) Understanding of the hybrid process. The better understanding of how the hybrid process affects the machined results, such as form accuracy, surface finish and sub-surface damage etc., deserves more research efforts.

Appendixes

A The RTIPC demonstration software

The demonstration software associated with the RTIPC, as detailed in Chapter 5, is openly available from:

http://dx.doi.org/10.15129/75c22cfe-2cee-4527-9c77-9611658876d1

B The toolpath smoothing demonstration software

The demonstrate software associated with the real-time global toolpath smoothing algorithm, as detailed in Chapter 6, is openly available from:

http://dx.doi.org/10.15129/a07cf57a-d18c-4764-b6cb-64052b184538

References

[1]   Y. Qin, *Micromanufacturing engineering and technology*. William Andrew, 2010.

[2]   F. K. Ehmann, D. Bourell, M. L. Culpepper, T. J. Hodgson, T. R. Kurfess, M. Madou, K. Rajuskar, and R. E. Devor, "International assessment of research and development in micromanufacturing," 2005.

[3]   Technology Strategy Board, "A landscape for the future of high value manufacturing in the UK," 2012.

[4]   K. Nakamoto, T. Ishida, N. Kitamura, and Y. Takeuchi, "Fabrication of microinducer by 5-axis control ultraprecision micromilling," *CIRP Ann. - Manuf. Technol.*, vol. 60, no. 1, pp. 407–410, 2011.

[5]   K. Cheng and D. Huo, *Micro-cutting: fundamentals and applications*. John Wiley & Sons, 2013.

[6]   B. Lauwers, F. Klocke, A. Klink, a. E. Tekkaya, R. Neugebauer, and D. McIntosh, "Hybrid processes in manufacturing," *CIRP Ann. - Manuf. Technol.*, vol. 63, no. 2, pp. 561–583, 2014.

[7]   W. Chang, "Development of Hybrid Micro Machining Approaches and Test-bed," Heriot-Watt University, 2012.

[8]   S. Z. Chavoshi and X. Luo, "Hybrid Micro-machining Processes: A Review," *Precis. Eng.*, vol. 41, pp. 1–23, 2015.

[9]   X. Liu, R. E. DeVor, S. G. Kapoor, and K. F. Ehmann, "The Mechanics of Machining at the Microscale: Assessment of the Current State of the Science," *J. Manuf. Sci. Eng.*, vol. 126, no. 4, p. 666, 2004.

[10]   D. Dornfeld, S. Min, and Y. Takeuchi, "Recent Advances in Mechanical Micromachining," *CIRP Ann. - Manuf. Technol.*, vol. 55, no. 2, pp. 745–768, Jan. 2006.

[11]   B. Bulla, F. Klocke, O. Dambon, and M. Hünten, "Ultrasonic Assisted Diamond Turning of Hardened Steel for Mould Manufacturing," *Key Eng. Mater.*, vol. 516, pp. 437–442, 2012.

[12]   M. Kumar and S. N. Melkote, "Process capability study of laser assisted micro milling of a hard-to-machine material," *J. Manuf. Process.*, vol. 14, no. 1, pp. 41–51,

2012.

[13]   "DT-110 Hybrid μEDM machine." [Online]. Available: http://mikrotools.com/hybriduedm/hybrid-uedm-introduction/. [Accessed: 22-Apr-2018].

[14]   "LUMEX Series." [Online]. Available: http://www.lumex-matsuura.com/english/. [Accessed: 23-Apr-2018].

[15]   "LASERTEC 65 3D hybrid." [Online]. Available: https://uk.dmgmori.com/products/machines/advanced-technology/additive-manufacturing/powder-nozzle/lasertec-65-3d-hybrid. [Accessed: 23-Apr-2018].

[16]   "Microfor FEMTO LASER." [Online]. Available: https://www.posalux.ch/site/en/products/microfor_laser/hp_femto_laser. [Accessed: 23-Apr-2018].

[17]   "ULTRASONIC 20 linear." [Online]. Available: https://uk.dmgmori.com/products/machines/advanced-technology/ultrasonic/ultrasonic-linear/ultrasonic-20-linear. [Accessed: 23-Apr-2018].

[18]   S. Fujita and T. Yoshida, "OSE: open system environment for controller," in *7th International Machine Tool Engineers Conference*, 1996, pp. 234–243.

[19]   J. Michaloski, S. Birla, C. J. Yen, R. Igou, and G. Weinert, "An open system framework for component-based CNC machines," *ACM Comput. Surv.*, vol. 32, no. 1es, p. 23–es, 2000.

[20]   G. Pritschow, C. Daniel, G. Junghans, and W. Sperling, "Open System Controllers - A Challenge for the Future of the Machine Tool Industry," *CIRP Ann. - Manuf. Technol.*, vol. 42, no. 1, pp. 449–452, 1993.

[21]   G. Pritschow, Y. Altintas, F. Jovane, Y. Koren, M. Mitsuishi, S. Takata, H. van Brussel, M. Weck, and K. Yamazaki, "Open controller architecture–past, present and future," *CIRP Ann. - Manuf. Technol.*, vol. 50, no. 2, pp. 463–470, 2001.

[22]   S.-H. Suh, S. K. Kang, D.-H. Chung, and I. Stroud, *Theory and design of CNC systems*. Springer Science & Business Media, 2008.

[23]   T. R. Kramer, F. M. Proctor, and E. Messina, "The NIST RS274NGC Interpreter - Version 3," NIST, 2000.

[24]   M. J. Pratt, "Introduction to ISO 10303—the STEP standard for product data

exchange," *J. Comput. Inf. Sci. Eng.*, vol. 1, no. 1, pp. 102–103, 2001.

[25]   U.S. Product Data Association, "Initial Graphics Exchange Specification. IGES 5.3."
         1996.

[26]   L. Piegl and W. Tiller, *The NURBS Book*, 2nd ed. New York, NY, USA: Springer-
         Verlag New York, Inc., 1996.

[27]   C. Brecher, S. Lange, M. Merz, F. Niehaus, C. Wenzel, and M. Winterschladen,
         "NURBS based ultra-precision free-form machining," *CIRP Ann. - Manuf. Technol.*,
         vol. 55, no. 1, pp. 547–550, 2006.

[28]   W. Zhong, X. Luo, W. Chang, F. Ding, and Y. Cai, "A real-time interpolator for
         parametric curves," *Int. J. Mach. Tools Manuf.*, vol. 125, no. August 2017, pp. 133–
         145, 2018.

[29]   D. F. Rogers, *An introduction to NURBS: with historical perspective*. Elsevier, 2000.

[30]   S. Tajima and B. Sencer, "Global tool-path smoothing for CNC machine tools with
         uninterrupted acceleration," *Int. J. Mach. Tools Manuf.*, vol. 121, no. February, pp.
         81–95, 2016.

[31]   "HEIDENHAIN   CNC."   [Online].   Available:
         https://www.heidenhain.com/en_US/products/cnc-controls/.   [Accessed: 11-Apr-
         2018].

[32]   "FANUC CNC." [Online]. Available: http://www.fanuc.eu/uk/en/cnc. [Accessed: 11-
         Apr-2018].

[33]   "SIEMENS   SINUMERIK   CNC."   [Online].   Available:
         https://www.siemens.com/global/en/home/products/automation/systems/cnc-
         sinumerik.html. [Accessed: 11-Apr-2018].

[34]   "Delta   Tau   Power   PMAC."   [Online].   Available:
         http://www.deltatau.com/dt_powerpmac/powerpmachome.aspx.   [Accessed: 11-Apr-
         2018].

[35]   "Aerotech   Motion   Controller."   [Online].   Available:
         https://www.aerotech.com/product-catalog/motion-controller.aspx.   [Accessed: 11-
         Apr-2018].

[36]   "KERN   Pyramid   Nano."   [Online].   Available: http://www.kern-
         microtechnik.com/en/machine-tool-manufacture/products/kern-pyramid-nano/.

[Accessed: 12-Apr-2018].

[37]   "FANUC ROBONANO." [Online]. Available: https://www.fanuc.co.jp/en/product/robonano/index.html. [Accessed: 12-Apr-2018].

[38]   W. Chang, W. Zhong, F. Ding, F. Wardie, and X. Luo, "Development of a compact ultra-precision six-axis hybrid micro-machine," in *2017 World Congress on Micro and Nano Manufacturing*, 2017.

[39]   S. D. Timar and R. T. Farouki, "Time-optimal traversal of curved paths by Cartesian CNC machines under both constant and speed-dependent axis acceleration bounds," *Robot. Comput. Integr. Manuf.*, vol. 23, no. 5, pp. 563–579, 2007.

[40]   B. Guenter and R. Parent, "Computing the Arc Length of Parametric Curves," *IEEE Comput. Graph. Appl.*, vol. 10, no. 3, pp. 72–78, 1990.

[41]   K. Erkorkmaz and Y. Altintas, "Quintic Spline Interpolation With Minimal Feed Fluctuation," *J. Manuf. Sci. Eng.*, vol. 127, no. 2, p. 339, 2005.

[42]   K. Erkorkmaz and M. Heng, "A heuristic feedrate optimization strategy for NURBS toolpaths," *CIRP Ann. - Manuf. Technol.*, vol. 57, no. 1, pp. 407–410, 2008.

[43]   M. Heng and K. Erkorkmaz, "Design of a NURBS interpolator with minimal feed fluctuation and continuous feed modulation capability," *Int. J. Mach. Tools Manuf.*, vol. 50, no. 3, pp. 281–293, 2010.

[44]   K. Erkorkmaz, S. E. Layegh, I. Lazoglu, and H. Erdim, "Feedrate optimization for freeform milling considering constraints from the feed drive system and process mechanics," *CIRP Ann. - Manuf. Technol.*, vol. 62, no. 1, pp. 395–398, 2013.

[45]   M. Liu, Y. Huang, L. Yin, J. Guo, X. Shao, and G. Zhang, "Development and implementation of a NURBS interpolator with smooth feedrate scheduling for CNC machine tools," *Int. J. Mach. Tools Manuf.*, vol. 87, pp. 1–15, 2014.

[46]   R. T. Farouki and Y. F. Tsai, "Exact Taylor series coefficients for variable-feedrate CNC curve interpolators," *CAD Comput. Aided Des.*, vol. 33, no. 2, pp. 155–165, 2001.

[47]   M. Shpitalni, Y. Koren, and C. C. Lo, "Realtime curve interpolators," *Comput. Des.*, vol. 26, no. 11, pp. 832–838, 1994.

[48]   T. Otsuki, H. Kozai, and Y. Wakinotani, "Free-form curve interpolation method and apparatus," United States Patent 5,815,401, 1998.

[49]   M.-Y. Cheng, M.-C. Tsai, and J.-C. Kuo, "Real-time NURBS command generators for CNC servo controllers," *Int. J. Mach. Tools Manuf.*, vol. 42, no. 7, pp. 801–813, May 2002.

[50]   H. Zhao, L. Zhu, and H. Ding, "A parametric interpolator with minimal feed fluctuation for CNC machine tools using arc-length compensation and feedback correction," *Int. J. Mach. Tools Manuf.*, vol. 75, pp. 1–8, 2013.

[51]   S. S. Yeh and P. L. Hsu, "Adaptive-feedrate interpolation for parametric curves with a confined chord error," *CAD Comput. Aided Des.*, vol. 34, no. 3, pp. 229–237, 2002.

[52]   T. Yong and R. Narayanaswami, "A parametric interpolator with confined chord errors, acceleration and deceleration for NC machining," *CAD Comput. Aided Des.*, vol. 35, no. 13, pp. 1249–1259, 2003.

[53]   S. H. Nam and M. Y. Yang, "A study on a generalized parametric interpolator with real-time jerk-limited acceleration," *CAD Comput. Aided Des.*, vol. 36, no. 1, pp. 27–36, 2004.

[54]   X. Liu, F. Ahmad, K. Yamazaki, and M. Mori, "Adaptive interpolation scheme for NURBS curves with the integration of machining dynamics," *Int. J. Mach. Tools Manuf.*, vol. 45, no. 4–5, pp. 433–444, 2005.

[55]   B. Sencer, Y. Altintas, and E. Croft, "Feed optimization for five-axis CNC machine tools with drive constraints," *Int. J. Mach. Tools Manuf.*, vol. 48, no. 7–8, pp. 733–745, 2008.

[56]   Y. Sun, Y. Zhao, J. Xu, and D. Guo, "The feedrate scheduling of parametric interpolator with geometry, process and drive constraints for multi-axis CNC machine tools," *Int. J. Mach. Tools Manuf.*, vol. 85, pp. 49–57, 2014.

[57]   X. Beudaert, S. Lavernhe, and C. Tournier, "Feedrate interpolation with axis jerk constraints on 5-axis NURBS and G1 tool path," *Int. J. Mach. Tools Manuf.*, vol. 57, pp. 73–82, Jun. 2012.

[58]   M. T. Lin, M. S. Tsai, and H. T. Yau, "Development of a dynamics-based NURBS interpolator with real-time look-ahead algorithm," *Int. J. Mach. Tools Manuf.*, vol. 47, no. 15, pp. 2246–2262, 2007.

[59]   M. Annoni, A. Bardine, S. Campanelli, P. Foglia, and C. A. Prete, "A real-time configurable NURBS interpolator with bounded acceleration, jerk and chord error," *CAD Comput. Aided Des.*, vol. 44, no. 6, pp. 509–521, 2012.

[60]   Y. A. Jin, Y. He, J. Z. Fu, Z. W. Lin, and W. F. Gan, "A fine-interpolation-based parametric interpolation method with a novel real-time look-ahead algorithm," *CAD Comput. Aided Des.*, vol. 55, pp. 37–48, 2014.

[61]   "SIEMENS SINUMERIK 840D sl/828D Basic Functions Function Manual." Siemens AG.

[62]   "A3200 Help file 4.09.000." Aerotech, Inc.

[63]   J. Huang, X. Du, and L. M. Zhu, "Real-time local smoothing for five-axis linear toolpath considering smoothing error constraints," *Int. J. Mach. Tools Manuf.*, vol. 124, no. October 2017, pp. 67–79, 2018.

[64]   J. Yang and A. Yuen, "An analytical local corner smoothing algorithm for five-axis CNC machining," *Int. J. Mach. Tools Manuf.*, vol. 123, no. May, pp. 22–35, 2017.

[65]   S. Sun, H. Lin, L. Zheng, J. Yu, and Y. Hu, "A real-time and look-ahead interpolation methodology with dynamic B-spline transition scheme for CNC machining of short line segments," *Int. J. Adv. Manuf. Technol.*, vol. 84, no. 5–8, pp. 1359–1370, 2016.

[66]   J. Shi, Q. Z. Bi, L. M. Zhu, and Y. H. Wang, "Corner rounding of linear five-axis tool path by dual PH curves blending," *Int. J. Mach. Tools Manuf.*, vol. 88, pp. 223–236, 2015.

[67]   Q. Bi, J. Shi, Y. Wang, L. Zhu, and H. Ding, "Analytical curvature-continuous dual-Bézier corner transition for five-axis linear tool path," *Int. J. Mach. Tools Manuf.*, vol. 91, pp. 96–108, 2015.

[68]   S. Tulsyan and Y. Altintas, "Local toolpath smoothing for five-axis machine tools," *Int. J. Mach. Tools Manuf.*, vol. 96, pp. 15–26, 2015.

[69]   B. Sencer, K. Ishizaki, and E. Shamoto, "A curvature optimal sharp corner smoothing algorithm for high-speed feed motion generation of NC systems along linear tool paths," *Int. J. Adv. Manuf. Technol.*, vol. 76, no. 9–12, pp. 1977–1992, 2014.

[70]   H. Zhao, L. Zhu, and H. Ding, "A real-time look-ahead interpolation methodology with curvature-continuous B-spline transition scheme for CNC machining of short line segments," *Int. J. Mach. Tools Manuf.*, vol. 65, pp. 88–98, 2013.

[71]   X. Beudaert, S. Lavernhe, and C. Tournier, "5-Axis Local Corner Rounding of Linear Tool Path Discontinuities," *Int. J. Mach. Tools Manuf.*, vol. 73, pp. 9–16, 2013.

[72]   V. Pateloup, E. Duc, and P. Ray, "Bspline approximation of circle arc and straight

line for pocket machining," *CAD Comput. Aided Des.*, vol. 42, no. 9, pp. 817–827, 2010.

[73] "FANUC Series 30i-LB Operator's Manual." FANUC Corporation.

[74] Z. Yang, L. Y. Shen, C. M. Yuan, and X. S. Gao, "Curve fitting and optimal interpolation for CNC machining under confined error using quadratic B-splines," *CAD Comput. Aided Des.*, vol. 66, pp. 62–72, 2015.

[75] W. Fan, C.-H. Lee, and J.-H. Chen, "A realtime curvature-smooth interpolation scheme and motion planning for CNC machining of short line segments," *Int. J. Mach. Tools Manuf.*, vol. 96, pp. 27–46, 2015.

[76] Y. Wang, D. Yang, and Y. Liu, "A real-time look-ahead interpolation algorithm based on Akima curve fitting," *Int. J. Mach. Tools Manuf.*, vol. 85, pp. 122–130, 2014.

[77] A. Yuen, K. Zhang, and Y. Altintas, "Smooth trajectory generation for five-axis machine tools," *Int. J. Mach. Tools Manuf.*, vol. 71, pp. 11–19, 2013.

[78] "Power PMAC User's Manual Rev. 8." Delta Tau Data Systems, Inc.

[79] S. Tajima and B. Sencer, "Kinematic corner smoothing for high speed machine tools," *Int. J. Mach. Tools Manuf.*, vol. 108, pp. 27–43, 2016.

[80] B. Sencer, K. Ishizaki, and E. Shamoto, "High speed cornering strategy with confined contour error and vibration suppression for CNC machine tools," *CIRP Ann. - Manuf. Technol.*, vol. 64, no. 1, pp. 369–372, 2015.

[81] T. Otsuki, S. Ide, and H. Shiobara, "Curve interpolating method," United States Patent 7,274,969 B2, 2007.

[82] Y. Koren and M. Shpitalni, "Design of reconfigurable manufacturing systems," *J. Manuf. Syst.*, vol. 29, no. 4, pp. 130–141, 2010.

[83] G. Putnik, A. Sluga, H. Elmaraghy, R. Teti, Y. Koren, T. Tolio, and B. Hon, "Scalability in manufacturing systems design and operation: State-of-the-art and future developments roadmap," *CIRP Ann. - Manuf. Technol.*, vol. 62, no. 2, pp. 751–774, 2013.

[84] L. Monostori, B. Kádár, T. Bauernhansl, S. Kondoh, S. Kumara, G. Reinhart, O. Sauer, G. Schuh, W. Sihn, and K. Ueda, "Cyber-physical systems in manufacturing," *CIRP Ann. - Manuf. Technol.*, vol. 65, no. 2, pp. 621–641, 2016.

[85]   J. Krüger, L. Wang, A. Verl, T. Bauernhansl, E. Carpanzano, S. Makris, J. Fleischer, G. Reinhart, J. Franke, and S. Pellegrinelli, "Innovative control of assembly systems and lines," *CIRP Ann. - Manuf. Technol.*, vol. 66, no. 2, pp. 707–730, 2017.

[86]   M. K. M. Nor and K. Cheng, "Development of a PC-based control system for a five-axis ultraprecision micromilling machine 'Ultra-Mill' and its performance assessment," *Proc. Inst. Mech. Eng. Part B J. Eng. Manuf.*, vol. 224, pp. 1631–1644, 2010.

[87]   W. Lutz, P and Sperling, "OSACA - the vendor neutral Control Architecture," *Conf. Integr. Manuf.*, 1997.

[88]   "EtherCAT Technology Group." [Online]. Available: https://ethercat.org/default.htm. [Accessed: 15-Apr-2018].

[89]   "Component-based software engineering." [Online]. Available: https://en.wikipedia.org/wiki/Component-based_software_engineering. [Accessed: 18-Apr-2018].

[90]   I. Crnkovic, S. Sentilles, A. Vulgarakis, and M. R. V. Chaudron, "A Classification Framework for Software Component Models," *IEEE Trans. Softw. Eng.*, vol. 37, no. 5, pp. 593–615, 2011.

[91]   H. Bruyninckx, M. Klotzbücher, N. Hochgeschwender, G. Kraetzschmar, L. Gherardi, and D. Brugali, "The BRICS component model: a model-based development paradigm for complex robotics software systems," *Proc. 28th Annu. ACM Symp. Appl. Comput.*, pp. 1758–1764, 2013.

[92]   "AUTOSAR." [Online]. Available: https://www.autosar.org/. [Accessed: 19-Apr-2018].

[93]   "OPC Foundation." [Online]. Available: https://opcfoundation.org/. [Accessed: 18-Apr-2018].

[94]   "OMG CORBA v3.3." [Online]. Available: https://www.omg.org/spec/CORBA/. [Accessed: 19-Apr-2018].

[95]   "OMG CCM v4.0." [Online]. Available: https://www.omg.org/spec/CCM/. [Accessed: 19-Apr-2018].

[96]   D. Box, *Essential COM*. Addison-Wesley Professional, 1998.

[97]   D. Box and T. Pattison, *Essential .NET: The Common Language Runtime*. Addison-

Wesley Longman Publishing Co., Inc., 2002.

[98]   "JavaBeans   Specification."   [Online].   Available: http://www.oracle.com/technetwork/java/javase/documentation/spec-136004.html. [Accessed: 19-Apr-2018].

[99]   "Enterprise   JavaBeans   Specification."   [Online].   Available: http://www.oracle.com/technetwork/java/javaee/ejb/index.html. [Accessed: 19-Apr-2018].

[100]   "TenAsys   INtime   for   Windows."   [Online].   Available: http://www.tenasys.com/products/intime-for-windows/. [Accessed: 20-Apr-2018].

[101]   "A3200 Programming Help (5.02.000)." Aerotech, Inc.

[102]   "KL-8056D Manual." [Online]. Available: www.kelinginc.net/KL-8056D. [Accessed: 24-Apr-2018].

[103]   "STM32F746ZG."   [Online].   Available: http://www.st.com/en/microcontrollers/stm32f746zg.html. [Accessed: 25-Apr-2018].

[104]   "ARM   Cortex-M7."   [Online].   Available: https://developer.arm.com/products/processors/cortex-m/cortex-m7. [Accessed: 25-Apr-2018].

[105]   "ST-LINK/V2." [Online]. Available: http://www.st.com/en/development-tools/st-link-v2.html. [Accessed: 25-Apr-2018].

[106]   "FPGA   Download   Cables."   [Online].   Available: https://www.altera.com/products/boards_and_kits/download-cables.html. [Accessed: 25-Apr-2018].

[107]   "SN75ALS192   Datasheet."   [Online].   Available: http://www.ti.com.cn/cn/lit/ds/symlink/sn75als192.pdf. [Accessed: 25-Apr-2018].

[108]   "USB   Device   Class   Specifications."   [Online].   Available: http://www.usb.org/developers/docs/devclass_docs/. [Accessed: 26-Apr-2018].

[109]   "RM0385   reference   manual."   [Online].   Available: www.st.com/resource/en/reference_manual/dm00124865.pdf. [Accessed: 26-Apr-2018].

[110]   "Application note: Floating point unit demonstration on STM32 microcontrollers," STMicroelectronics, Geneva, Switzerland, 2016.

[111] Y. B. Bai, J. H. Yong, C. Y. Liu, X. M. Liu, and Y. Meng, "Polyline approach for approximating Hausdorff distance between planar free-form curves," *CAD Comput. Aided Des.*, vol. 43, no. 6, pp. 687–698, 2011.

[112] "Hausdorff distance." [Online]. Available: https://en.wikipedia.org/wiki/Hausdorff_distance. [Accessed: 26-Jun-2018].

[113] P. J. Hartley and C. J. Judd, "Parametrization and shape of B-spline curves for CAD," *Comput. Des.*, vol. 12, no. 5, pp. 235–238, Sep. 1980.